ITER DOCUMENTATION SERIES No. 22

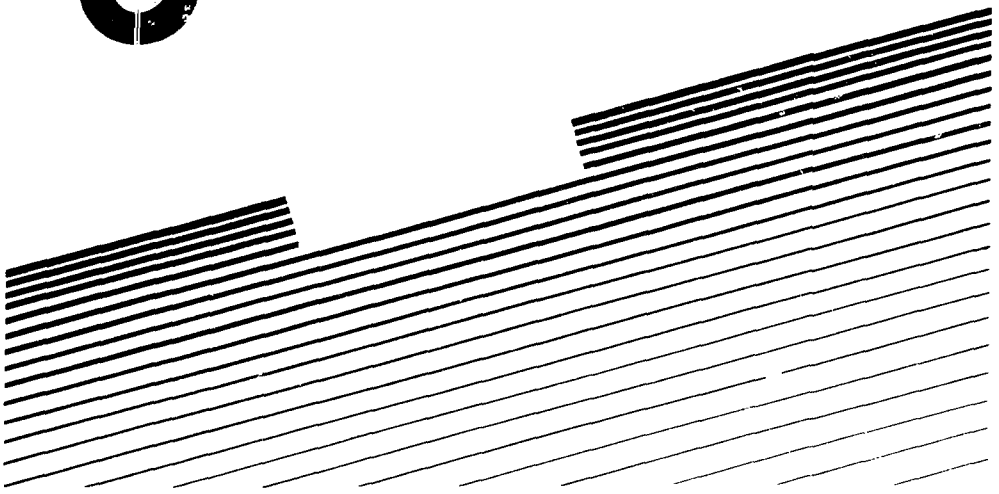

ITER PARAMETRIC ANALYSIS AND OPERATIONAL PERFORMANCE

INTERNATIONAL ATOMIC ENERGY AGENCY, VIENNA, 1991

ITER PARAMETRIC ANALYSIS AND OPERATIONAL PERFORMANCE

ITER DOCUMENTATION SERIES, No. 22

ITER PARAMETRIC ANALYSIS AND OPERATIONAL PERFORMANCE

L.J. PERKINS, W.R. SPEARS, J.D. GALAMBOS, H. IIDA,
T. MIZOGUCHI, S.V. PUTVINSKI, D.T. BLACKFIELD,
S.J. BRERETON, S.A. COHEN, G.A. EMMERT, F. ENGELMANN,
C.A. FLANAGAN, G. HARRIS, M.F.A. HARRISON,
A.I. KOSTENKO, J.R. MILLER, T. NAKAZATO, G.W. PACHER
H.D. PACHER, D.E. POST, Y. SHIMOMURA

INTERNATIONAL ATOMIC ENERGY AGENCY
VIENNA, 1991

ITER PARAMETRIC ANALYSIS AND
OPERATIONAL PERFORMANCE
IAEA, VIENNA, 1991
IAEA/ITER/DS/22

Printed by the IAEA in Austria
April 1991

FOREWORD

Development of nuclear fusion as a practical energy source could provide great benefits. This fact has been widely recognized and fusion research has enjoyed a level of international co-operation unusual in other scientific areas. From its inception, the International Atomic Energy Agency has actively promoted the international exchange of fusion information.

In this context, the IAEA responded in 1986 to calls for expansion of international co-operation in fusion energy development expressed at summit meetings of governmental leaders. At the invitation of the Director General there was a series of meetings in Vienna during 1987, at which representatives of the world's four major fusion programmes developed a detailed proposal for a joint venture called International Thermonuclear Experimental Reactor (ITER) Conceptual Design Activities (CDA). The Director General then invited each interested party to co-operate in the CDA in accordance with the Terms of Reference that had been worked out. All four Parties accepted this invitation.

The ITER CDA, under the auspices of the IAEA, began in April 1988 and were successfully completed in December 1990. This work included two phases, the definition phase and the design phase. In 1988 the first phase produced a concept with a consistent set of technical characteristics and preliminary plans for co-ordinated R&D in support of ITER. The design phase produced a conceptual design, a description of site requirements, and preliminary construction schedule and cost estimate, as well as an ITER R&D plan.

The information produced within the CDA has been made available for the ITER Parties to use either in their own programme or as part of an international collaboration.

As part of its support of ITER, the IAEA is pleased to publish the documents that summarize the results of the Conceptual Design Activities.

CONTENTS

I. INTRODUCTION

The goal of the International Thermonuclear Reactor (ITER) project is the development of an experimental tokamak reactor to establish the scientific and technological feasibility of fusion power [1]. To meet this goal it will demonstrate plasma ignition and extended burn, with steady-state as the ultimate goal. In doing so, it will provide the physics database needed for a demonstration tokamak power reactor, evaluate many of the reactor technologies needed for fusion power and act as an integrated test bed for high heat flux and nuclear components. This report describes the activities in parametric analysis and operational performance studies which have been performed over the past three years of the international ITER Conceptual Design Activities (CDA). These studies have encompassed the following activities:

- Determination of the optimum machine design characteristics to meet the ITER mission goals.
- Investigation of operational performance under various modes including inductive-ignition, steady-state current-drive and hybrid operation.
- Recommendation of baseline performance specifications.
- Studies of the sensitivity of the ITER design to uncertainties in the physics and technology databases.
- Investigation of operational flexibility.
- Continuing assessment of alternative candidate designs which would accommodate changes in either the ITER mission goals or the world tokamak database.
- Implications for extrapolation to prospective DEMO reactors and commercial power reactors.

In performing this work, we have evolved novel analysis tools including optimization systems codes and phase-space methods which are applicable not only to ITER but serve to clearly delineate the cost and performance of any tokamak relative to the major database constraints.

Companion reports in this series describe complementary activities [2, 3, 4, 5]. Of particular interest is Ref 2 which documents the underlying physics rationale of ITER and provides the main physics database constraints on which the present report is based. Similarly, Ref. 3 discusses the operations and research program and formulates the operating scenarios developed in the present report in terms of the overall machine strategy.

This report is organized as follows: Chapter II is the executive summary. Chapter III discusses the rationale leading to the selection of the ITER baseline design and underscores the relationship of the ITER mission goals relative to the database constraints. Chapter IV examines the inductive-ignited operation of the ITER baseline

and assesses the sensitivity of its performance to the major database uncertainties The technology phase performance of ITER is addressed in Chapter 6 where the problems associated with steady-state, current-driven operation -- in particular compatible divertor operation -- are shown to be somewhat alleviated by hybrid operation. Chapter VI provides a preliminary assessment of the prospects for future higher-aspect-ratio ITER designs with emphasis on the potential for improved technology phase performance. As ITER may ultimately be able to perform at levels better than those required to meet the basic mission objectives, Chapter VII examines two potential advanced operating modes, namely an advanced technology phase with possible net electric power generation and D-^{3}He operation. Finally, Chapter VIII assesses the implications for commercial fusion reactors from the standpoint of existing conceptual design studies based on ITER database assumptions or extrapolations thereof.

REFERENCES

[1] *ITER Conceptual Design Report*, ITER Documentation Series No. 18, IAEA, Vienna, (1990)

[2] *ITER Physics*, ITER Documentation Series No. 21, IAEA, Vienna, (1990)

[3] *ITER Operation and Research Program*, ITER Documentation Series No. 23, IAEA, Vienna, (1990)

[4] *ITER Test Program*, ITER Documentation Series No. 24, IAEA, Vienna, (1990)

[5] *ITER Tokamak Device*, ITER Documentation Series No. 25, IAEA, Vienna, (1990)

II. EXECUTIVE SUMMARY

II.1 RATIONALE FOR THE ITER BASELINE DESIGN

II.1.1 I-A-B_{tf} Design Space

In Chapter III, we examine the rationale leading to the choice of the ITER baseline design. This choice was dominated by considerations of prospective ignition performance under inductive operation. Formalisms for steady-state and divertor operation were only fully developed and applied in the later stages of the project. To arrive at an optimum ITER design point, we must meld the set of ITER mission objectives with our present tokamak physics and engineering database and search parameter space within constraint boundaries for, typically, the minimum size/cost machine which meets these objectives at acceptable risk. Constraint boundaries include confinement, beta, divertor heat loads, vertical stability, inductive burn time, radial-build, etc.

Although our optimization systems codes can be directed to arrive at a single optimum design point, we have developed a phase space technique to make the decision analysis more transparent. We emphasize that three datum parameters are required to define a unique design, i.e plasma current (I), aspect ratio (A), and peak field at the TF coil (B_{tf}). The philosophy of trading I for A alone without accounting for peak toroidal field results in an incomplete evaluation. Constraint surfaces applied in this I-A-B_{tf} phase space then restrict the region of optimum design choice. This methodology can be used to clearly delineate the cost and performance of any tokamak from test machines to power reactors, and differs only in the particular mission and physics/technology constraints applied.

Fig. II-1 shows this ITER I-A-B_{tf} design space as a succession of 2-D I-A plots of plasma current -v- aspect ratio with B_{tf} as a parameter in the range 10-13T. Each {I,A,B_{tf}} grid point in Fig. II-1 completely defines a unique machine with unique specifications of major radius, minor radius, axial field, TF/PF magnet geometries, capital cost, etc; contours of major radius are shown in the figure. Note that although the peak toroidal field (B_{tf}) is varied for the plots in Fig II-1(a)-(d), magnet modelling at each grid point is performed with the same design constraints on stress, coil-protection and stability. The location of the ITER baseline (I=22MA, A=2.79, R=6m) is shown in the B_{tf}=11T plane in Fig. II-1(b).

II.1.2 Constraints

The 3-D constraint surfaces of beta limit, minimum permissible inductive burn time (400s at li_3=0.65), energy confinement* , and TF magnet radial build, are shown as slices in the 2-D space of Fig II-1. Other constraints are discussed in

---

* Confinement constraints are expressed in terms of a maximum permissible enhancement (H) over L-mode energy confinement scalins. In this summary, we consider only *ITER Power* scaling with $H_{ITER\text{-}power} \leq 2$,. Other favored scalings are considered in Chapters III and IV.

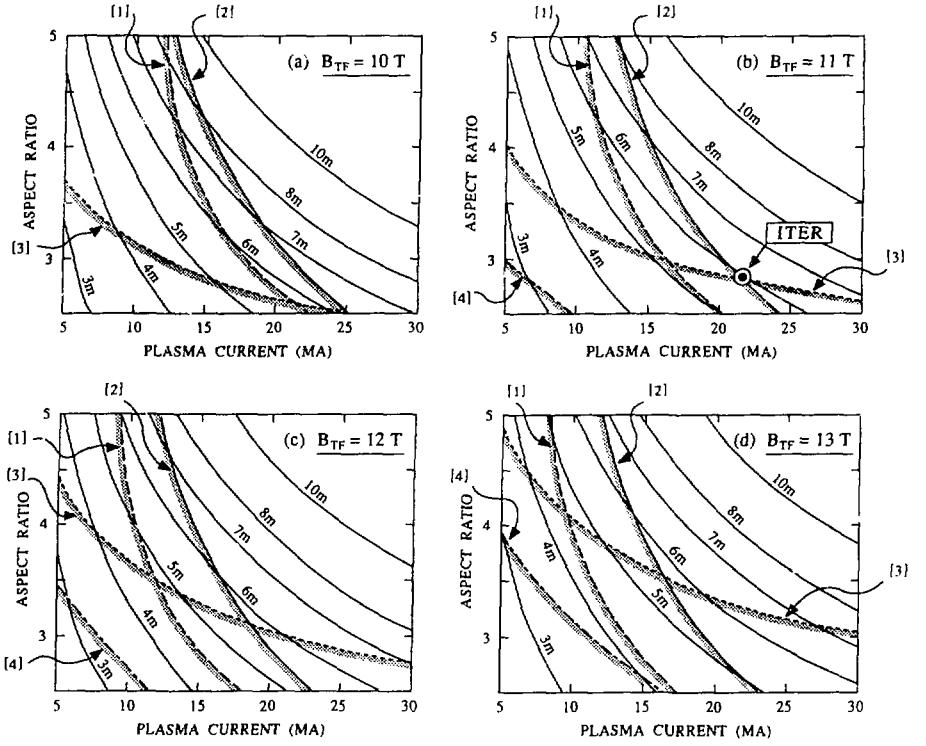

Fig. II-1(a)-(d). Two-dimensional I-A representation of I-A-B_{tf} space with B_{tf} in the range 10-13T. Contours of major radius for ITER-like machines are shown. Constraint boundaries for inductive-ignited operation at a neutron wall load of 1MW/m^2 are: [1] beta limit (g_{Troyon}=2.5), [2] confinement limit ($H_{ITER\text{-}power}$=2.0), [3] inductive burn time (t_{burn}=400s at li_3=0.65), and [4] TF radial build. The location of the ITER baseline is shown in (b).

Chapter III. Candidate ITER machines must necessarily lie on or outside all applicable constraint boundaries. For example, smaller machines located inside the $H_{ITER\text{-}power}$=2.0* confinement boundary would require better than twice L-mode confinement capability to ignite. The constraints of inductive burn time and TF magnet radial build are two facets of the same phenomenon: machines located inside the inductive burn time constraint boundary will have a burn time less than 400s. For even smaller machines located on the TF radial build constraint boundary, the hole within the TF coil inner legs has completely closed leaving no room for a central solenoid.

* Confinement constraints are expressed in terms of a maximum permissible enhancement (H) over L-mode energy confinement scalins. In this summary, we consider only *ITER Power* scaling with $H_{ITER\text{-}power}$≤2,. Other favored scalings are considered in Chapters III and IV.

II.1.3 Selection of the ITER Baseline

From Fig. II-1 we see that at lower values of B_{tf}, requirements of minimizing size/cost favor low aspect ratio machines due to the form of the confinement constraint boundary at constant H. The converse is true at higher values of B_{tf}, i.e. high aspect ratio machines are required due to the inductive burn time constraint boundary. Of course, if the inductive constraint were to be dropped in, say, the design selection of a purely current-driven machine, then low aspect ratio designs would be available at any toroidal field. However, as discussed in Chapter VI, optimization of current-driven performance tends to direct us to back to higher aspect ratio.

For brevity in Fig. II-1, we have shown only confinement predictions from the *ITER Power* energy confinement scaling. In Chapter III we show that all common confinement scalings converge at the ITER design point at low aspect ratio and high plasma current whereas, at higher aspect ratios and lower currents, the scalings differ in their prediction of τ_E. Accordingly, ITER is located at the convergence of the various energy confinement scalings at low aspect ratio together with the inductive burn time constraint. Therefore, our baseline has a reasonable chance of achieving ignition under all of the considered scalings.

II.2 ITER INDUCTIVE-IGNITED PERFORMANCE AND SENSITIVITIES

Parametric and design space analyses are performed for ITER under the agreed physics guidelines of the project. Such guidelines provide the present best estimates for constraints such as beta limits, impurity specifications, profiles, etc. and are subject to the uncertainties inherent in the present tokamak physics database. In Chapter IV, we examine the inductive, ignited operation of ITER and assess the sensitivity of the major performance parameters to the following :

- Thermal alpha particle fraction,
- Impurity content and Z_{eff},
- Fusion power and neutron wall loading,
- Driven operation at high and low Q,
- Density profile,
- Plasma current

Table II-1 shows the major characteristics of the ITER baseline design point and illustrates its nominal performance under inductive, ignited operation ($Q=\infty$). Operation at the beta limit is shown in parentheses. Required enhancement factors, H, for the common L-mode energy confinement scalings are seen to be all about 2.0, a consequence of the selection of the design point (Chapter III). The recent ITER H-mode scaling for ELM free discharges (see Chapter VI for discussion) predicts a required enhancement factor -- note relative to an H-mode scaling -- of only 0.66. ELMs might be expected to increase theis by ~25% or more. The nominal burn time

TABLE II-1. ITER BASELINE: NOMINAL PERFORMANCE UNDER INDUCTIVE, IGNITED OPERATION

(Operation at the beta limit is shown in parentheses)

Characteristics		
Aspect ratio	2.79	
Major/minor radius (m)	6.0/2.15	
Plasma current (MA)	22.0	
Toroidal field, axis/coil-peak (T)	4.85/11.1	
Elongation/triangularity (95%, at li_3=0.65)	1.98/0.383	
q_ψ(95%) at li_3=0.65	3.01	
Ignition Performance		
Neutron wall loading (MW/m^2)	1.0	(1.6[1])
Fusion power (MW)	1080	(1720)
β/β_p	0.042/0.62	(0.053/0.78)
Troyon beta coefficient (%)	1.99	(2.5[1])
Average electron temperature, n_e-weighted (keV)	10.0	
Average electron density / density limit (10^{20} m^{-3})	1.22/1.96	(1.53/2.69)
Zeff	1.66	(1.60)
Plasma thermal stored energy, thermal/total[2] (GJ)	0.58/0.64	(0.73/0.80)
Plasma inductive stored energy at li_3=0.65/0.75 (GJ)	2.24/2.36	
Divertor peak heat load[3] (MW/m^2)	16.5	(35.5)
Required energy confinement time (s)	3.82	(2.87)
$n_{DT}(0).\tau_E.T_i(0)$ (10^{21}s keV m^{-3})	8.46	(7.99)
Required H-mode enhancement over the following scaling predictions: -		
ITER power (L-mode)	2.0	(1.9)
ITER offset (L-mode)	2.0	(1.6)
Shimomura Odajima	1.9	(1.6)
Rebut-Lallia	2.1	(1.6)
Goldston	1.9	(1.8)
T-10	2.1	(2.0)
ITER H-mode	0.66[4]	
Inductive Performance for li_3=0.65		
Plasma inductance (μH)	9.26	
Volt-sec capability (Vs)	326	
Volt-sec for burn (Vs)	46.1	
Loop voltage (V)	0.115	
Burn time (s)	400	

1. At beta limit (max permitted Troyon factor=2.5% for ignited operation)
2. i.e, including fast alpha pressure
3. Systems code models benchmarked to 2D runs.Includes safety/peaking factors of 4.1
4. No allowance for ELMs; might be expected to increase the req'd enhancement factor by ~1.25

under inductive operation is seen to be ~400s for an internal inductance of li_3=0.65 and ~300s for li_3=0.75.

Sensitivity to Thermal Alpha Particle Fraction. As the thermal alpha particle fraction increases from zero to 20%, the Z_{eff} increases only slightly whereas the required confinement time and, therefore, the required enhancement (H) over L-mode scaling increase strongly due to an increase in both the plasma stored energy and radiation losses, both cosequences of increasing n_e. Above an alpha fraction of ~24%, the radiation losses exceed the fusion alpha power, irrespective of the confinement (conduction) losses and no power balance solution is possible. A density limit due to radiative collapse of the plasma edge might be expected to be reached at alpha particle fractions in the vicinity of 15-20% although operation at higher plasma temperatures (and, therefore, lower n_e for the same fusion power) may ease this problem.

Sensitivity to Impurities: By contrast to increasing thermal alpha fractions, increasing higher-z impurity content causes only a modest increase in electron density but an appreciable increase in Z_{eff}. At an impurity content 2.5 times higher than our nominal specifications (causing an increase of Z_{eff} from the nominal baseline of 1.66 to 2.25), ITER would require L-mode enhancement factors of about H~3 to ignite due to the large radiation losses. Density limits may, however, be reached at multipliers of only ~2.0. Above a Z_{eff} of 2.25, radiation losses exceed alpha heating power and power balance cannot be maintained irrespective of the confinement (conduction) performance.

Sensitivity to Neutron Wall Load (Fusion Power): ITER inductive, ignited performance is assessed as a function of wall load in the range 0.3 to 3 MW/m^2 (fusion power in the range 320 to 3240MW). Below $0.3MW/m^2$, the radiation losses exceed the internal alpha power, while operation at a minimum wall load of ~$0.4MW/m^2$ (or equivalent total heating power of $P_\alpha + P_{aux}$) might anyway be required to operate below the density limit.. Such behavior warrants careful attention both to start-up scenarios and operation at fractional power. As the wall loading increases, there is a strong improvement in the confinement requirements under the offset-linear scalings while only a very modest increase in the power law scalings, a consequence of the $\sim P^{-0.5}$ dependence of the latter. Any increase of confinement capability with power is, of course, obtained at the expense of divertor operation. Moreover, the Troyon beta limit of 2.5 would, in any case, be reached for ignited operation at a neutron wall load of ~$1.6MW/m^2$. An appreciable increase in inductive burn time with fusion power is seen as a consequence of the response of the vertical field to increasing poloidal beta.

Sensitivity to Driven Operation at Finite Q: One way to offset uncertainties in energy confinement is to supplement the internal alpha particle heating with external auxiliary power and, therefore, run sub-ignited at a finite Q ($Q=P_{fusion}/P_{aux}$). We assess ITER inductive operation with Q in the range from ∞ (i.e ideal ignition) down to 5 and the required confinement decreases strongly with decreasing Q. Again we see the different trend of the offset-linear scalings relative to the power laws. Under the former, for example, operation at a Q of 5 results in the requirement for less than L-

mode confinement, while the *ITER Power* scaling still requires ~1.3 times L-mode. Operation at Q=20, for example, decreases the ignition confinement requirements from H~2 to H~1.5-1.7. The penalty of lower Q operation is that considerable external power is required, e.g. 54MW for Q=20 and (an impossibly large) 216MW for Q=5,. The effect of this additional power is a highly non-linear increase in the peak divertor heat flux, e.g. a factor of ~2 for Q=20 and a factor of ~5 for Q=5. We note that operation at, say, Q~20 as distinct from ideal ignition can be used as a margin against uncertainty in confinement capability. Alternatively, if we were certain of confinement capabilities of ~2 times L-mode and only demand Q=20 operation, we could, in principle, consider a smaller (R~5m), lower current (I~15MA) machine.

Sensitivity to Density Profile: Performance is assessed as a function of the density profile $n(r)=n(0)\{1-(r/a)^2\}^{\alpha n}$ ranging from hollow (α_n=-0.5), flat (α_n=0) to peaked (α_n~1-3). The significant feature of increasing density profile peaking is a strong increase in the peak to average beta. Moreover, fusion power production scales as n^2 while the thermal stored energy is only proportional to n. Consequently, increasing profile peaking while maintaining a constant neutron wall loading produces a decrease in the required average DT density, the average electron density and thermal stored energy. Radiation powers decrease only slowly due to the competing effect of increasing Z_{eff} with reducing n_e. The net result for a constant wall load is a marked reduction in required energy confinement time and, therefore, in the required H-factors. The required Troyon coefficient (expressing the average beta condition) also falls appreciably at higher values of α_n, while pressure profiles become markedly more peaked (i.e, average beta decreases while peak beta increases). Accordingly, a consistent MHD analysis would be required to determine the limiting values.

Sensitivity to Plasma Current: Sensitivity to plasma current is shown for the range I=15 to 28MA. Given the large dependence of all confinement scalings on plasma current, we see a large variation in the required energy confinement enhancement factors. At 15MA, ~2.5-2.8 times L-mode would be required while the Troyon beta limit of 2.5 would in any case be reached at I~17MA. At 28MA, the required enhancement factors are only ~1.6-1.7 and could be as low as ~1.2 for ignition at the start of burn where the thermal alpha fraction is essentially zero. Two benefits of reducing plasma current are: (a) a large increase in volt-seconds for burn from the baseline value of 400s at 22MA to, for example, almost 2000s at 15MA for the same plasma conditions, (b) the divertor peak heat loads are reduced due, in part, to longer field-line connection lengths, albeit with smaller values of the field line grazing angle at the divertor plate, (c).the disruption loads are reduced due to lower inductive stored energy .

II.3 ITER TECHNOLOGY PHASE PERFORMANCE

II.3.1 Rationale for Analysis

The ITER technology testing mission requires operating scenarios with long pulse length (>1000s and preferably steady state) and adequate neutron wall loads (>0.8MW/m^2 and preferably in excess of 1MW/m^2). Steady-state, non-inductive

current drive is most efficient at low plasma density and, even so, requires large external power injection. Both of these features considerably exacerbate the conditions at the divertor, notably the local plasma temperature (a problem for enhanced erosion), peak heat flux, He pumping and impurity retention. Our present understanding of the expected divertor conditions precludes steady-state operation in the present design at neutron wall loads sufficiently high for useful technology testing. A compromise solution is *hybrid* operation, which combines both inductive and noninductive current drive to achieve scenarios with pulse lengths of thousands of seconds and wall loads near 1 MW/m^2. A feature of some of our operating scenarios is the employment of impurity seeding of the edge plasma to ameliorate divertor heat loads by enhancing the impurity radiation, a scheme that requires validation.

We evaluate the technology phase operating points through systems code optimization of: plasma density, temperature, $q_\psi(95\%)$ (i.e., plasma current), current drive power, fraction of noninductive current drive, and additional impurity concentration (seeded cases only), subject to the following constraints:

- Beta ≤ Troyon limit (g=3); • Confinement enhancement (H) over L-mode ≤ 2.2 (*ITER Power* and *ITER Offset* L-mode scalings); • Density ≤ density limit; • Current drive power ≤ 90% of maximum installed limit; • Divertor heat load ≤ 21 MW/m^2 (includes uncertainties and peaking factors); • $q_{95} \geq 3.0$; • Burn time ≥ 1000 s (hybrid operation only); • Iron impurity = base specifications (unseeded cases) or ≥ base specifications (impurity-seeded cases); • Noninductive current-driven fraction ≥ 30% (for adequate profile control)

For steady-state operating points we maximize the neutron wall load. For hybrid cases, we maximize the fluence (product of wall load, burn time, and number of hybrid cycles)) unless the wall load is unable to attain at least 0.8 MW/m^2 in which case we maximize wall load. Table II-2 provides a subset of representative ITER technology phase scenarios.

II.3.2 Steady-State Operation

Cases 1-3 in Table II-2 show parameters for three steady-state cases, each at the maximum-attainable neutron wall load. In cases 1-2, the divertor heat load constraint is applied and demonstrates the effect of impurity seeding. The divertor heat load is clearly a dominant constraint, and as seen, reducing the power flow to the divertor plate by enhancing the radiation losses through impurity seeding, permits higher wall load operation. However both cases 1 and 2 are limited to maximum wall loads too low for technology testing. If we remove the divertor heat load constraint (case 3), the maximum wall load approaches values of interest for technology testing. Such operation may be possible should improved divertor concepts be realized or if present divertor models prove to be too pessimistic.

II.3.3 Hybrid Operation

Both inductive and non-inductive current drive is used in hybrid operation. However, the total current is reduced to extend the burn time and the power balance is

TABLE II-2. ITER TECHNOLOGY PHASE: STEADY-STATE AND HYBRID OPERATIONAL MODES

Case:	1	2	3	4	5
Mode:	s.state	s.state	s.state	hybrid	hybrid
Seeded?:	no	yes	no	no	yes
Div. constraint?:	yes	yes	no	yes	yes
wall load (MW/m^2)	0.27	0.42	0.71	0.40	1.01
P_{fus} (GW)	0.29	0.46	0.77	0.43	1.09
Q	2.6	4.1	6.8	7.4	9.76
P_{inj} (MW)	113*	113*	113*	58	113 *
burn time (s)	∞	∞	∞	1380	3100
I_p (MA)	10.2	14.5	18.9	17.3	15.6
$I_{cd}/I_{ind}/I_{bs}$(%)	53/-/47	67/-/33	70/-/30	30/51/19	30/32/38
H_{IP} / H_{IO} [a]	2.2*/1.8	2.2*/2.0	2.1/1.8	2.1/2.2*	2.2*/1.7
Impty. seed. fract.[b]	0	0.0013	0	0	0.0007
n_e ($10^{20}m^{-3}$)	0.76	0.64	0.64	0.61	1.13
T_e (keV)	8.5	14	20	14.	11
g-Troyon	2.38	2.54	3.0*	1.93	3.00*
H_{div} (MW/m^2)[c]	21*	21 *	66	21*	21*
T_{div} (eV)[c]	41	35	>100	37	11

*Optimization variable at a constraint bound.

[a] Confinement enhancement factors over L-mode for ITER Power and Offset-linear scalings

[b] Additional fraction of medium-Z impurity seeding (e.g Fe) to alleviate divertor heat loads

[c] Divertor peak heat load and temperature from system code models benchmarked to 2D runs. Peaking factors of 2.75 (physics) and 1.5 (engineering) are applied to the heat loads.

partly maintained by.heating from the current drive power. Higher density operation is then possible which relieves the divertor conditions. The penalty is a finite burn duration. Cases 4 and 5 of Table II-2 show hybrid cases with divertor constraints applied, with and without impurity seeding, respectively. As with steady-state, the use of impurity seeding has a large impact on the attainable wall load. With seeding, wall loads of 1 MW/m^2 and burn times of ~3000 s are possible. The seeded hybrid case attains a wall load more than twice that of the respective steady-state case. The parameters of hybrid case 4 are adequate for technology testing in ITER but this operating point relies on significant impurity seeding to promote edge radiation.

II.3.4 Discussion

A general observation on all technology phase scenarios in Table II-2 are that they are at, or very near, the confinement limit. Although this may seem surprising in view of the large auxiliary power supplied, we note that the optimum plasma current for these scenarios is somewhat less than the 22MA specified for ignited operation. Accordingly, assurance of confinement capabilitiy of ~2 times L-mode will be important for all phases of operation. We show in Chapter V that both the predicted performance for steady-state and hybrid operation can be improved significantly through the use of alternative, more favorable, formalisms for beta limits and bootstrap current. For such conditions, for example, wall loads of 1.5 MW/m^2 and burn times of 6000 s under hybrid operation would be possible. General sensitivities of ITER performance in steady-state and hybrid modes are also discussed in Chapter V relative to uncertainties in divertor heat load constraint, confinement, bootstrap current, beta limit and installed power. The first three of these are seen to be the dominant factors.

II.4 THE PROSPECTS FOR HIGHER ASPECT RATIOS: A PRELIMINARY ASSESSMENT

The present ITER design has a reasonable chance of achieving ignition under all of the presently considered energy-confinement scalings. The choice of this baseline design was primarily dictated by inductive-ignited performance requirements. However, in the later stages of the CDA, formalisms for modelling technology phase and divertor operation were developed further. In Chapter VI we examine the implications of the aspect-ratio-dependence of confinement scaling on the ITER design point and suggest that there may be benefits for high aspect ratio ITER designs, especially regarding steady state operation in the technology phase.

The present experimental confinement database is derived mainly from low aspect ratio machines in the vicinity of 3. In addition, as each of these aspect ratios remained either fixed or varied over only a narrow range, the aspect-ratio-dependence of all scalings for energy confinement derived from this database is uncertain. At high aspect ratios, these scalings diverge considerably in their predictions of τ_E. Experimental results reported as part of the ITER physics R&D program and the analysis of data from higher aspect ratio machines in the new ITER H-mode confinement database, has provided some evidence that the current -v- aspect ratio dependence predicted by both the *ITER Power* and *ITER H-mode* confinement scalings may be about right.

In Chapter VI, we examine a high aspect ratio study point (A=4 I=14.8MA) which has the same confinement capability for ignition as the ITER baseline (A=2.79, I=22MA) under the above scalings but possesses the potential for improved technology phase performance, a consequence of, amongst other factors, higher attainable bootstrap current fractions. A comparison of the major parameters of this study point with those of the ITER baseline is provided in Table II-3. Note, especially, the large improvement in steady-state and hybrid performance. We caution that these high aspect ratio performance parameters are preliminary and have yet to be subjected to the scrutiny employed for the present baseline.

TABLE II-3. COMPARISON OF ITER AND A HIGH ASPECT RATIO STUDY POINT

	ITER BASELINE	*HIGH ASPECT RATIO STUDY POINT*
Characteristics		
Aspect ratio	2.79	4.0
Major/minor radius (m)	6.0/2.15	5.98/1.50
Plasma current (MA) / q_ψ(95%)	22.0 / 3.0	14.8 / 3.0
Toroidal field, axis/coil (T)	4.85/11.1	7.0/13.3[a]
Thermal/inductive stored energies (GJ)	0.580/2.24	0.346/1.35
Relative capital cost	1.00	~0.95[b]
Inductive, ignited performance		
Neutron wall loading (MW/m^2)	1.0	1.0
Fusion power (MW)	1080	784
Required Troyon beta coefficient (%)	1.99	1.73
Required H-mode enhancement for:		
ITER power confinement scaling	2.0	2.0[f]
ITER H-mode confinement scaling	0.66 - ~0.85[d]	0.62 - ~0.85[d]
Divertor peak heat load[c] (MW/m^2)	16.5	11.5
Volt-seconds: capability/burn (Vs)	326/46.1	417/179
Burn pulse length (s)	400	1660
No. of cycles for 1 - 3 MWy/m^2 fluence under purely inductive operation only	78,000 - 237,000	19,000 - 57,000
Technology phase performance[e]		
Steady-state operation under original beta and bootstrap models:		
Maximum attainable wall load[e] (MW/m^2)	0.42	1.10
Q	3.7	7.6
Bootstrap current fraction	0.33	0.46
Steady-state operation under alternative, enhanced beta and bootstrap models :		
Maximum attainable wall load[e] (MW/m^2)	0.65	2.84[g]
Q	6.2	20
Bootstrap current fraction	0.54	0.82
Hybrid operation:		
Pulse length at $1MW/m^2$ wall load[e] (s)	~3,000	~9,000
No. of cycles for 1 - 3 MWy/m^2 fluence	11,000-32,000	4,000-11,000

a. At same coil design constraints as ITER (i.e same stress, protection and stability).
b. Would need validating under present ITER bottoms-up costing procedures
c. Includes safety factors of 2.75 (physics) and 1.5 (engineering)
d. Range reflects possible degradation due to ELMs; lowest values are for basic scaling.
e. Impurity-seeded operation with divertor, beta, and confinement constraints applied
f. Maintained constant relative to ITER baseline, i.e same confinement capability
g. Maximum wall load. Shielding and volumetric heat load constraints may preclude the realization of this high value in practice

With the accumulated knowledge of three years of the ITER CDA, design selection based equally on optimization of both ignited and technology phase operation would have caused more attention to be paid to high aspect ratio designs. In view of the potential impact on the rest of the ITER Engineering Design Activity (EDA), ITER prospects at higher aspect ratio merit early study. Experimental aspect-ratio-dependent confinement data is, therefore, an important part of the EDA physics R&D program.

II.5 FEASIBILITY STUDIES OF ADVANCED OPERATING MODES

II.5.1 Scope

In Chapter VII, we examine how the machine would perform under two operating modes which lie beyond the normal operational scenarios: (1) "advanced" operation at higher power densities more akin to those expected in a commercial power reactor together with an assessment of the capability of net electric power generation, and (2) D-^{3}He operation such as might be undertaken to assess plasma physics performance extrapolations to this case.

II.5.2 Advanced Operation

Performance was assessed using net electric power as a figure of merit under two sets of operating constraints: the base set of ITER physics and technology constraints, and an optimistic set where the constraints were relaxed to more optimistic values. Three operating modes were examined: purely inductive, conventional current drive, and a speculative advanced current drive based on divertor-biased, helicity injection. The results indicate that net electric power generation might be possible, depending on operating constraints, operating mode, and wall loading. Not surprisingly, advanced current drive, which pushes on the whole electron population with high inherent efficiency, appears most attractive, but has yet to be proven.

The impact on various ITER systems was assessed. Divertor heat loads and erosion may limit the wall loading to below the level required for net electric power. If, depending on operating mode and operating constraints, higher fusion power were required to achieve net electric power, or if the machine mission were extended, additional shielding would be required. To obtain net electric power from ITER, it would be necessary to provide a high temperature, high efficiency thermal conversion system. If higher fusion power were required to generate net electricity, it would be necessary to breed more tritium or significantly increase external sources of supply. Demands on tritium systems performance would increase, and safety assurance would become more demanding as fusion power and integral machine operation time increase. Configurational changes will be necessary to accommodate the various needs of this phase. Clearly, extending the ITER mission in this way would add to its cost, safety risk and complexity.

The challenge of extracting net electric power from ITER may be more easily met if only a single sector (1/16) were considered. Many of the concerns associated with energy extraction from the full blanket would be considerably reduced. Obtaining net electric power from a single sector of the ITER blanket during an Advanced Phase would be a more manageable objective.

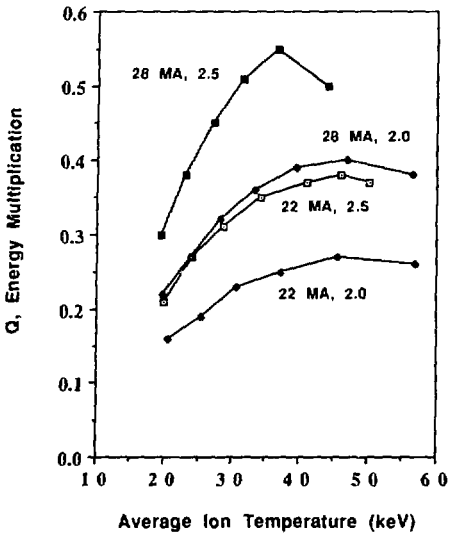

Fig. II-2. D-^{3}He operation in ITER: Variation of Q with average ion temperature. The four curves are parameterized by the plasma current and H-mode multiplier (ITER Power scaling).

II.5.3 D-^{3}He Operation

D-^{3}He operation in ITER would require high temperature plasma conditions (T_e~30keV, T_i~40keV) in order to study plasma transport, power balance, fueling mechanisms, impurity control, etc. In Chapter VII, we investigate the value of energy multiplication Q, the ratio of the fusion power produced in the plasma to the injected power required to sustain the plasma, which might be expected.

Shown in Fig. II-2 is the Q we might achieve in ITER under D-^{3}He operation versus ion temperature and parameterized in terms of plasma current and confinement enhancement factor H for the ITER Power scaling. All other ITER constraints are applied. Q improves with ion temperature and reaches a maximum at about 35 to 50 keV depending on the case. Under the nominal constraints assumed for conventional ITER operation, a D-^{3}He plasma might be expected to achieve Q values of ~0.3, providing ~190MW of auxiliary heating can be supplied. Confinement enhancement of up to H=2.5 and higher plasma currents up to 28MA would increase this value to Q~0.6. Note, however, that from the point of view of the impact of fusion reactions on the plasma power balance, a given Q in D-^{3}He is equivalent to a Q five times larger in D-T. This is because essentially 100 % of the fusion energy is in the form of charged particles for the D-^{3}He reaction, whereas it is only 20 % for the D-T reaction However, for the same reason, power exhaust problems on the divertor may, depending on radiation losses, be much more severe.

Problems requiring further analysis for D-^{3}He operation in ITER include the effect of low density and the large proportion of charged particles on divertor operation, and ripple loss of fast ions. Attention must also be paid to the accuracy of modelling the loss of especially synchrotron radiation power, the production of which will be appreciable at these temperatures.

II.6 IMPLICATIONS FOR COMMERCIAL FUSION REACTORS

During the ITER Conceptual Design Activity a number of parametric surveys and design studies of commercial tokamak power reactors have been made, based to varying extents on ITER physics assumptions. A common assumption of these studies has been to consider higher peak field values than in ITER. Some studies assume a beta scaling coefficient higher or plasma safety factor lower than ITER, and higher bootstrap current contributions and current drive system efficiencies.

Even a machine the size of ITER would under the right circumstances be able to produce a few hundred MW of electricity. For the 1200 MW_e devices from the above studies, the increase in size over that of ITER is rather modest, and the results show that the range covered by conceivable plasma parameter options which are planned to be studied in the ITER experimental programme may even allow some overall size reduction in devices after ITER.

To attain this reactor performance, the main plasma physics and technological objectives that will need to be achieved relative to those expected in basic ITER operation are:

- magnet stress levels about 25% higher;
- thermal conversion efficiencies of about 40%;
- about 2x higher current drive efficiency, or an enhanced bootstrap effect;
- an energy efficient blanket of similar attenuation to the driver blanket;
- control of the scrape-off layer physics, so that heat and particle loads on the first wall and divertor are not 3 times higher than in ITER;
- material damage levels 3-10 times that attainable in ITER;

Confidence in the ability to overcome these challenges in subsequent machines will to a large extent be demonstrated by the studies to be carried out on the ITER device and additional facilities, e.g. for materials testing.

III. RATIONALE FOR THE ITER BASELINE DESIGN

III.1. INTRODUCTION

In this chapter, we examine the rationale leading to the choice of the ITER baseline design. This choice was dominated by considerations of prospective ignition performance under inductive operation rather than by attention to both ignited and steady-state, current-driven performance. This was, in part, due to the fact that formalisms for steady-state and divertor operation were only fully developed in the later stages of the Conceptual Design Activity and, consequently, ITER technology phase performance could only be fully investigated only after the design had been finalized. Accordingly, our discussion of ITER design selection in this chapter will be centered on inductive, ignited operation. Optimization of the baseline technology phase performance will be considered separately in Chapter V, while Chapter VI provides recent preliminary assessment of technology phase prospects at high aspect ratio. Details of the inductive, ignited performance of the baseline and sensitivities to input assumptions will be considered in Chapter IV.

III.2. ITER DESIGN OPTIONS IN I-A-B_{tf} SPACE

III.2.1 I-A-Btf Phase Space

In arriving at an optimum design point, we must meld a set of ITER mission objectives (e.g.: ignition, extended burn under inductive operation, provision of performance parameters sufficient for technology testing, etc), with our present physics and engineering database (e.g.: energy-confinement scalings, plasma impurity models, magnet models for stress, protection, stability, etc) and then search parameter space within constraint boundaries for, typically, the minimum size/cost machine which meets these objectives. Constraint boundaries include confinement limits, beta limits, divertor heat loads, radial-build/volt-seconds, etc).

Although the systems codes available within each of the four ITER parties give similar results, the codes TETRA and QUICK were used for the analysis in this report as they have been kept most up to date with developing ITER physics and engineering assumptions. These codes are capable of performing non-linear optimization of, say, machine size/cost, subject to our set of constraints and, thereby, can determine a single optimum design point. However, while this process quickly arrives at an answer, it is not particularly conducive to making the decision method transparent. Accordingly, here we will employ the I-A-B_{tf} analysis methodology introduced in the early stages of the ITER Conceptual Design Activity [1]. We emphasize that this powerful methodology, where tradeoffs in design space can be viewed relative to physics and technology constraints, can be applied to delineate the cost and performance of any tokamak from test machines to commercial power reactors. The only differences would be in the particular mission and physics/technology constraints applied.

Fig III-1 displays schematically the three-dimensional I-A-B_{tf} space where the axes are plasma current(I), aspect ratio(A), and peak field at the TF coil (B_{tf}). This is

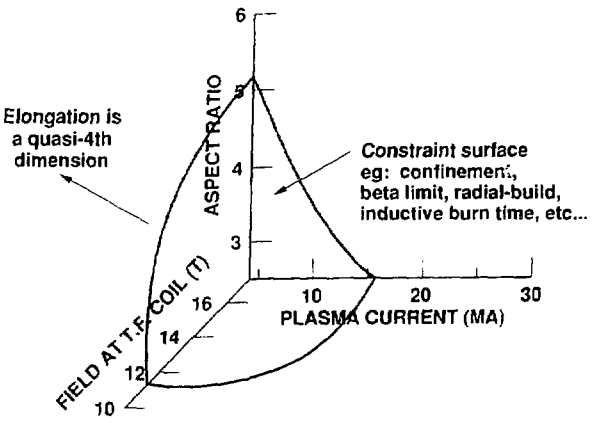

Fig. III-1. Schematic of I-A-B_{tf} phase space for performing tokamak design and confinement trade studies. This methodology is applicable to any type of tokamak; only the database and mission constraint would differ. Elongation, κ, could appear as a fourth axis in an "I-A-B_{tf}-κ" representation.

not a unique set of axes and the datum dimensional variables of either plasma major or minor radius could be substituted for aspect ratio; the latter would then appear as a parameter in this space. The significance of this particular phase space is that providing the following are defined: (1) minimum safety factor at the plasma edge $[q_\psi(95\%)=3.0]^*$, (2) radial build between plasma and inner leg of TF coil which includes inboard scrapeoff, first-wall, shield and vacuum vessel [1.05m], and (3) elongation $[\kappa(95\%)=2.0]$, then each $\{I,A,B_{tf}\}$ grid point completely defines a unique machine with a unique specifications of major radius, minor radius, axial field, TF/PF magnet geometries, capital cost, etc. Furthermore, if a nominal neutron wall loading performance is specified at each grid point (typically 1 MW/m^2) together with the nominal ITER physics specifications [2], then each machine also has a unique set of plasma performance parameters such as energy confinement margin, beta, inductive burn time, etc. Permissible designs then lie on or outside (i.e at higher I, A or B_{tf} values) a set of constraint surfaces in the 3-D space (Fig. 2-1), that is the designs are at at or within the constraint limits. These surfaces may be mission constraints (e.g., minimum required inductive burn time, etc), physics database constraints (e.g., Troyon beta limit, confinement limit, etc), or technology database constraints (e.g., divertor heat load, magnet radial build due to stress limits, etc).

Formally, elongation (κ) should really appear as a fourth axis in a "I-A-B_{tf}-κ" space representation, as it is the fourth key datum parameter in tokamak design. However, here, for ease of understanding and display, we choose to define a typical maximum value of $\kappa(95\%)=2$ which is fixed over the 3-D space of Fig II-1 and then examine its impact by means of a constraint surface of vertical stability.

---

* The values in square brackets indicate those assumed for this analysis

III.2.2. Operational and Database Constraints

As 3-D surfaces are difficult to interpret, we show in Fig. III-2(a) through (e), the ITER I-A-B_{tf} design space as a succession of 2-D I-A plots of plasma current versus aspect ratio at constant values of B_{tf} in the range 10 to 14T. Contours of major radius are shown in each I-A plot. As each I-A-B_{tf} grid point is a unique machine, we could also plot corresponding contours of minor radius, field on axis, etc although they are omitted in these figures for clarity. Within the same B_{tf} plot, for example, the toroidal field on axis increases strongly as aspect ratio increases. Note also that, at a given {I,A} coordinate, the corresponding major radius decreases as B_{tf} increases from plot to plot, a consequence of the minimum specified value of $q_\psi(95\%)=3.0$. It is also important to appreciate that although the peak toroidal field (B_{tf}) is varied for each of the plots in Fig 2-2a through e, magnet modelling at each grid point is performed with the same design constraints on stress, protection and stability. The location of the ITER baseline (I=22MA, A=2.79, R=6m) is shown in the B_{tf}=11T plane in Fig. 1(b).

Contours of capital cost could also be plotted in this space and trends would be approximately similar to those of major radius although high aspect ratio, low current machines are somewhat cheaper than low aspect ratio, high current machines of the same major radius. As an example, consider the position of the ITER baseline in Fig III-2(b) (B_{tf}=11T) with A=2.79, I=22MA and relative cost of, say, 1.0. Proceeding along the same major radius contour of 6m in this figure to a coordinate with A=4, I=12.5MA results in a machine with a relative cost of ~0.83.

The 3-D constraint surfaces of: (1) beta limit (Troyon coefficient =2.5), (2) confinement limit (enhancement factor over L-mode for *ITER Power* scaling of $H_{ITER\text{-}power}$=2.0 -- consideration will be given to other confinement scalings below), (3) inductive burn time (t_{burn}=400s*), and (4) TF magnet radial build, are shown as slices in the 2-D space of Fig III-2 and pertain to ignited operation at a neutron wall load of 1MW/m^2. Other constraints such as vertical stability growth rates, divertor heat loads, etc also apply over this space but, for brevity, are not shown here. Generally, growth rates for vertical stability are seen to vary only very slowly over I-A-B_{tf} space provided elongation is constant and there seems to be little or no dependence on aspect ratio; this will be discussed further in Chapter VI.

In Fig. III-2 (a) - (e), candidate ITER machines must necessarily lie on or outside all such applicable constraint boundaries. For example, larger machines located outside the $H_{ITER\text{-}power}$=2.0 boundary (i.e at higher I or A values) require less than an enhancement factor of two to ignite. Conversely, smaller machines located inside the boundary (i.e at lower I or A values) require better than twice L-mode confinement capability (as predicted by *ITER Power* scaling) to ignite.

The constraints of inductive burn time and TF magnet radial build in Fig. III-2 are two facets of the same phenomenon and are interpreted as follows: Smaller machines located inside the inductive burn time constraint boundary, will have a burn

---

* The required minimum ITER inductive burn time is 200s at a plasma inductance of li_3=0.75. A less conservative assumption of li_3=0.65 results in a corresponding minimum burn time requirement of 400s. All points in Fig 2-2 have li_3=0.65.

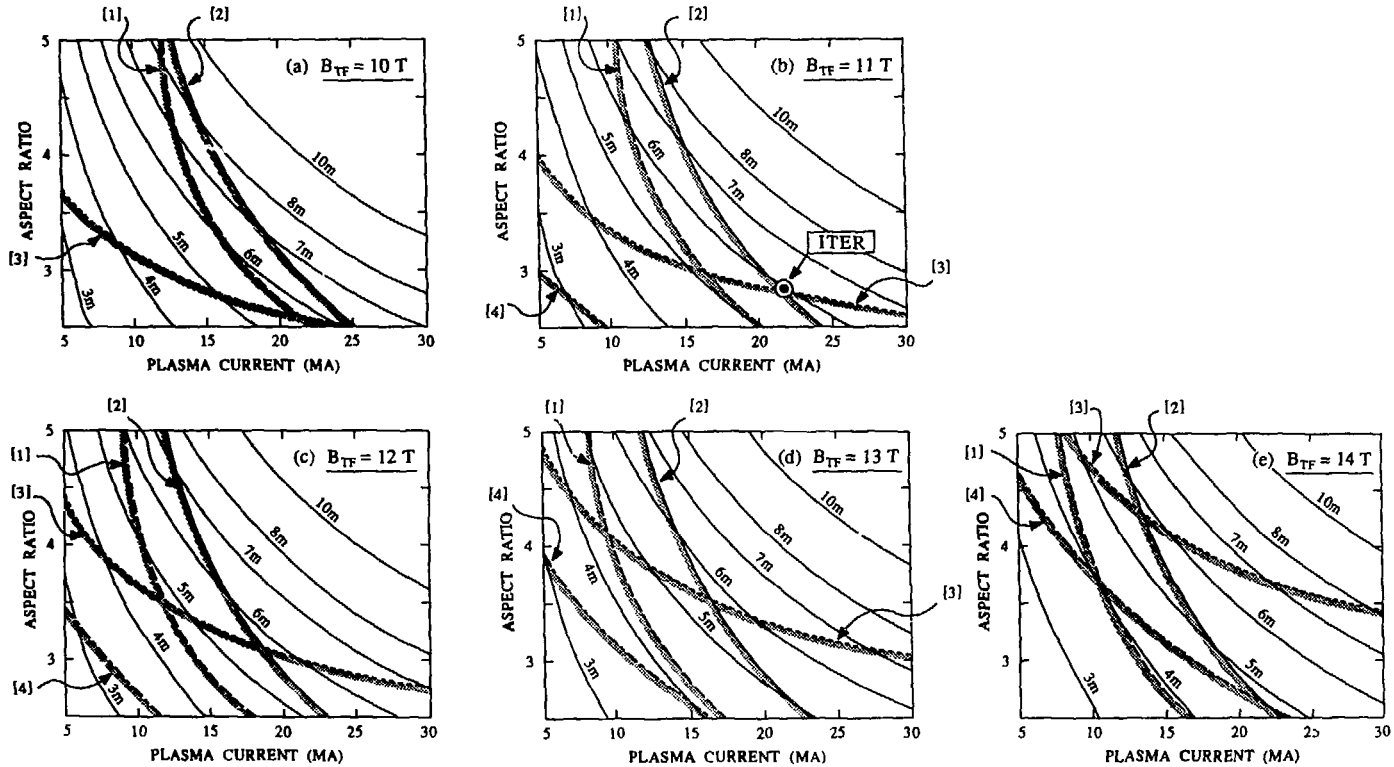

Fig. III-2(a)-(e). Two-dimensional I-A representation of I-A-B_{tf} space for B_{tf} in the range 10-14T. Contours of major radius for ITER-like machines are shown. Constraint boundaries for inductive ignited operation at a neutron wall loading of 1MW/m^2 are: [1] beta limit (g_{Troyon}=2.5), [2] confinement limit ($H_{ITER\text{-}power}$=2.0), [3] inductive burn time (t_{burn}=400s/200s for li_3=0.65/0.75), and [4] TF radial build.

time less than 400s for li_3=0.65 (or less than ~200s for li_3=0.75). For even smaller machines located on the TF radial build constraint boundary, the hole within the TF coil inner legs has completely closed leaving no room for a central solenoid. These machines will still retain some volt-second capability because of the outer PF coils but this would be significantly less than that required to provide for the inductive and resistive volt-seconds consumed during current ramp-up. Such machines could, in principle, be considered as minimum size devices which could operate with non-inductive current-drive**. For machines located inside the TF build constraint boundary, it would be impossible to produce the required value of the peak field (B_{tf}) at the coil and, consequently, such machines would only be viable by permitting B_{tf} (and thus B and q_ψ) to decrease.

III.3. SELECTION OF THE ITER BASELINE

It is important to appreciate from Fig. III-1 and III-2 that three datum parameters are required to perform confinement and design tradeoff studies for tokamaks, i.e. I, A and B_{tf}. The philosophy of trading current for aspect ratio alone without considering toroidal field at the coil results in an incomplete evaluation. Furthermore, from Fig. III-2, we see that at lower values of B_{tf}, requirements of reasonable size/cost favor low aspect ratio machines due to the form of the confinement constraint boundary at constant H. The converse is true at higher values of B_{tf}, i.e. high aspect ratio machines are favored cost-wise, this time due to the inductive burn time constraint boundary. Of course, if the inductive constraint were to be dropped in, say, the design selection of a purely current-driven machine, then low aspect ratio designs would be available at any toroidal field. However, optimization of current-driven performance tends to direct us to back to higher aspect ratio machines because of the larger bootstrap current fractions available [3]; this will be discussed further in Chapter VI.

The reason for the selection of the present ITER baseline is shown in Fig III-3, where we repeat the I-A plot from Fig III-2(b) at B_{tf}=11T. Here, we include the H=2.0 confinement constraint boundaries for all energy-confinement scalings in vogue during earlier phases of the project when the baseline was selected. Note that the scalings tend to converge at the ITER design point at low aspect ratio and high plasma current and selection of this point minimizes the uncertainties in their prediction. By contrast, at higher aspect ratios and lower currents, the scalings diverge in their prediction of τ_E. In particular, scalings such as *Goldston*, *T-10* , and the new *ITER H-mode* scaling (see Chapter VI) predict a strong impact of trading I for A, *ITER Power* predicts a moderate impact, while *Rebut-Lallia*, *Shimomura-Odajima* and *ITER Offset-linear* predict a weak effect and require considerably larger machines at high aspect ratio to obtain the same confinement margin over L-mode.

Accordingly, ITER is located at the confluence of these various scalings at low aspect ratio together with the inductive burn time constraint. Note that the combined constraints of confinement and burn time determined the ITER design in parameter

** In practice, however, such current-driven machines will probably have some need for poloidal currents on the inboard for plasma shaping purposes.

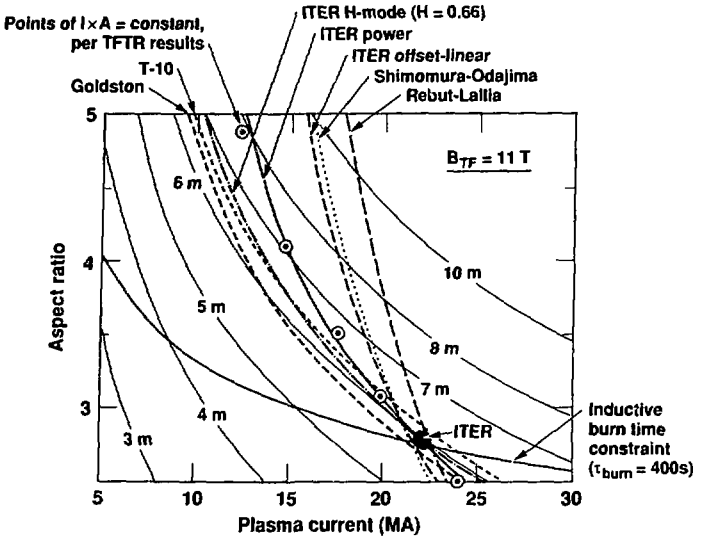

*Fig. III-3. I-A space for ITER-like machines at B_{tf}= 11T and a more detailed version of Fig. III-2(b) above. Contours are shown for various energy-confinement L-mode scalings at an enhancement factor over L-mode of H = 2. The contour for the recent ITER H-mode scaling has an effective "H" factor of 0.66 as required for the ITER baseline. The individual points are for I*A = constant per TFTR results of Grisham et al. and are discussed in Chapter VI; note the excellent agreement with ITER Power scaling.*

space and that, for ignited operation at 1MW/m^2, the beta limit (i.e. a Troyon coefficient of 2.5) is not a limiting constraint. As we will see in Chapter V, the same is not necessarily true for steady-state operation where beta limits can be a major constraint on performance when reasonable wall loadings are required.

REFERENCES

[1] W.R.SPEARS, T.MIZOGUCHI, L.J.PERKINS, S.PUTVINSKI, C.A.FLANAGAN, *Design Point Selection for an Ignited ITER*, ITER Document Series No. 5, IAEA, Vienna, (1989)

[2] N.A.UCKAN, "ITER Physics Design Guidelines" in *ITER Design Information Document*, C.A.Flanagan (Ed.), ITER team, Garching, IAEA, Vienna (to be published 1990).

[3] L.J.PERKINS, J.D.GALAMBOS, J.R.GILLELAND, et al., *The International Thermonuclear Reactor at High Aspect Ratio*, Lawrence Livermore National Laboratory, UCRL-ID-104178, (1990)

IV. ITER INDUCTIVE IGNITED PERFORMANCE AND SENSITIVITIES

IV.1. INTRODUCTION

Systems and design space analysis is performed for ITER under the physics guidelines of Ref 1. However, such guidelines provide only the present best estimates for constraints such as beta limits, impurity specifications, profiles, e.t.c. and are necessarily subject to the uncertainties inherent in the present tokamak physics database. In this chapter, we examine the inductive, ignited performance of ITER and assess the sensitivity of its performance to the following :

- Thermal alpha particle fraction
- Impurity content and Zeff
- Fusion power and neutron wall loading
- Driven operation at high and low Q
- Density profile
- Plasma current

IV.2. NOMINAL ITER PERFORMANCE UNDER INDUCTIVE, IGNITED OPERATION

Table IV-1 shows the major characteristics of the ITER baseline design point and illustrates its nominal performance under inductive, ignited operation ($Q=\infty$). Nominal physics specifications include a thermal alpha particle fraction of 10%, baseline impurity specifications, a neutron wall load of $1MW/m^2$, a density profile exponent of $\alpha_n=0.5$ (where $n(r)=n(0)\{1-(r/a)^2\}^{\alpha n}$), and a plasma current of 22MA. The values in parentheses in the table show the performance at the beta limit, i.e. a Troyon coefficient of 2.5 yielding a wall loading of $\sim 1.6MW/m^2$.

Required enhancement factors, H, for the common L-mode energy confinement scalings are seen to be all about 2.0, a consequence of the selection of the design point (See Chapter III). The new ITER H-mode scaling (see Chapter VI for discussion) predicts a required enhancement factor of only 0.66. ITER ignition performance under this scaling looks rather beneficial but we should appreciate that no allowance is made for ELMs, a feature which might be expected to increase the H factor by ~20% or more.

The nominal burn time under inductive operation is seen to be ~400s for an internal inductance of $li_3=0.65$ and ~300s for $li_3=0.75$. However, given the rather large uncertainties in both the volt-seconds supplied by the PF system and that consumed during ramp-up to 22MA, these resulting burn time numbers have large uncertainties. If current-driven ramp-up assist could be employed to offset some of the start-up volt-seconds, the burn time can be extended by ~100s per 10Vs saved. For example, if 50Vs out of the total start-up requirements of 280Vs could be offset, a burn time of ~830Vs would result. Similarly, if all the resistive volt-seconds (~76Vs) were saved, a burn time of ~1060s would result.

TABLE IV-1. ITER BASELINE: NOMINAL PERFORMANCE UNDER INDUCTIVE, IGNITED OPERATION

(Operation at the beta limit is shown in parentheses)

Characteristics		
Aspect ratio	2.79	
Major/minor radius (m)	6.0/2.15	
Plasma current (MA)	22.0	
Toroidal field, axis/coil-peak (T)	4.85/11.1	
Elongation/triangularity (95%, at li_3=0.65)	1.98/0.383	
q_ψ(95%) at li_3=0.65	3.01	
Ignition Performance		
Neutron wall loading (MW/m^2)	1.0	(1.6[1])
Fusion power (MW)	1080	(1720)
β/β_p	0.042/0.62	(0.053/0.78)
Troyon beta coefficient (%)	1.99	(2.5[1])
Average electron temperature, n_e-weighted (keV)	10.0	
Average electron density / density limit (10^{20} m^{-3})	1.22/1.96	(1.53/2.69)
Zeff	1.66	(1.60)
Plasma thermal stored energy, thermal/total[2] (GJ)	0.58/0.64	(0.73/0.80)
Plasma inductive stored energy at li_3=0.65/0.75 (GJ)	2.24/2.36	
Divertor peak heat load[3] (MW/m^2)	16.5	(35.5)
Required energy confinement time (s)	3.82	(2.87)
$n_{DT}(0).\tau_E.T_i(0)$ (10^{21}s keV m^{-3})	8.46	(7.99)
Required H-mode enhancement over the following scaling predictions: -		
ITER power (L-mode)	2.0	(1.9)
ITER offset (L-mode)	2.0	(1.6)
Shimomura Odajima	1.9	(1.6)
Rebut-Lallia	2.1	(1.6)
Goldston	1.9	(1.8)
T-10	2.1	(2.0)
ITER H-mode	0.66[4]	
Inductive Performance for li_3=0.65		
Plasma inductance (μH)	9.26	
Volt-sec capability (Vs)	326	
Volt-sec for burn (Vs)	46.1	
Loop voltage (V)	0.115	
Burn time (s)	400	

1. At beta limit (max permitted Troyon factor=2.5% for ignited operation [1])
2. i.e, including fast alpha pressure
3. Systems code models benchmarked to 2D runs.Includes safety/peaking factors of 4.1
4. No allowance for ELMs; might be expected to increase the req'd enhancement factor by ~1.25

No current-drive power is applied for the case in Table IV-1. Accordingly, current profiles will evolve in a global skin time. Auxiliary power will, however, be applied for burn control purposes and is discussed further in Section IV-6 below. This power (~25MW nominal) might also provide some current-profile control.

IV.3. SENSITIVITY TO THERMAL ALPHA FRACTION

Table IV-2 shows the sensitivity of the ITER inductive, ignited performance as a function of the equilibrium thermal alpha concentration f_α in the plasma. All other physics specifications are maintained at their baseline values [1]. Note that as neutron wall load is maintained at 1MW/m^2, the DT density remains fixed. The values in the third column correspond to the nominal baseline with f_α=10%. The values in the first column (i.e. f_α=0) would be representative of the situation for the first few seconds after at the start of burn before the equilibrium alpha fraction is established.

Note from the table that, as the alpha fraction increases from zero to 20%, the Zeff increases only slightly. With constant neutron wall loading (i.e constant n_{DT}) this is a consequence of both the low atomic number of helium and the increasing electron density which dilutes impurity fractions under our present impurity models. Note, however, that the confinement requirements in terms of confinement time and required enhancement (H) over L-mode scaling increase strongly. The reason for this behavior is due to the effect of increasing density on the plasma power balance:

$$P_{alpha} + P_{aux} + P_{ohmic} = W_{thermal}/\tau_E + P_{radiation}$$

where P_{alpha}, P_{aux}, P_{ohmic} are, respectively, the fusion alpha power, external axiliary power (zero for ignition) and ohmic powers (small, ~2MW, at these conditions), $W_{thermal}$ is the plasma thermal stored energy, and $P_{radiation}$ is the core radiation losses (bremmstrahlung, synchrotron, and impurity line). τ_E is the required energy confinement time and is expressed in terms of an enhancement factor times an L-mode scaling as $\tau_E = H^*\tau_{E\text{-scaling}}$.

At constant neutron wall load (i.e constant n_{DT}), the electron density increases strongly with increasing f_α. Accordingly, both the plasma thermal stored energy $W_{thermal}$ and radiation (mainly bremmstrahlung ~n_e^2*Zeff) increase strongly with a consequent deleterious increase in the confinement H factors required for power balance.

Note also that above an alpha particle fraction of ~24%, the radiation losses exceed the fusion alpha power, irrespective of the confinement (conduction) losses and no power balance solution is possible. In fact, as shown, a density limit due to radiative collapse of the plasma edge might be expected to occur at f_α values in the vicinity of 15-20%. Although these limits have appreciable uncertainty (~factor of two) they might be allieviated, at constant fusion power, by increasing the temperature.

An interesting feature of higher alpha fractions is that the increasing plasma density ameliorates somewhat the divertor heat fluxes[1]. An alternative way to reduce divertor heat loads is through controlled seeding of medium-z impurities and the effect on confinement requirements would be less severe. This technique is discussed

---

[1] The systems code employs a divertor module based on the Harrison-Kukushkin model, benchmarked to 2D runs. The edge density is assumed to scale with the average core density as n_e/3.5. Peaking and safety factors of 2.75 (physics) and 1.5 (engineering) -- i.e a total multiplier of 4.1 -- are applied to the peak heat loads in the tables to cover uncertainties

TABLE IV-2. SENSITIVITY OF ITER INDUCTIVE, IGNITED PERFORMANCE TO THERMAL ALPHA PARTICLE FRACTION

	THERMAL PARTICLE ALPHA FRACTION					
	0%	**5%**	**10%** **	**15%**	**20%**	**≥ 24%**
Zeff	1.56	1.61	1.66	1.72	1.79	
$n_e/n_{e\ limit}$ (10^{20} m^{-3})	0.97/2.21	1.08/2.11	1.22/1.96	1.41/1.73	1.66/1.32	No solution--
$W_{thermal}$ (MJ)	482	525	580	652	750	radiation powers
β(%)	3.67	3.90	4.20	4.61	5.21	(core + edge) exceed
g_{Troyon}(%)	1.74	1.85	1.99	2.19	2.47	alpha power irrespective
P_{rad}/P_{rad} (MW) -core -edge	43/29	53/31	67/35	86/40	115/47	of confinement properties
τ_E (s)	2.75	3.18	3.82	4.93	7.31	
$n_{DT}(0)\,\tau_E\,T_i(0)$ (10^{21} s.keV.m^{-3})	6.09	7.03	8.46	10.9	16.2	
H_{ITER} / H_{ITER} -power -offset	1.6/1.5	1.7/1.7	2.0/2.0	2.4/2.4	3.1/3.3	
t_{burn} (s)	394	396	400	409	427	
$H_{divertor}$ (MW/m^2)*	28	22.7	16.5	9.9	4.2	

* Includes safety factors of 2.75 (physics) and 1.5 (engineering) ** Reference baseline: f_α = 10%

further in Chapter V. Also in Table IV-2, inductive burn times are seen to increase slightly due to increasing beta poloidal and, therefore, a greater volt-seconds contribution from the vertical field coils.

IV.4. SENSITIVITY TO IMPURITIES AND Zeff

Table IV-3 shows the sensitivity of ITER inductive, ignited performance to impurity concentration and Zeff. The baseline impurity specifications are a function of n_e [1]. Consequently, we simply apply a multiplier on these concentrations in the range zero to 2.5. The values in the second column corresponding to the nominal baseline performance with a multiplier of unity (yielding Zeff=1.66). All other physics specifications are maintained at their baseline values

By contrast to increasing alpha fraction in Sect. IV.3 above, increasing the higher-z impurity content causes only a modest increase in electron density but an appreciable increase in Zeff. For a factor of 2.5 times the baseline impurity specifications (causing an increase of Zeff from the nominal baseline of 1.66 to 2.25), ITER would require H-mode enhancement factors of about 3 to ignite due to the large radiation losses. Density limits would, however, be reached at only ~2 times our nominal specifications. Above a Zeff of 2.25, radiation losses exceed alpha heating power and power balance cannot be maintained irrespective of the confinement (conduction) performance. Also by contrast to the behavior under increasing alpha fractions above, the inductive burn time is seen to decrease with increasing Zeff, a consequence of the fact that the increasing volt-seconds from the β_p-dependent vertical field is unable to compensate for the increasing loop voltage.

IV.5. SENSITIVITY TO FUSION POWER AND NEUTRON WALL LOADING

Nominal ignited performance of ITER was assessed above at an average neutron wall load of 1MW/m^2 and corresponding to a fusion power of 1080MW. Table IV-4 shows the ITER inductive, ignited performance as a function of wall load in the range 0.3 to 3 MW/m^2 (i.e. fusion power in the range 320 to 3240MW) with the third column showing the nominal reference performance. All other physics specifications are maintained at their baseline values.

The first column in the table, 0.3MW/m^2, is the lowest wall loading at which operation can be sustained without externally-applied auxiliary power, i.e. below this fusion power the radiation losses exceed the internal alpha power. However, as shown, operation at a minimum wall load of ~0.4MW/m^2 (or equivalent total heating power of $P_\alpha + P_{aux}$) would anyway be required to operate below the density limit. Such behavior warrants careful attention both to start-up scenarios and operation at fractional power

As the wall loading increases, there is a strong improvement in the confinement requirements under the *ITER Offset-linear* scaling while only a modest increase in the *ITER Power* scaling. This rather disparate behavior is typical of the two groups of scaling relations. Scalings of the offset-linear type show considerable improvement in

TABLE IV-3. SENSITIVITY OF ITER INDUCTIVE, IGNITED PERFORMANCE TO IMPURITY CONCENTRATION AND Zeff

	MULTIPLIER ON BASELINE IMPURITY SPECIFICATIONS				
	0	**x1.0****	**x1.84**	**x2.50**	**>x2.5**
Zeff	1.20	1.66	2.0	2.25	>2.25
$n_e/n_{e\ limit}(10^{20}\ m^{-3})$	1.11/2.47	1.22/1.96	1.32/1.32	1.42/0.08	No solution--
$W_{thermal}$ (MJ)	544	580	613	642	radiation
ß(%)	4.01	4.20	4.38	4.55	powers (core + edge) exceed
g_{Troyon}(%)	1.	1.99	2.08	2.16	alpha power
P_{rad}/P_{rad} (MW) -core -edge	36/<10	67/35	97/67	124/95	irrespective of confinement properties
τ_E (s)	2.99	3.82	5.03	6.76	
$n_{DT}(0)\ \tau_E\ T_i(0)\ (10^{21} s.keV.m^{-3})$	6.62	8.46	11.1	15.0	
H_{ITER} / H_{ITER} -power -offset	1.7/1.6	2.0/2.0	2.3/2.5	2.8/3.0	
t_{burn} (s)	538	400	340	310	
$H_{divertor}$ (MW/m²)*	36	16.5	4.7	~0	

* Includes safety factors of 2.75 (physics) and 1.5 (engineering)

** Reference baseline: $f_C = 1.04\%$, $f_O = 0.1\%$, $f_{Fe} = 0.014\%$ ($f_\alpha = 10\%$), => Zeff = 1.66

TABLE IV-4. SENSITIVITY OF ITER INDUCTIVE, IGNITED PERFORMANCE TO NEUTRON LOAD AND FUSION POWER

	NEUTRON WALL LOAD (MW/m^2)					
	0.3+	0.5	1.0**	1.5	2.0	3.0
Fusion power (MW)	320	540	1080	1620	2160	3240
$n_e/n_{e\ limit}(10^{20}\ m^{-3})$	0.70/0.46	0.88/1.08	1.22/1.96	1.48/2.59	1.71/3.12	2.09/4.0
Zeff	2.03	1.82	1.66	1.61	1.58	1.56
$W_{thermal}$ (MJ)	329	416	580	707	814	996
ß(%)	2.36	3.00	4.20	5.13	5.91	7.23
g_{Troyon}(%)	1.12	1.42	1.99	2.43	2.80	3.43
P_{rad}/P_{rad} (MW) -core -edge	35/26	44/28	67/35	88/41	108/46	148/56
τ_E (s)	9.90	6.26	3.82	2.97	2.50	1.98
$n_{DT}(0)\ \tau_E\ T_i(0)\ (10^{21}s.keV.m^{-3})$	12.0	9.79	8.46	8.04	7.82	7.59
H_{ITER} / H_{ITER} -power -offset	2.6/3.6	2.2/2.8	2.0/2.0	1.9/1.6	1.8/1.4	1.8/1.2
t_{burn} (s)	251	307	400	470	532	652
$H_{divertor}\ (MW/m^2)$*	<1	3.7	16.5	32.5	50.0	88.6

* Includes safety factors of 2.75 (physics) and 1.5 (engineering) ** Reference baseline: (1 MW/m^2)

\+ Minimum wall load sustainable by ignited plasma, ie sustainable with alpha heating only

TABLE IV-5. SENSITIVITY OF ITER INDUCTIVE, IGNITED PERFORMANCE TO DRIVEN OPERATION AT HIGH AND LOW Q

	$Q = P_{fusion}/P_{aux}$				
	$Q = \infty$ **	Q = 40	Q = 20	Q = 10	Q = 5
Auxiliary power, P_{aux} (MW)	0	27	54	108	216
$n_e(10^{20}\ m^{-3})$	1.22	<-	<-	<-	<-
$\beta(\%)$	4.20	<-	<-	<-	<-
$g_{Troyon}(\%)$	1.99	<-	<-	<-	<-
τ_E (s)	3.82	3.25	2.82	2.23	1.58
$n_{DT}(0)\,\tau_E\,T_i(0)\ (10^{21}s.keV.m^{-3})$	8.46	7.18	6.24	4.94	3.49
H_{ITER} / H_{ITER} -power -offset	2.0/2.0	1.8/1.7	1.7/1.5	1.5/1.3	1.3/0.9
$H_{divertor}\ (MW/m^2)$*	16.5	22.9	29.9	45.0	77.6

* Includes safety factors of 2.75 (physics) and 1.5 (engineering)

** Reference baseline: $Q = \infty$

confinement capability for increasing fusion power, while power laws, with their ~$P^{0.5}$ dependence, show much smaller increases. The power laws are virtually insensitive to fusion powers at higher values of the latter.

The increase of confinement capability with power is, of course, bought at the expense of divertor operation where an increase in fusion power from 1 to 3MW/m2 results in a highly non-linear increase in peak divertor heat fluxes from ~16MW/m^2 to ~90MW/m^2. Moreover, the Troyon beta limit of 2.5 would, in any case, be reached at a neutron wall load of ~1.6MW/m^2 (for operation at this point see Table IV-1). An appreciable increase in inductive burn time with fusion power is also seen for the reasons discussed above.

IV.6. SENSITIVITY TO DRIVEN OPERATION AT HIGH AND LOW Q

One way to offset uncertainties in energy confinement is to supplement the internal alpha heating with external auxiliary power and, therefore, run sub-ignited at a finite Q ($Q=P_{fusion}/P_{aux}$). In fact, stability requirements for ITER in ignited mode will necessitate sub-ignited operation for control purposes [2,3]. Accordingly, Table V-5 shows ITER inductive operation with Q in the range ∞ (i.e true ignition) down to 5 where requirements on τ_E is reduced as Paux increases (i.e Q decreases). All other physics specifications are maintained at their baseline values

Required confinement enhancement factors are seen to decrease strongly for decreasing Q, i.e. for increasing auxiliary power. Again we see the different trend of the offset-linear scalings relative to the power laws. Under the former, for example, operation at a Q of 5 results in the requirement for less than L-mode confinement, while the *ITER Power* scaling still requires ~1.3 times L-mode. Operation at Q=20 decreases the ignition confinement requirements from H~2 to H~1.5-1.7.

The penalty of lower-Q operation is two-fold: First, considerable external power is required, e.g. 54MW for Q=20 and (an impossibly large) 216MW for Q=5. Second, the effect of this additional power is a highly non-linear increase in the peak divertor heat flux, e.g. factor of ~2 for Q=20 operation and factor of ~5 for Q=5 operation.

As mentioned above, our ignited or near-ignited operating points at these low temperatures (~10keV) and high density (~1.2 $10^{20}m^{-3}$) are susceptible to thermal instabilities that, if uncontrolled, can terminate an ITER discharge within 3–15 seconds by means of disruptions resulting from violations in beta or density limits. Furthermore, it is possible for these excursions to produce elevated fusion powers ($\geq$ 2000 MW), thus significantly increasing the possibility of damage to plasma facing components. Accordingly, our present baseline method for control of thermal instabilities in ITER is to operate in any case at a slightly sub-ignited operating point (Q~40-50) and provide feedback control of the equilibrium auxiliary power (~20-25MW) based on total neutron flux measurements [2,3]. The resulting increase in divertor heat fluxes can be offset by judicious choices of operating density and temperature.

Finally, as noted above, operation of Q~20 as distinct from true ignition, results in an appreciable improvement in confinement requirements. There are, therefore, two

TABLE IV-6. SENSITIVITY OF ITER INDUCTIVE, IGNITED PERFORMANCE TO DENSITY PROFILE

	DENSITY PROFILE EXPONENT α_n					
	-0.5	**0**	**0.5****	**1.0**	**1.5**	**3.0**
$n_{DT}(10^{20}\ m^{-3})$	1.05	0.969	0.885	0.816	0.753	0.671
$n_e/n_{e\ limit}(10^{20}\ m^{-3})$	1.44/1.83	1.33/1.91	1.22/1.96	1.13/2.0	1.05/2.04	0.939/2.07
<ß>(%)	4.99	4.59	4.20	3.88	3.59	3.21
ß(0)(%)	7.50	9.18	10.5	11.6	12.6	16.1
Ratio of ß(0)/<ß>	1.5	2.0	2.5	3	3.5	5.0
$W_{thermal}$ (MJ)	692	637	580	536	496	447
P_{rad}/P_{rad} (MW) -core -edge	77/40	71/37	67/35	64/33	61/31	61/29
Zeff	1.61	1.63	1.66	1.69	1.72	1.78
g_{Troyon}(%)	2.36	2.17	1.99	1.84	1.70	1.52
τ_E (s)	4.88	4.29	3.82	3.47	3.15	2.82
H_{ITER} / H_{ITER} -power -offset	2.5/2.6	2.2/2.6	2.0/2.0	1.8/1.8	1.7/1.6	1.5/1.4
t_{burn} (s)	460	430	400	376	354	324
$H_{divertor}$ (MW/m^2)*	11.6	14.3	16.5	18.6	21.0	23.2

* Includes safety factors of 2.75 (physics) and 1.5 (engineering) ** Reference baseline (α_n=0.5)

ways in which this can be exploited: It can be used as a margin against uncertainty in either confinement capability or the other nominal physics specifications employed in evaluating the baseline design. Alternatively, if we were certain of confinement capabilities of ~2 times L-mode and only demand Q=20 operation, we can then consider a smaller, lower current machine. For example, relative to the R=6m, I=22MA ITER design which has Q=∞ at H~2, we could obtain a machine at R~5m, I~15MA which has Q=20, again at H~2. Injected powers for this machine at 1MW/m^2 wall load (fusion power of only ~750MW) would be ~38MW..

IV.7. SENSITIVITY TO DENSITY PROFILE

Table IV-6 shows the inductive, ignited performance as a function of the density profile exponent α_n, where the density profile is expressed as $n(r)=n(o)\{1-(r/a)^2\}^{\alpha n}$. Profiles range from hollow (α_n=-0.5), flat (α_n=0) to peaked (α_n~1-3). The nominal baseline with its rather flat profile (α_n=0.5) is shown in column 3. ITER studies of density profile evolution under H-mode operation and with present fueling methods (edge gas puffing or relatively low velocity pellets) indicate rather flat profiles will result [4]. Hollow profiles may occur under strong edge fueling. More peaked profiles would result from stronger anomalous inward-pinching of fuel, higher pellet injection velocities, or novel central fueling techniques such as compact toroid injection [5].

From the table, we see that the significant feature of increasing density profile peaking is a strong increase in the peak to average beta. Maintenance of a neutron wall load of 1MW/m^2 requires that the volume integral of $n(r)^2.\langle\sigma v(r)\rangle$ be constant. Note that fusion power production scales as n^2 while the thermal stored energy is only proportional to n. Accordingly, with our peaked temperature profile specifications (α_T=1.0) and a constant fusion power, we see a corresponding decrease in the required average DT density, the average electron density and thermal stored energy as α_n increases. Radiation powers decrease only slowly due to the competing effect of increasing Zeff with reducing n_e. The net result for a constant wall load is a marked reduction in required energy confinement time and, therefore, in the required H-factors.

We also note that the required Troyon coefficient (expressing the average beta condition) falls appreciably at higher values of α_n, a fortunate trend as pressure profiles become markedly more peaked (i.e, average beta decreases while peak beta increases). Accordingly, while MHD stability may still be maintainable, a consistent MHD analysis would be required to determine the limiting beta values. As above, burn times decrease because less V-s are available at the poloidal beta. Divertor heat loads increase by virtue of decreasing average core density (the edge density is assumed to be a constant fraction of edge density); however, this characteristic might perhaps be ameliorated by separate control of edge density via gas puffing.

IV.8. SENSITIVITY TO PLASMA CURRENT

ITER has sufficient volt-seconds capability for inductive ramp-up to its reference plasma current of 22MA and an inductive burn length of ~400s at li_3=0.65 (~300s at li_3=0.75) -- see Table IV-1 above. Table IV-7 illustrates the sensitivity of

TABLE IV-7. SENSITIVITY OF ITER INDUCTIVE, IGNITED PERFORMANCE TO PLASMA CURRENT

	PLASMA CURRENT				
	15 MA	20 MA	22 MA**	25 MA	28 MA
q_ψ(95%)	4.41	3.31	3.01	2.65	2.36
g_{Troyon}(%)	2.92	2.19	1.99	1.75	1.56
β_p	1.34	0.751	0.621	0.481	0.383
τ_E(s)	3.86	3.84	3.82	3.80	3.78
H_{ITER} / H_{ITER} -power -offset	2.8/2.5	2.2/2.	2.0/2.0	1.8/1.8	1.6/1.7
t_{burn} (s)	1930	661	400	115	<0+
$H_{divertor}$ (MW/m^2)	13.7	15.7	16.5	17.7	18.8

* Includes safety factors of 2.75 (physics) and 1.5 (engineering)

** Reference baseline (22 MA)

+ No burn possible under pure inductive operation. Burn time may be extended by LH ramp-up, i.e. for 20 Vs saved, t_{burn}=40s; for all resistive Vs saved during startup (94.4 Vs), t_{burn}=510 s.

the inductive, ignited performance as a function of current in the range 15 to 28MA. All other parameters are retained at their reference values. Column 3 shows the nominal reference case.

Given the large dependence of all confinement scalings to plasma current, we see a large reduction in the required energy confinement enhancement factors for increasing current for an essentially constant τ_E requirement (the small change in required τ_E with plasma current is due to the change in ohmic power). At 15MA, ~2.5-2.8 times L-mode would be required while the Troyon beta limit of 2.5 would in any case be reached at I~17MA. At 28MA, the required enhancement factors are only ~1.6-1.7 and would be as low as ~1.2 for ignition at the start of burn where the thermal alpha particle fraction is essentially zero.

Two benefits of reducing plasma current can, however, be seen from Table IV-7. First, there is a large increase in burn time from the baseline of 400s at 22MA to almost 2000s at 15MA but, by contrast, no burn volt-seconds available at 28MA due to the large inductive consumption (LI) during current ramp· as described in the table, use of LH current assist during ramp-up may provide for a finite burn time at these higher currents. Second, the divertor peak heat loads are reduced due, in part, to longer field-line connection lengths. A caveat, however, is that lower plasma currents result in smaller values of the field line grazing angle at the divertor plate. Just how small this can reasonably be due to alignment tolerances is still under consideration.

REFERENCES

[1] N.A.UCKAN, "ITER Physics Design Guidelines" in *ITER Design Information Document*, C.A.Flanagan (Ed.), ITER team, Garching, to be published by the IAEA (1990). See also Sect. 1 and 2 in Ref. 2

[2] "Burning Plasmas: Properties and Control", Sect. 2.4.4 in *ITER Physics* , IAEA ITER Documentation Series No.21, IAEA Vienna, to be published (1990)

[3] L.J.PERKINS, et al, *US Studies in ITER Burn Control* --Final Report, Lawrence Livermore National Laboratory, to be published 1990

[4] "Fueling", Sect. 8 in *ITER Physics* , IAEA ITER Documentation Series No.21, IAEA Vienna, to be published (1990)*ITER Physics Basis*, IAEA, Vienna, to be published (1990)

[5] L.J.PERKINS, S.K.HO, and J.H.HAMMER, "Deep Penetration Fueling of Reactor-Grade Tokamak Plasmas by Accelerated Compact Toroids", *Nucl. Fusion*, **28**, 1365 (1988)

V. TECHNOLOGY PHASE OPERATION: RATIONALE, METHODOLOGY AND OPTIMIZATION

V.1 INTRODUCTION

In this section, we investigate operating scenarios for the ITER device to satisfy the steady-state and technology testing objectives of the ITER mission (the technology phase). Ideally, a pure steady-state operational mode should be used for the technology phase accomplished by non-inductive current drive means. This technique is hindered by divertor operation considerations. Since noninductive current drive efficiencies are low compared to inductive current drive, large injection power levels (>100 MW) are needed to maintain steady-state plasma current levels. This additional power and the low density associated with efficient current-driven operation considerably exacerbate divertor operation.

Our present understanding of the divertor problem indicates that steady-state operation will be limited to wall loads below 1 MW/m^2, with Q near 5-6. If the divertor conditions are not as severe as presently envisioned, operation at higher wall loads will be possible. Given the problems associated with pure steady-state operation, recourse is necessary to *hybrid* operation, a combination of inductive and noninductive current drive at higher plasma densities to provide long pulses with reduced injected power requirements. With the hybrid mode, we show attractive scenarios at wall loads up to 1 MW/m^2, with Q near 10 and with extended burn times >1000 s. Operational parameters for a range of steady-state and hybrid scenarios are presented in Section V-3.

A key ingredient of the plasma modeling used here is the use of medium-Z (for example Fe) impurity seeding to enhance the radiation losses. This concept has been previously identified as a possible method of controlling the divertor power loads (Refs. 3-5) and initial modeling for ITER has now commenced [15]. The compatibility with other constraints such as density limits and PPC conditions requires assessment. Despite the detrimental effects of impurity seeding on the global plasma power balance, we will show that the enhanced radiation greatly expands the potential operational space, due to the reduction of the power load flowing to the divertor plates. Possible problems are either a deposition of non-recycling medium-z impurities (e.g Fe) on the divertor plates or sputtering from recycling medium-z impurities (e.g Fe). Also we show results for cases which do not include any divertor constraints to demonstrate the effect of the divertor requirements on the technology phase performance. These examples represent the upper bound of possible performance, then being constrained only by the major plasma limits.

This chapter is organized as follows: In Section V.2 the modeling procedure is described. In Section V.3 we present nominal operating points for steady-state and hybrid operation optimized with the U.S TETRA systems code, and show the impact of some of the primary modelling assumptions. In section V.4 we present a broader set of sensitivity studies for the technology phase operation. In section V.5 some complementary studies using the Japanese TRESCODE are presented.

V.2 MODEL

The TETRA systems code [6] is used to perform the trade studies discussed here. Since we are considering a fixed device configuration, few of the "engineering" constraints in the code are employed and emphasis is primarily on the physics operational constraints The physics model is a profile averaged global treatment which generally follows the prescriptions discussed in Ref. 7. The nominal set of constraints considered in the technology phase modeling are :

plasma beta $\leq$ the Troyon limit,

energy confinement (H) factors ≤ 2.2 (ITER scalings),

plasma density $\leq$ density limit ,

current drive power $\leq$ 113 MW -- nominal max. supply (NB and LH in a 2/1 ratio),

divertor peak heat load ≤ 21 MW/m^2 (includes a factor of 4.1 to account for physics and engineering peaking factors)

edge $q_{95} \geq 3.0$ (i.e. I≤22MA)

iron impurity = base specification for unseeded cases
$\geq$ base specification for seeded cases ,

burn time $\geq$ 1000 s (hybrid cases only).

available flux must be sufficient to provide the initial plasma current and maintain the specified inductive fraction for the entire burn (hybrid cases only)

PF coil current densities $\leq$ allowable (function of field).

Although the basic device build is taken to be that of the reference ITER, a number of quantities are allowed to vary, subject to certain limitations. These include the plasma density and temperature, edge safety factor q_{95} (i.e. plasma current), the current drive power, the fraction of noninductive current drive (hybrid cases only), and additional iron (Fe) impurity concentration (seeded cases only). The solution method is iteration of the free variables to satisfy the above constraints and to also maximize a prescribed figure of merit. Unless otherwise stated, for steady-state we maximize the wall load, and for hybrid cases we maximize the fluence (product of the wall load and burn time). A standard optimization package [8] is used to perform the optimization. The TETRA code follows, in general, the physics guidelines of Ref. 7. Appendix V-A at the end of this chapter describes briefly other, mainly engineering-related, models employed in the following analyses. Full details are available in Ref. 9.

In the sensitivity studies to follow in this chapter, we will apply two new alternative physics models presently under consideration [12]; one for the plasma beta

$$
\begin{aligned}
g_{Troyon} = f_s [\ & 3.3856334706\ 10^1 && - 1.64436574637\ 10^2\ li_3 + \\
& 2.86100967657\ 10^2\ li_3^2 && - 2.12477156514\ 10^2\ li_3^3 + \\
& 5.76396735205\ 10^1\ li_3^4 && - 3.66476803251\ 10^1\ q_\psi + \\
& 1.8144578445\ 10^2\ li_3\ q_\psi && - 3.20938196681\ 10^2\ li_3^2\ q_\psi + \\
& 2.41868447689\ 10^2\ li_3^3\ q_\psi && - 6.65086560422\ 10^1\ li_3^4\ q_\psi + \\
& 1.34584893934\ 10^1\ q_\psi^2 && - 6.79456049307\ 10^1\ li_3\ q_\psi^2 + \\
& 1.22134225313\ 10^2\ li_3^2\ q_\psi^2 && - 9.32797750077\ 10^1\ li_3^3\ q_\psi^2 + \\
& 2.59454960183\ 10^1\ li_3^4\ q_\psi^2 && - 2.1099362792\ q_\psi^3 + \\
& 1.08543067109\ 10^1\ li_3\ q_\psi^3 && - 1.9806255199\ 10^1\ li_3^2\ q_\psi^3 + \\
& 1.53138218078\ 10^1\ li_3^3\ q_\psi^3 && - 4.30372169484\ li_3^4\ q_\psi^3 + \\
& 1.19035563668\ 10^{-1}\ q_\psi^4 && - 6.24869191608\ 10^{-1}\ li_3\ q_\psi^4 + \\
& 1.15770687802\ li_3^2\ q_\psi^4 && - 9.05907639827\ 10^{-1}\ li_3^3\ q_\psi^4 + \\
& 2.57101698394\ 10^{-1}\ li_3^4\ q_\psi^4\ ]
\end{aligned}
$$

Fig. V-1. Bi-quartic fit to the DIII-D data from Ref. 13 for the Troyon beta coefficient. A safety factor of $f_s = 0.9$ is employed for modelling applications. The range of validity of the fit is $2.25 \leq q_\psi \leq 5.5$, $0.5 \leq li_3 \leq 1.15$ and should be strictly adhered to. Due to roundoff errors, all significant figures should be used.

limit, and another for the bootstrap current fraction. Neither has been adopted by ITER at this point but we use them to indicate sensitivities to the resulting technology phase performance. These effects are especially important for technology phase operation, as the beta limit and noninductive plasma current drive can be dominant constraints in the operating space.

The alternative beta limit is based on recent DIII-D results [13] and the fitting is described in Ref 12.. These results show the beta limit expressed in terms of a Troyon coefficient, as a function of the internal plasma inductivity (li) and the edge safety factor (q). The D-III data is fit with the bi-quartic expression in li and q95, as shown in Fig. V-1, where a safety factor of 0.9 is employed to avoid operation right at the stability boundary.

The present ITER bootstrap current formulation was chosen to fit selected bootstrap current calculations by Fujisawa in 1989 [17], which were for a single plasma configuration. Recent work at Lawrence Livermore National Laboratory [14],

has applied the Hirshman bootstrap model, which accounts for finite aspect ratio and non-circular plasma effects. This model can yield bootstrap fraction ≥1.5 times that predicted by the nominal ITER scaling.

The systems code employs a divertor module based on the Harrison-Kukushkin model, benchmarked to 2D runs. The edge density is assumed to scale with the average core density as $n_e/3.5$. Peaking and safety factors of 2.75 (physics) and 1.5 (engineering) -- i.e a total multiplier of 4.1 -- are applied to the peak heat loads to obtained design constraint values.

V.3 NOMINAL TECHNOLOGY PHASE OPERATING SCENARIOS

A primary concern for long pulse operation is divertor survivability. Operation with high densities and low temperatures at the divertor plate is required to reduce the divertor peak heat flux, decrease erosion, increase He pumping, improve impurity retention by the divertor, and reduce the liklihood and severity of runaways during disruptions. However, this regime is opposite to that desired for good current drive efficiencies (low density, high temperature). Thus, results which satisfy the divertor constraints tend to be unattractive from the point of view of required injection power. The divertor models, however, are subject to large uncertainty. Therefore we do calculations in two ways, (1) cases which incorporate the divertor constraints (*divertor constrained*) and (2) cases which do not use the divertor constraints (*divertor unconstrained*). The divertor unconstrained cases are limited only by the main plasma constraints, and represent the best possible situation should improved divertor concepts emerge in the future. In this way we offer a range of possible operating points, with lower performance cases given by the divertor constrained cases, and upper performance bounds set by the divertor unconstrained cases.

V.3.1 Steady-State Operation

Demonstration of extended burn DT plasmas, with steady-state as an ultimate goal is part of the ITER objectives. Initially, in the physics phase, short pulse ignited conditions are expected to be demonstrated. Following this, steady-state experiments will begin, initially at low fusion powers and gradually going to higher wall loads. The ITER terms of Ref. state that the steady-state energy multiplication Q (= P_{fusion}/P_{inj}) should be greater than 5, and if steady-state is to be used to perform technology testing, wall loads of about 0.8-1 MW/m^2 are needed to adequately simulate a fusion reactor environment. In order to scope out the feasibility of attaining these steady-state goals, we investigate divertor constrained operation, and divertor unconstrained operation. We also look at the impact of seeding the plasma with additional impurity to enhance radiation losses, and lessen the divertor heat load. For steady-state, no volt-second constraints, or burn time limits are used.

Table V-1 shows parameters for several maximum steady-state wall load scenarios. The first two columns are divertor constrained, use the nominal physics models, and are for both impurity unseeded and seeded examples. Both cases are seen to be limited to low wall loads (0.27 MW/m^2 without seeding and 0.40 MW/m^2 with seeding), primarily due to the divertor heat load constraint. A common feature of

TABLE V-1. SENSITIVITY OF ITER PERFORMANCE UNDER STEADY-STATE, CURRENT-DRIVEN OPERATION

Case:	1	2**	3	4	5+	6
divrtr. constraint?	yes	yes	yes	yes	no	no
impurity seeded?	no	yes	no	yes	no	no
beta/BS model	present	present	alternative	alternative	present	alternative
wall load MW/m^2	0.27	0.42	0.31	0.65	0.71	1.85
P_{fus} (GW)	0.29	0.46	0.33	0.70	0.77	1.99
Q	2.6	4.1	3.7	6.2	6.8	17.7
P_{inj} (MW)	113*	113*	90	113*	113*	113*
I_p (MA)	10.2	14.5	12.2	16.8	18.9	15.9
q95	6.5	4.6	5.5*	4.0	3.5	4.2
I_{cd}/I_{bs}	53/47	67/33	48/52	46/54	70/30	28/72
l_i	0.65	0.65	0.64	0.62	0.65	0.77
H_{IP} / H_{IO}	2.2*/1.8	2.2*/2.0	2.2*/2.0	2.2*/1.9	2.1/1.8	2.1/13
f_{seed} (10^{-3})	0	1.3	0.0	1.50	0	0
Z_{eff}	1.9	3.0	2.1	2.9	2.2	1.6
n_e ($10^{20}m^{-3}$)	0.76	0.64	0.67	0.74	0.64	1.35
T_e (keV)	8.5	14	11	15	20	12
gTroyon	2.38	2.54	2.23*	2.71	3.0*	4.01*
beta/ beta limit(%)	2.3/2.9	3.6/4.2	2.6/2.6	4.4/4.5	5.5/5.5	6.1/6.1
$beta_{pol}$	1.59	1.20	1.26	1.11	1.08	1.73
P_{rad-c}/ P_{rad-e} (MW)	36/27	53/56	34/25	73/80	49/27	83/37
H_{div} (MW/m^2)	21*	21 *	21 *	21 *	66	123
T_{div} (ev)	41	35	44	23	>100	>100

* variable at a constraint bound. ** similar to case B.7 in ITER reference scenarios
+ similar to case B.6 in ITER reference scenarios

the technology phase results is that the edge q is typically above the lower bound of 3.0 (in these cases it is > 4.5). This reduces the plasma current level, which eases the injection power requirements. Alpha particle ripple losses are, however, an increasing concern Using the alternative beta and bootstrap formulation (as discussed in section V.2) has a positive effect on the attainable wall load, as indicated in columns 3-4 of Table V-1. (Note. that when the alternative beta formulation is used the plasma inductivity, l_i, is allowed to vary). The additional bootstrap fraction predicted with the alternative model allows for a 50% increase in the peak wall load, when seeding is permitted. However the maximum wall load is still below the level needed for technology testing.

For comparative purposes, the last two columns of Table V-1 show maximum wall-load cases for the divertor unconstrained examples. These examples may be possible should improved divertor concepts be realized, or if the present divertor modeling proves to be too pessimistic. As expected, without the divertor constraints,

impurity seeding goes to zero. The case with the alternative beta and bootstrap formulation has a very high attainable wall load of 1.85 MW/m^2. The divertor heat load is about 6 times the nominal level in this latter case - but should the predictions of the present models prove too severe, or alternative power exhaust concepts be developed, this case gives an indication that steady-state operation could be used to accomplish the technology testing mission. We note that all of the divertor constrained cases are confinement limited (i.e. the H-factor is at the upper bound of 2.2). The divertor unconstrained cases are limited by the beta limit.

Steady-state tests in the physics phase are possible at reduced wall loading, but for technology testing (where wall loads of ≥0.8MW/m^2 are required), an improved divertor concept is required. Alternatively, strong impurity seeding together with enhanced bootstrap currents and beta limits greater than g_{Troyon}=3 must be assumed. If neither of these scenarios obtain then technology testing would have to depend on hybrid operation.

V.3.2 *Hybrid Operation*

Under hybrid operation both noninductive and inductive current drive are employed. Compared to steady-state, hybrid operation has lower injection power requirements to maintain the plasma current and higher density operation is possible, which tends to relieve the divertor conditions. The penalty incurred with the hybrid operation is, of course, finite burn times. For these runs we use the volt-second constraints discussed in Appendix V-A, with a minimum burn time of 1000 s. The latter is needed for some tritium breeding blanket components to approach their steady-state operational parameters. We also require that ≥30% of the current is to be driven non-inductively to retain adequate current profile control.

Table V-2 shows the hybrid cases, for seeded and unseeded, with the present ITER modeling and with the alternative beta and bootstrap models. Cases shown here are for a maximum fluence (or burn-time times wall load) for all cases where the wall load is able to reach at least 0.8 MW/m^2, otherwise we show the maximum wall load scenarios. Both of the unseeded cases (1 and 3) are unable to reach a 0.8 MW/m^2 wall load. The primary limits met here are the energy confinement (H-factor) and the divertor heat load. Since the beta limit is not met in the unseeded example, use of the alternative beta and bootstrap models has little impact. When seeding is included, wall loads of 1 MW/m^2 and burn times of 3000 s are possible - with the present physics models (case 2). The hybrid cases that use seeding have wall loads more than twice that of the respective steady-state cases, and also have burn times of several thousand seconds. With alternative beta and bootstrap models, wall loads of 1.5 MW/m^2 and burn times of 6000 s are obtained (case 4). Both of the seeded hybrid cases are adequate for technology testing. Case 5 in Table 2 shows the maximum fluence of the nominal hybrid point (case 2) when the divertor heat load constraint is removed. The fluence is increased only about 33% when the divertor constraint is ignored. This sensitivity is less than that of the steady-state cases, and is due to the smaller fraction of current driven non-inductively.

The final case shown in Table V-2 is a case with the maximum confinement margin. Here we minimize the confinement H-factor, while restricting the wall load to be at least 0.8 MW/m^2. To permit a large confinement margin the plasma current is

TABLE V-2. SENSITIVITY OF ITER PERFORMANCE UNDER HYBRID OPERATION

Case	1	2**	3	4	5	6
Impurity seeded?	no	yes	no	yes	no	yes
beta/BS model	present	present	alternative	alternative	present	present
fig. of merit	wall load	fluence	wall load	fluence	fluence	H-factor
divertor constrained?	yes	yes	yes	yes	no	yes
wall load MW/m^2	0.40	1.01	0.41	1.51	0.94	0.8*
P_{fus} (GW)	0.43	1.09	0.44	1.69	1.01	0.86
Q	7.4	9.76	7.4	14.5	13.5	7.6
P_{inj} (MW)	58	113 *	58	113 *	75	113*
burn time (s)	1380	3100*	1320	6000 *	4400 *	1000*
I_p (MA)	17.3	15.6	16.4	17.7	16.3	19.2
q_{95}	3.9	4.3	4.1	3.8	4.5	3.5
$I_{cd}/I_{ind}/I_{bs}$(%)	30/51/19	30/32/38	30/35/35	30/14/56	30/34/36	30/50/20
l_i	0.65	0.65	0.83	0.65	0.65	0.65
H_{IP} / H_{IO}	2.1/2.2*	2.2*/1.7	2.2*/2.2*	2.2*/1.7	2.2*/1.8	1.8*/1.6
f_{seed} (10^{-3})	0	0.70	0	1.46	0.	0.9
Z_{eff}	2.2	2.1	2.2	2.6	1.8	2.3
n_e ($10^{20} m^{-3}$)	0.61	1.13	0.64	1.18	0.88	0.96
T_e (keV)	14.	11	13.	14.	14.	12.
g-Troyon	1.93	3.00*	2.00	3.43	3.0 *	2.25
beta/ beta limit(%)	3.2/5.0	4.5/4.5	3.2/6.1	5.8/5.9	4.7/4.7	4.2/5.5
$beta_{pol}$	0.76	1.35	0.84	1.31	1.26	0.82
P_{rad-c}/P_{rad-e} (MW)	36/24	100/103	36/25	142/165	51/28	85/91
H_{div} (MW/m^2)	21*	21*	21*	21*	21 *	21*
T_{div} (ev)	37	11	37	<10	83	13

* variable at a constraint bound ** similar to case B.1 in the ITER reference scenarios but with better performance due to improved optimization techniques

high, compared to the previous cases, and results in a shorter burn time (we imposed a minimum burn time of 1000 sec). This case represents the best confinement margin possible, using the lower bounds of wall load and burn time requirements. With these parameters though, the total accumulated fluence would be lower than that of the previous cases.

V.3.3 Hybrid Operation with Pulsed Fatigue Limits

All the previous hybrid results used an allowable stress in the central solenoid of 450 MPa. The allowable stress actually depends on the number of cycles, due to fatigue effects such as crack growth propagation. The correlation of permissible number of cycles with allowable stress of the ITER central solenoid is is indicated in

TABLE V-3. IMPACT OF FATIGUE STRESS LIMITS IN THE CENTRAL SOLENOID ON THE MAXIMUM POSSIBLE FLUENCE FOR HYBRID CASE NO. 2

Maximum CS stress (MPa)	450	375	350	250
permissable cycles	6763	12,800	26,981	50,273
total volt-sec. capability (Vs)	318	303	283	266
burn volt-sec capability (Vs)	106	91	71	54
burn time (s)	3084	2660	2063	1567
total fluence (MWy/m^2)	0.67	1.09	1.78	2.52

Table V-3 for hybrid case 2 taken from the previous table (this correlation also includes the cycles needed to perform the physics phase mission). As the allowable stress drops below about 350 MPa, the number of permissible cycles increases rapidly, whereas the burn time reduction is not so severe. Thus the accumulated fluence (product of burn time x wall load x number of cycles) maximizes at the lower stress levels in the coils. As the operating stress approaches 250 MPa, an accumulated fluence of about 2.5 MWy/m^2 is possible, requiring about 50,000 hybrid pulses.

V.4 SENSITIVITIES

Many of the ITER modeling procedures involve uncertainties. In this section we show the effect on the attainable technology phase performance when some of these assumptions are varied over their range of uncertainty. In particular we look at the divertor heat load, injection power level, bootstrap fraction, confinement assumption, and beta limit. All of these studies are done for both seeded and unseeded cases. The steady-state cases are optimized for maximum wall load, and the hybrid cases for maximum fluence. In all cases, only one sensitivity is examined at a time.

V.4.1 Divertor Heat Load

Fig. V-2 shows the effect of the allowable heat load on the maximum attainable steady-state wall load. The solid lines correspond to seeded cases and the dotted lines to unseeded cases. Note that the divertor heat load shown in these figures are base model predictions and must be multiplied by the peaking factor of 4.1, which was included in the results of the previous section. As the divertor heat load increases from 5.0 to 13 MW/m^2 (times 4.1 for peaking) , there is a strong increase in the wall load. At about 13 MW/m^2 (x4.1), the beta limit is met, and further increases in the divertor heat load have only a small effect. Also, as the allowable divertor heat load increases, the impurity seeding concentration (= seeded iron density / electron density)

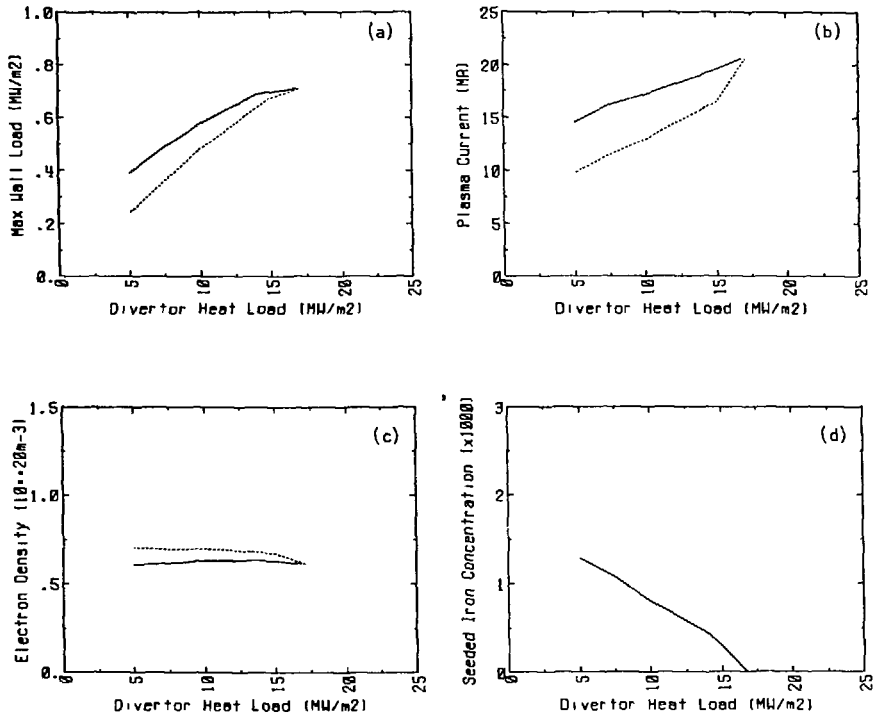

Fig. V-2. Sensitivity of the maximum steady-state wall load to the allowable divertor heat load. The solid curves are of seeded cases, and the dotted lines for unseeded cases. a) shows the maximum wall load, b) shows the plasma current, c) shows the plasma density and d) shows the seeded impurity iron concentration. Note that the heat loads shown here are the base model predictions and do not include the peaking factors of 4.1 used earlier in the chapter. They should be multiplied by 4.1 to obtain the design heat load.

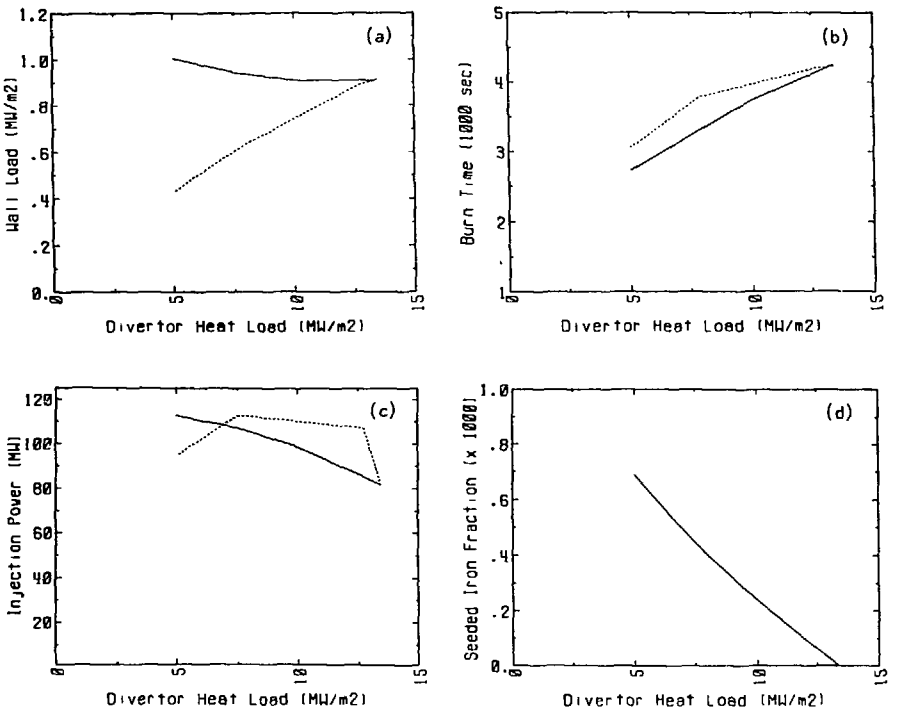

Fig. V-3. Sensitivity of the hybrid operational performance to the allowable divertor heat load. The solid curves are of seeded cases, and the dotted lines for unseeded cases. a) shows the wall load, b) shows the burn time, c) shows the injection power and d) shows the seeded impurity iron concentration. Note that the heat loads shown here are the base model predictions and do not include the peaking factors of 4.1 used earlier in the chapter. They should be multiplied by 4.1 to obtain the design heat load.

goes to zero. All cases shown in this figure are at the upper bound of the injection power (113 MW).

The hybrid divertor heat load sensitivity is shown in Fig. V-3. Here we show both the wall load and the burn time, since it is their product which is being maximized. When seeding is permitted, the increase in fluence is attained by increasing the burn time - as the wall load actually drops slightly. The increased burn time is possible due to the lower impurity seeding levels and resultant lower loop voltages. For the unseeded case, the fluence increases with increasing divertor heat load due to increases in both the wall load and burn time. However, without seeding the attainable wall load is too low for technology testing, unless high divertor heat loads can be accommodated (> 10 MW/m^2 without safety factors applied, or >40MW/m^2 with).

V.4.2 Injection Power Level

The amount of available injection power has an impact on the attainable wall loads. Previous results used 113 MW (nominal maximum) as the upper limit of injection power. Fig. V-4 shows the impact on the steady-state wall load when the upper bound on injection power is varied. For the unseeded case, there is little advantage to increasing the injection power, as the divertor heat load is the dominant constraint. The maximum useful power level in this case is about 115 MW. When seeding is allowed, there is a larger impact on the achievable wall load. With higher injection powers, larger impurity seeding concentrations are used, which eases the divertor heat load constraint. With injection powers near 150 MW, the seeded steady-state case approaches wall load levels useful for technology testing.

For the unseeded hybrid scenario, there is very little effect on performance with increasing injection powers (see Fig. V-5). With seeding, the wall load increases steadily with larger injection powers, and the burn time remains near 3000 sec. As injection power increases, the plasma density increases and the temperature decreases. This tendency is favorable for the divertor heat load, and helps maintain the specified limit even though the fusion power and injection power increase. We note that at least 100 MW is needed to achieve wall loads of 0.8 MW/m^2.

V.4.3 Bootstrap Fraction

Here we examine the effect of enhanced bootstrap current fractions. Modification of the bootstrap scaling is done by introducing a multiplying factor on the bootstrap scaling from Ref. 17. Results are plotted vs. the calculated bootstrap fraction, which includes the effect of the multiplying factor. The actual bootstrap fraction is generally proportional to the multiplying factor, and the nominal bootstrap fraction points are indicated with a triangle on the following figures.

Fig. V-6 shows the impact of bootstrap current fraction on the steady-state wall load. When the bootstrap current fraction is lowered from the nominal level, only moderate decreases in the wall load are observed, especially for the unseeded case. When the bootstrap current fraction is increased to levels above 50% for the seeded case and above 60% for the unseeded case substantial improvements are seen (this represents about a 50% improvement over the nominal scaling). If the bootstrap

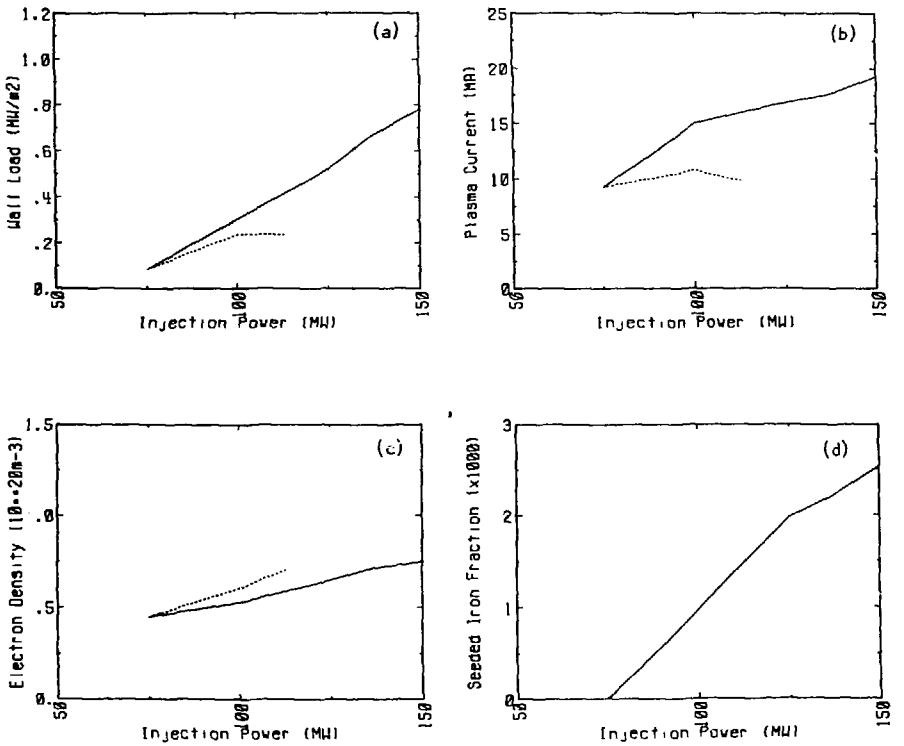

Fig. V-4. Sensitivity of the maximum steady-state wall load to the allowable injection power level. The solid curves are of seeded cases, and the dotted lines for unseeded cases. a) shows the maximum wall load, b) shows the plasma current, c) shows the plasma density and d) shows the seeded impurity iron concentration.

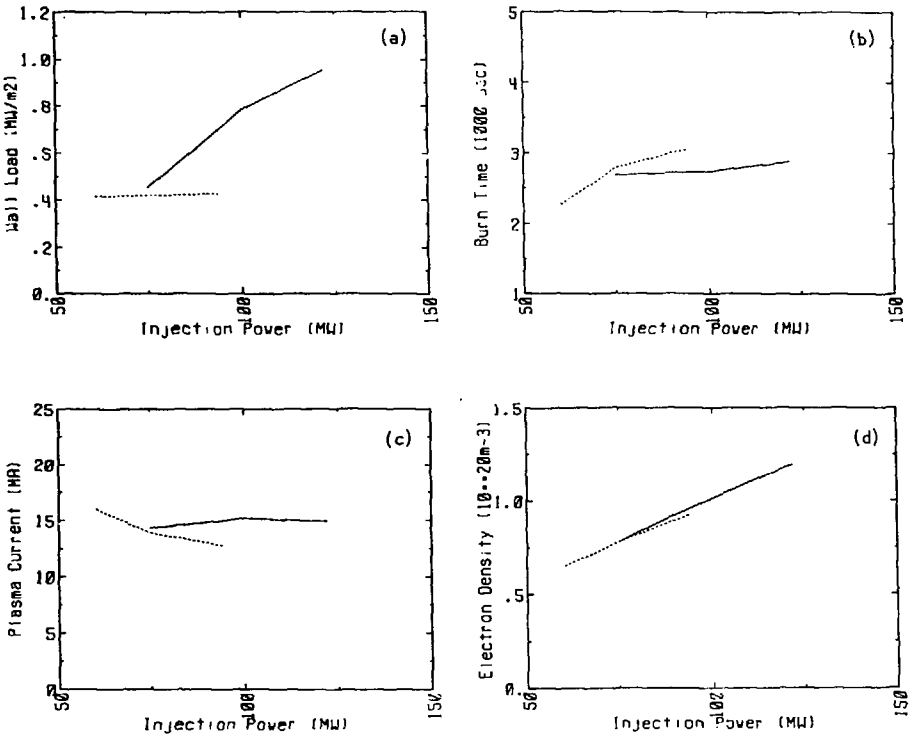

Fig. V-5. Sensitivity of the hybrid operational performance to the injection power level. The solid curves are of seeded cases, and the dotted lines for unseeded cases. a) shows the wall load, b) shows the burn time, c) shows the plasma current and d) shows the plasma density.

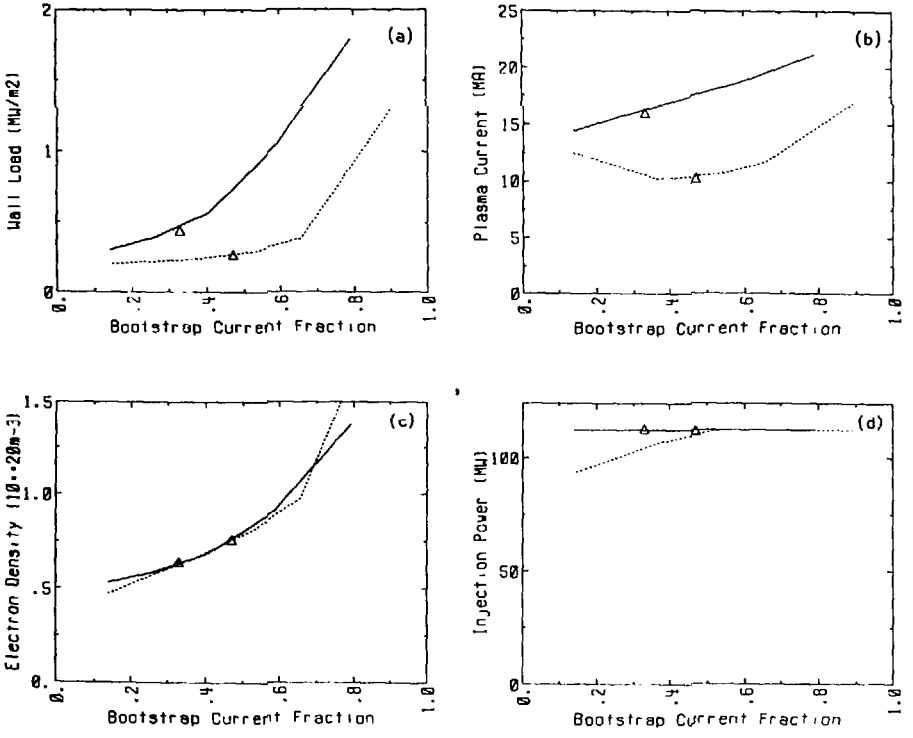

Fig. V-6. Sensitivity of the maximum steady-state wall load to the bootstrap current fraction. The solid curves are of seeded cases, and the dotted lines for unseeded cases. a) shows the maximum wall load, b) shows the plasma current, c) shows the plasma density and d) shows the seeded impurity iron concentration. The triangle indicate the points using the nominal bootstrap scaling.

fraction is twice the presently predicted level, steady-state wall loads approaching 0.8 MW/m^2 are possible. The main reason for this benefit is that with larger bootstrap fractions, the plasma density can increase, as less current must be driven non-inductively. This eases the conditions for the divertor heat load constraint. Presumably, increasing the current-drive efficiency would have a similar affect.

With hybrid operation, increasing the bootstrap fraction has little impact on the wall load, but does allow for significant gains in the burn time for both seeded and unseeded cases (see Fig. V-7). There is little variation in the optimal hybrid scenario plasma parameters as the bootstrap fraction increases - the increase in the burn time is simply a result of the reduced loop voltage from the enhanced bootstrap fraction. Also, the injection power is at or near the upper limit of 113 MW for all cases shown in Fig. V-7.

Although not indicated above, almost all the cases shown in this section are limited by the energy confinement ($H \leq 2.2$). Only the cases with a) unconstrained divertor heat load, and b) the steady-state seeded case with injection power = 150 MW are not at the H factor limit (these cases hit the beta limit). Even though the technology phase cases have the benefit of external heating, confinement is generally as critical as with the physics phase because of the operation at lower plasma current levels.

V.4.4. Confinement H factor

Even though the technology phase operational scenarios have additional heating power to the plasma from the non-inductive current drive, these operational scenarios are still sensitive to confinement. Figure V-8 shows the steady-state wall load vs the confinement H-factor (considering both ITER power and Offset scalings). For H-factors approaching 2.5, the steady-state wall load approaches attractive levels for technology testing. The sensitivity to the H-factor is due to the fact that these scenarios operate at lower plasma current levels than the ignition scenarios. Also they tend to have larger radiation fractions (i.e., the impurity seeded cases), which also increases the sensitivity to the needed confinement. Fig. V-9 shows the sensitivity of the hybrid performance to the confinement. Most of the increase in the product (burn time x wall load) with increasing H factors occurs in the burn time, with less change in the wall load.

V.4.5. Beta Level

The previous section showed that the technology phase operational scenarios are sensitive to energy confinement. Generally, they are not beta limited. In figure V-10, we show the steady-state wall load sensitivity to the Troyon factor. Above g_{Troyon} of about 2.5, the beta limit is no longer met and confinement is a stronger constraint. But if the Troyon coefficient is limited to below 2.5, the wall load is strongly affected.

V.5 ADDITIONAL STEADY STATE OPERATION STUDIES

Steady state operation is the ultimate goal of the technology phase operation. However, as noted above, the compatibility of the steady state operation and divertor performance is a serious problem. Here, some improvements of those operations are investigated, using alternate models from the Japanese TRESCODE [18]

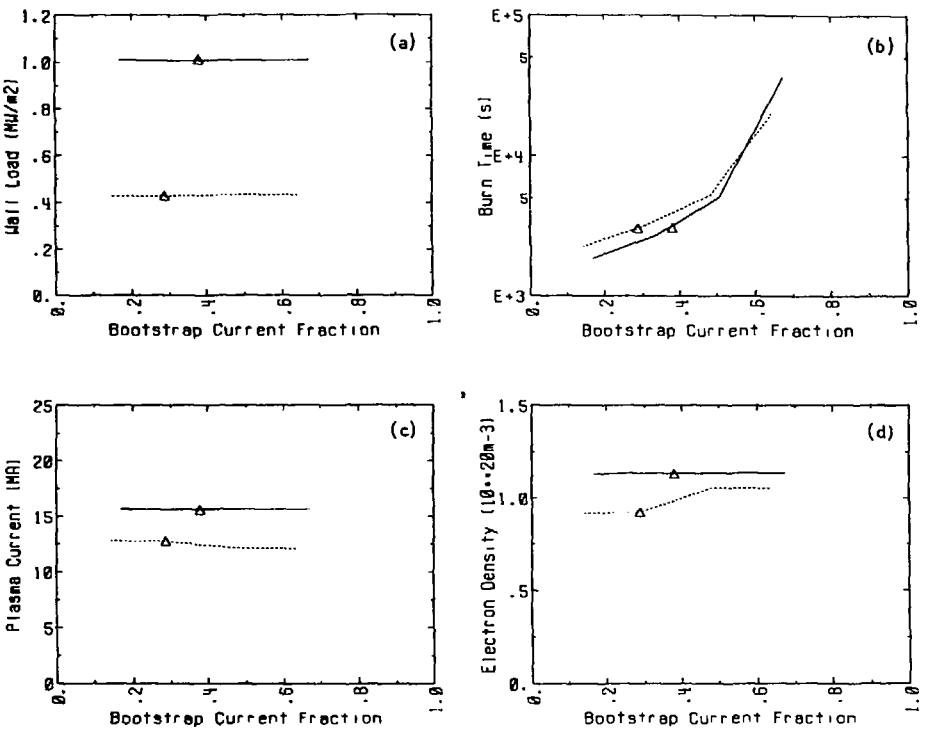

Fig. V-7. Sensitivity of the hybrid operational performance to the bootstrap current fraction. The solid curves are of seeded cases, and the dotted lines for unseeded cases. a) shows the wall load, b) shows the burn time, c) shows the plasma current and d) shows the plasma density. The triangle indicate the points using the nominal bootstrap scaling.

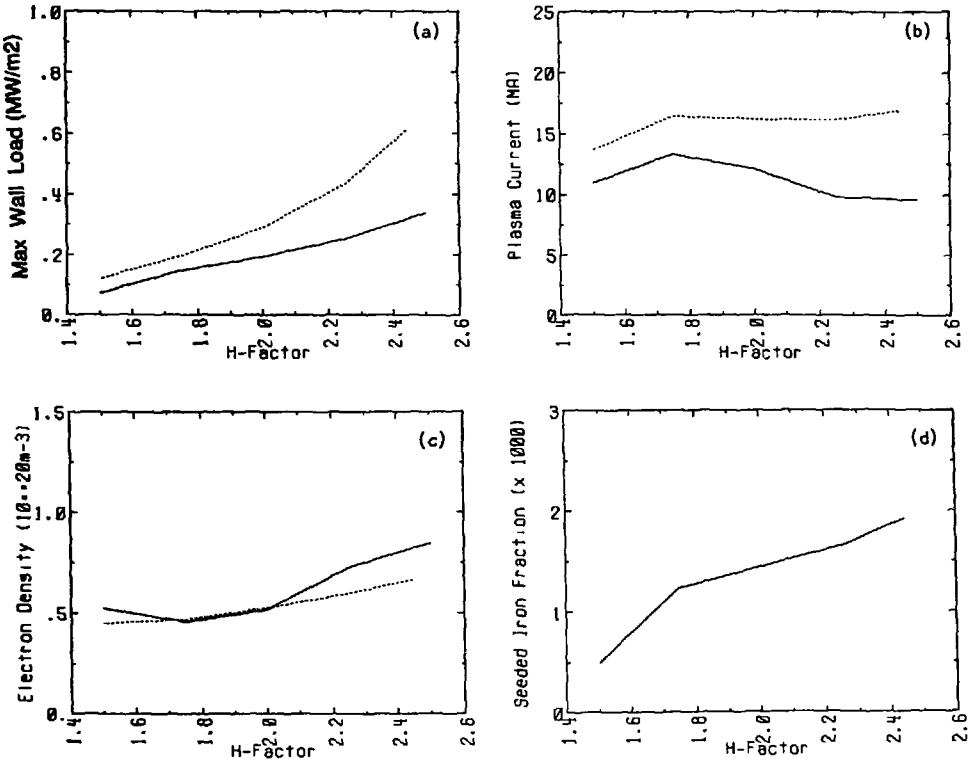

Fig. V-8. Sensitivity of the steady-state wall load to H-factor (confinement) uncertainties. The solid curves are for unseeded cases and the dotted curves are for seeded cases. a) shows the maximum wall load, b) shows the plasma current, c) shows the plasma density and d) shows the seeded impurity content.

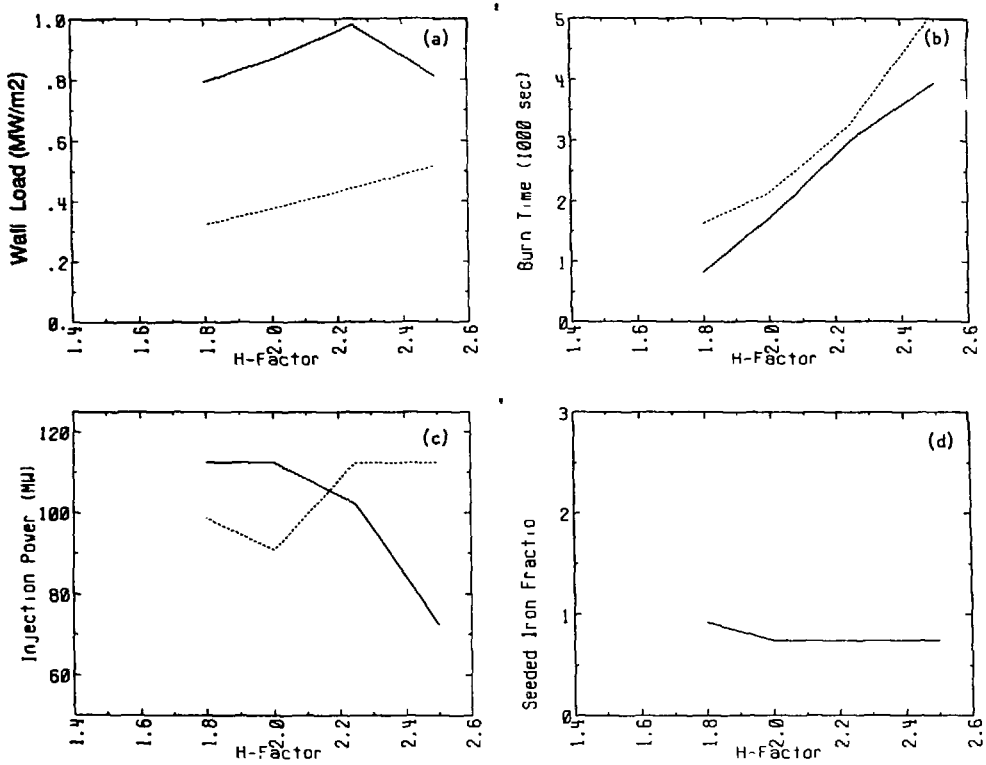

Fig. V-9. Sensitivity of the hybrid operation performance to H-factor (confinement) uncertainties. The solid curves are for unseeded cases and the dotted curves are for seeded cases. a) shows the wall load, b) shows the burn time, c) shows the plasma current and d) shows the seeded impurity content.

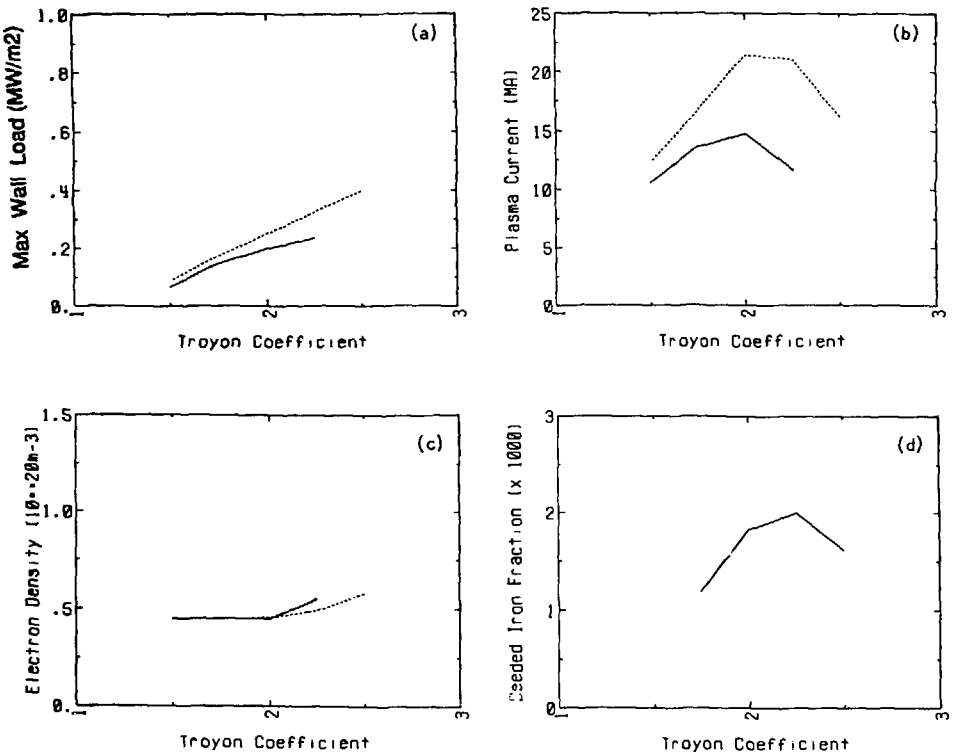

Fig. V-10. Sensitivity of the steady-state wall load to the Troyon coefficient. The solid curves are for unseeded cases and the dotted curves are for seeded cases. a) shows the maximum wall load, b) shows the plasma current, c) shows the plasma density and d) shows the seeded impurity content.

V.5.1. Boundaries for Steady-State Operation

Analysis of the steady state operation space has been carried out in an operational temperature-plasma current (T-I) space. The boundary constraints for the operation space are the following:

H_{ITER-P}	≤ 2.0
$H_{ITER-OL}$	≤ 2.0
gTroyon	≤ 3.0
q(95)	≥ 3
Q	≥ 5

The required current drive power, bootstrap current fraction divertor heat load etc., are examined in the resultant operation space, named *Operation Space I (OpeS I)*.

H-mode Experiments in JET and ASDEX show that the enhancement factor for ITER power law scaling, H_{ITER-P}, is about a factor of 2.2. It may be considered that $H_{ITER-P} \leq 2.2$ could be achievable. Another point is that there is some uncertainty for a beam pressure contribution to MHD beta limits. It is not clear at present whether only the perpendicular component of the injected beam pressure should be included in the MHD beta limit or whether the entire beam pressure should contribute. As a rather optimistic assumption, only one third of the beam pressure is used in calculation of the toroidal beta limit. We incorporate these new assumptions of optimistic energy confinement and NB beta contributions in an extended operation space, called *Operation Space II (OpeS II)*, namely:

H_{ITER-P}	≤ 2.2
$H_{ITER-OL}$	≤ 2.0
gTroyon	≤ 3.0
q(95)	≥ 3
Q	≥ 5

V.5.2. Models

In this study, we used a simplified Harrison-Kukushukin (HK) model [16] for the divertor heat load analysis. A simplified HK model is introduced with the divertor heat load proportional to $P_Q^{14/9}/n_e^{7/9}$, where P_Q is a net input power to the divertor plate and n_e is an average electron density . A coefficient is adjusted to match the result of the standard ignition operation. With this particular model, the divertor heat load for the standard ignition operation is estimated to be 9.1MW/m ^{2} at the outer divertor plate including a physics peaking factor. Full 2D modelling of the baseline ignition case (A.1) has indicated a heat load of 20MW/m^2, albeit with different models and different assumptions of peaking factors. These values have not been normalized against the previous results of this section.

V.5.3 Impact of Neutron Wall Loading

Fig.V-11 shows the steady state operation space in T-I plane, for the case of 0.8MW/m^2. Fig.V-12 shows the associated contours of the neutral beam power. The operational space is bounded by the beta limit and the minimum Q value of 5. The

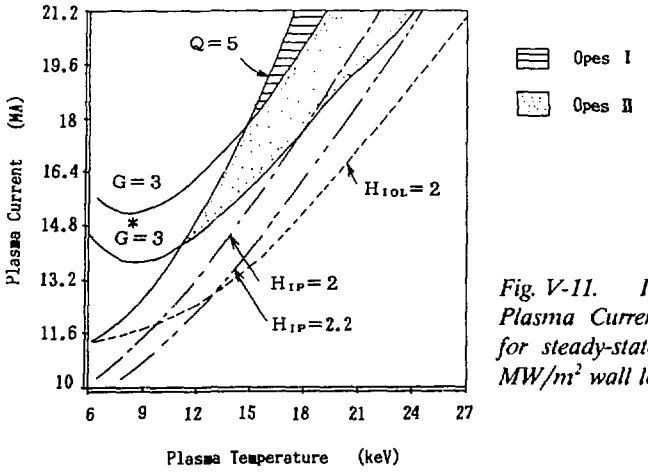

Fig. V-11. ITER Temperature/ Plasma Current operation space, for steady-state operation at 0.8 MW/m² wall load.

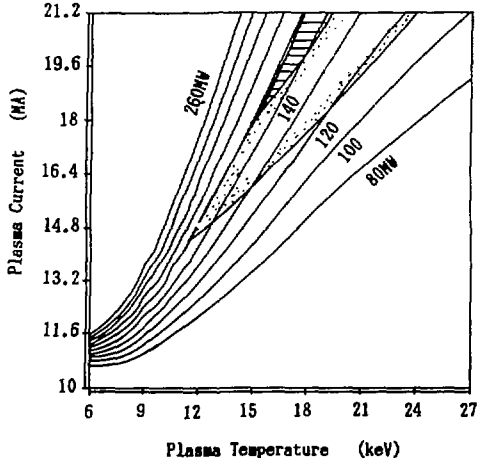

Fig. V-12. The neutral beam power levels associated with Fig. V-8.

plasma current must be larger than 17MA and the operational temperature higher than 14keV at the OpeS I. NB current drive power requirements go from 160MW to 180MW. The correspondind achievable Q value is only 5 to 6 as shown in Fig. V-13. The fraction of bootstrap current is less than 30%. Since the total heating power (i.e., summation of alpha power, NBCD power and ohmic power) is quite large, the divertor heat load will exceed 35MW/m^2 as shown in Fig. V-14. Steady state operation keeping the wall load condition of 0.8MW/m^2 is very difficult since the current drive power is too low (NB power 75MW and LH power 45MW), and the divertor heat load is critical.

If one could operate at the OpeS II where only one-third of the beam pressure is taken into account for the beta limit, the needed plasma current can be reduced. As a result, the required current drive power reduces to 120MW and Q value is improved to

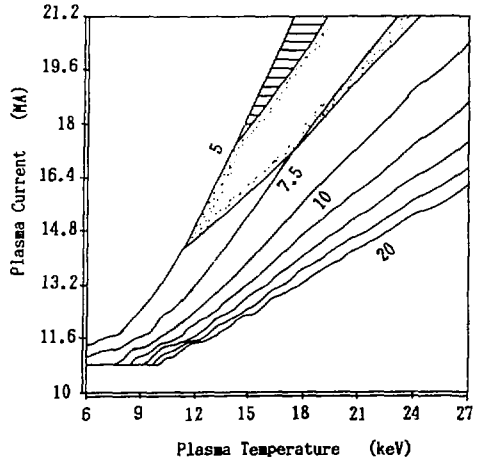

Fig. V-13. The Q values associated with Fig. V-8.

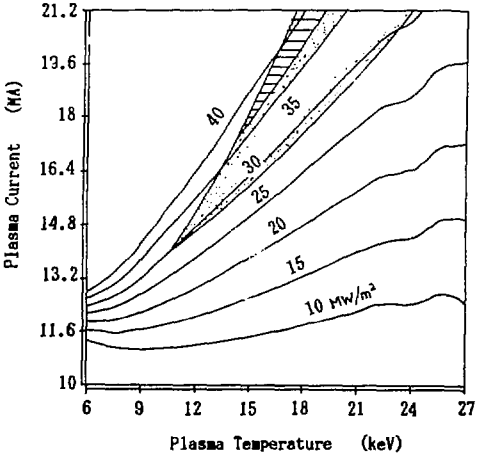

Fig V-14. The divertor heat load levels associated with Fig. V-8.

about 8. Therefore, the improvement of beta limit gives a substantial impact on the steady state performance at high power. However, divertor heat load is still nearly 30MW/m^2.

Fig. V-15 shows the operation space in the case of 0.6MW/m^2 wall load. In this case the required minimum current at a given temperature is bounded by the confinement capability instead of the beta limit. The required current drive power is between 120MW and 140MW at OpeS I and down to 110MW at OpeS II. Maximum Q values are 6 and 7 at OpeS I and OpeS II, respectively. The divertor heat load can be reduced to around 23MW/m^2. Therefore, the reduction of the wall load requirement down to 0.6MW/m^2 is quite substantial for both current drive and divertor performance. It is noted that a local neutron wall load near the midplane will be about 1MW/m^2 so that .nuclear testing could possibly be done satisfactorily, if a proper location is selected for testing modules.

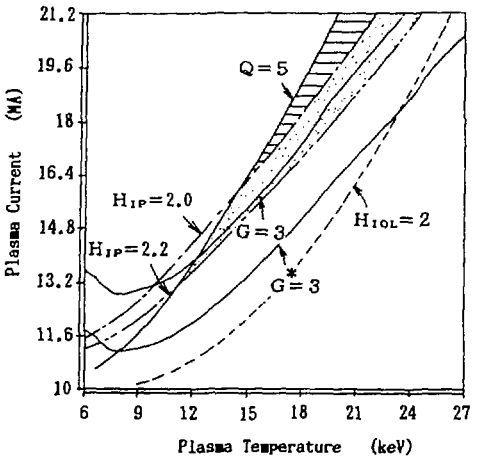

Fig. V-15. ITER Temperature/Plasma Current steady-state operation space with a 0.6 MW/m² wall load.

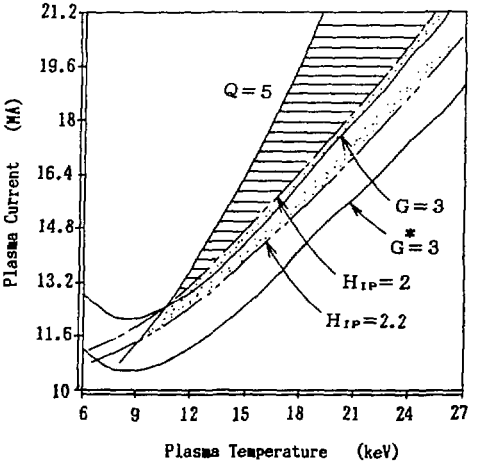

Fig. V-16. Temperature/Plasma Current steady-state operation space with 0.8 MW/m² wall load and a higher magnetic field (B_{max}=12.5T)

V.5.4 Effect of High Magnetic Field

The steady state operation space is generally restricted by the beta limit. It is possible to remove this boundary if a slightly higher field is applied. This would, of course, result in higher stress in the TF coils.

Fig.V-16 shows the case with the maximum field at the coil increase to 12.5T from the design value of 11.5T. The magnetic field at the plasma axis increases from 4.85T to 5.32T. As seen in the figure, the operation space is restricted not by the beta limit but by the confinement requirement. The operation space is expanded and the required current drive is reduced to about 140MW (Fig.V-17). In OpeS II, steady state operation become possible with 120MW. On the other hand, the divertor heat load is reduced to about 30MW/m^2 and 25MW/m^2 at OpeS I and OpeS II, respectively (Fig.V-18). To reach a wall load of 0.8MW/m^2 an increase of the

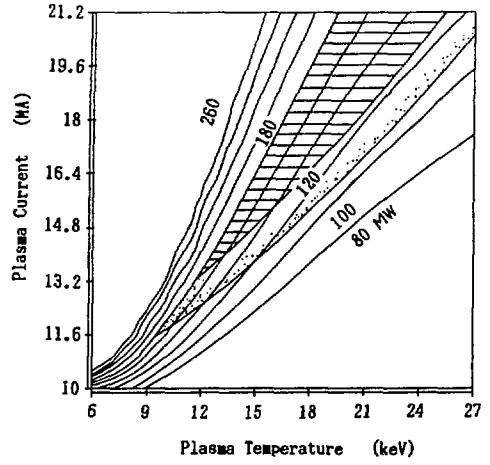

Fig. V-17. Neutral beam power levels associated with Fig. V-13.

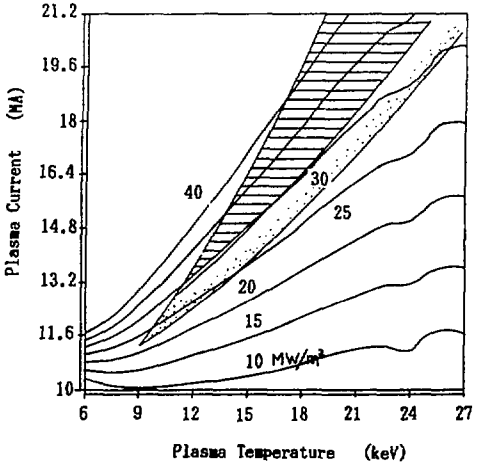

Fig. V-18. Divertor heat load power levels associated with Fig. V-13.

magnetic field would be an alternative option. Of course, the device design may have to be altered to accommodate higher field magnets.

V.5.5 Hybrid and High Q Cases

The I_p - T space analysis can be used to systematically investigate long pulsed high Q cases in addition to steady-state cases. Characteristics and sensitivities of the reference points are also revealed in the I_p - T space analysis. For high Q hybrid operation, suitable temperatures are in the range $9 < T_e < 14$ keV, as shown in figure V-19. The point A1* is similar to the physics phase operation point (with some

* Note that the following dscenario designatios, A1, A2, A3 etc, do not necessarily correspond to the ITER baseline operating points.

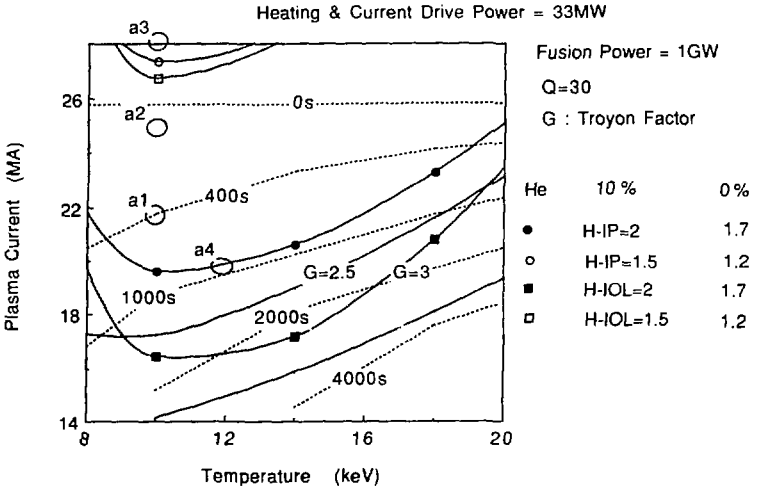

Fig. V-19. Plasma current - Temperature (I-T) operational space for high Q.

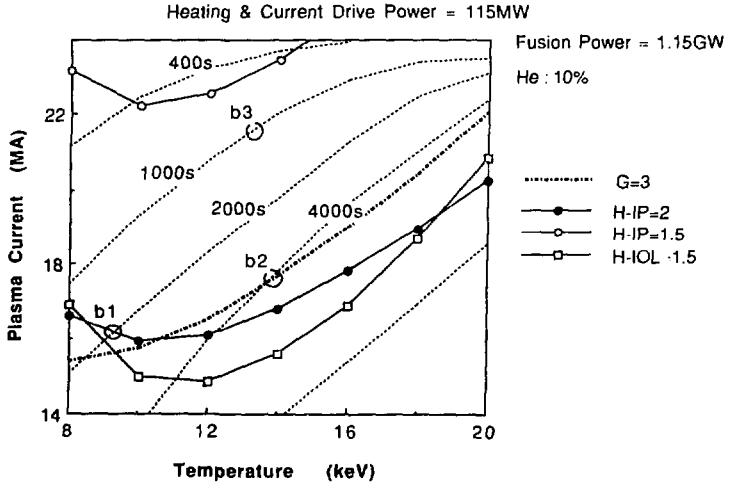

Fig. V-20. Plasma current - Temperature (I-T) operational space for long pulse operation.

injection power for burn control). Point A2 represents an alternate operating point with more confinement margin (H_{IP} / H_{IO}= 1.7 / 1.6), but the burn time is lower (50 s). If about 20 VS flux savings were possible during current ramp up, and operation at low edge q is possible, point A3 is acceptable, with even higher confinement margins. Should the confinement margin be acceptable, point A4 offers burn time of 1000s (H=2) in a pure inductive scenario. Increasing the injection power (decreasing Q) increases the pulse length, as shown in Figure V-20, which uses Q=10.

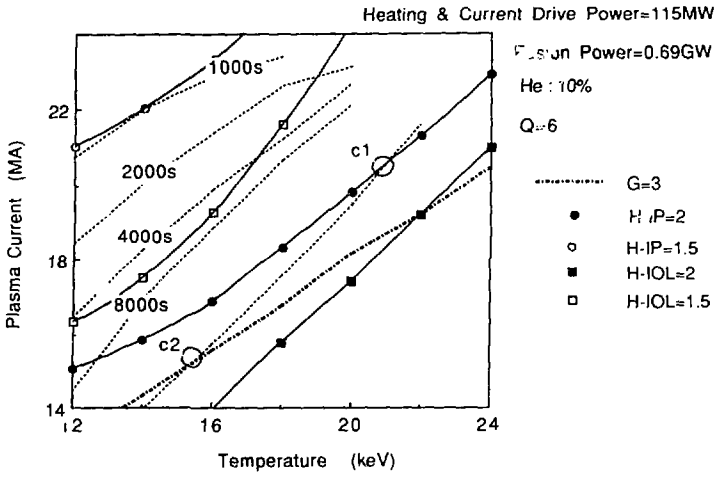

Fig. V-21. Plasma current - Temperature (I-T) operational space for low Q operation.

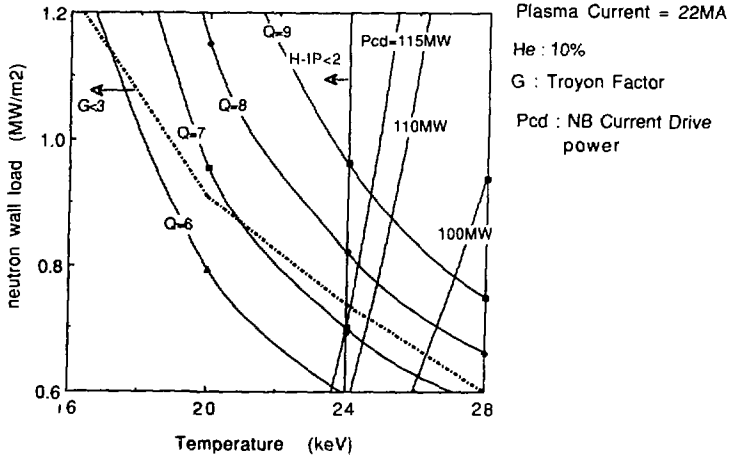

Fig. V-22. Steady-state operation in wall load/temperature space.

A steady state operation point with an acceptable Troyon factor does not exist in the high Q, high wall load example shown in figure V-20. Some optimum points can be considered here with regards to different constraints. Point B1 has the best divertor conditions, point B2 has the longest pulse duration, and point B3 has the best confinement margin. These characteristics are similar to those described in previous sections.

A steady-state operational point appears achievable with a relatively low Q value and wall load. As shown in figure V-21 (for Q=6 and wall load =0.69 MW/m^2), the

current is driven entirely by non-inductive means at operational points c1 and c2. Point C1 is most demanding with respect to the divertor conditions since it has a high temperature and low density plasma conditions, as well as high plasma current. Point C2 has better divertor conditions, but requires slightly better confinement margin.

The maximum Q constraint for steady-state operation is beta limited at high neutron wall loads and is confinement limited (H factor) at low neutron wall loads, as indicated in figure V-22. The maximum steady state Q value is 7, as shown in figure V-19., bounded by the conditions $H \leq 2$, and the injection power ≤ 115 MW.

V.6 SUMMARY

The steady-state and technology phase operation requirements place extra difficulty on the divertor, due to the large injection powers needed to sustain the energy balance and mainatain the plasma current over these long burn times. Identifying operational parameters which satisfy the desired performance, yet remain within the bounds of acceptable divertor and main plasma constraints is difficult. A key ingredient included in our modeling, which eases the divertor conditions, is the use of additional impurity seeding to enhance the radiative losses. Before such a method is to be adopted, careful attention to the critical issues is required. These are addressed in Ref. 15.

For steady-state operation under the baseline assumptions, wall loads of only about 0.4 MW/m^2 are possible, even with seeding. Steady-state wall loads approaching 0.8 MW/m^2 are possible if either 1) the bootstrap current fraction were about twice the nominal scaling level, 2) the permitted divertor peak power density could approach about 3-4 times the presently expected limit, or, alternatively, advanced divertor methods employed (He pumping, erosion and impurity retention would still a problem), 3) the injection power approaches 150 MW (seeded case only), or 4) some combination of the above effects.

Higher wall loads are possible with the nominal set of modeling assumptions if hybrid operation, a combination of inductive and noninductive current drive methods, is used. Under hybrid operation, wall loads near 1 MW/m^2 for burn times over 3000 s are possible with the baseline assumptions. However, both steady-state and hybrid scenarios are dependent on the viability of a radiation enhancement scheme which utilizes the seeding the plasma with medium Z impurities. in concentrations of the order of ~0.1%

If the divertor issues were not as severe as presently envisioned, the technology-phase operation prospects would be somewhat improved. In this situation steady-state scenarios are found for the technology phase demonstration, with wall loads near 0.7 MW/m^2. Also, steady-state wall loads over 1.5 MW/m^2 would be possible if the bootstrap current fraction is about twice that predicted by the present modeling. Finally, additional studies indicate steady-state operation conditions are improved if lower wall-loads are permitted, or if higher field levels are possible.

APPENDIX V-A

A BRIEF OVERVIEW OF *TETRA* SYSTEMS CODE MODELS OF RELEVANCE TO ITER TECHNOLOGY PHASE OPTIMIZATION

For the hybrid studies it is necessary to check the volt-second balance due to the long burn times required (1000s of seconds). The flux linkage between the plasma and PF coil system is governed by two constraints:

plasma startup flux requirement $\leq$ PF coil set flux capability during startup

plasma burn flux requirement $\leq$ PF coil set flux capability during flattop

The plasma startup requirement (VSsu) is taken to be :

$$VSsu\ (V\text{-}sec) = Ip\ (A)\ Lp\ (H) + (\ 0.40\ Ip\ (A)\ R\ (m) + 10\ ),$$

where I_p is the plasma current, L_p is the plasma inductance (see Ref. 7), and R is the major radius. The first term is the flux requirement associated with the plasma inductance and the second term represents the startup flux requirements. The plasma burn flux requirement is

$$VS_{bu}\ (V\text{-}sec) = I_p(A)\ V_{loop}(V)\ t_b\ (1 - F_{ni} - F_{bs}),$$

where V_{loop} is the plasma loop voltage (from Ref. 7), t_b is the burn time, F_{ni} is the fraction of the current driven non-inductively and F_{bs} is the bootstrap current fraction.

The PF coil set flux linkage to the plasma is calculated at three times, the beginning of the plasma current ramp up (BOP), the end of the plasma current ramp up, and at the end of the flattop (EOF). The coil set startup flux capability and the burn flux capability are found from these values. A key part of this calculation is the evaluation of the coil currents at the three specified times. This is done with a fixed boundary MHD model, as described in Ref. (9).

We use a combination of neutral beam and lower hybrid injection for the noninductive current drive, as per the ITER baseline design. The beams provide noninductive current drive for the central part of the plasma, and the lower hybrid drives current in the outer plasma region. The neutral beam current drive efficiency follows the Mickelson-Singer formulation. The beam energy is held at 1.3 MeV, and the tangency radius of injection is held at 1.05 x R. The lower hybrid current drive efficiency is taken from Ref. 10. The fraction of the current driven by neutral beams is adjusted to provide the nominal 75/25 ITER power split between neutral beams and lower hybrid thus providing an approximate profile consistency in our 0D plasma representation.

The currents in the central Ohmic Heating stack coils are constrained by (from Ref. 11) :

$$J_{alw}\ (A/m^2) = 1.45 \times 10^8/[32\ X/s_{alw}\ (B_i + B_o)\ (r_i + r_o) + 1.0 + 0.6\ Z/Y].$$

The first term in the denominator represents the structure requirements from stress considerations, where s_{alw} is the allowable stress (MPa), $B_{i(o)}$ is the field at the inner (outer) radius (T), and $r_{i(o)}$ is the coil inner (outer) radius (m). The second term in the denominator represents magnet protection constraints. The last term in the denominator is the superconductor (ie stability) contribution, and

$$X = 0.1 + 0.925\ (r_o / r_i) - 0.053(r_o / r_i)^2$$

$$Y = 1 - T_m/[T_c\ (1 - B_i/B_c) - T_b]\ , \text{and}$$

$$Z = 0.036\ (B_i).5\ /\ (1 - B_i/B_c)^2).$$

Here T_m is the temperature margin (= 1 K), T_c is the critical temperature at zero field (= 16.0 K), B_c is the critical field at zero temperature (= 23 T), and T_b is the bulk He temperature (= 5.0 K). The factors in the first and second terms in the current denisty equation were arrived at to match the ITER OH coil current density at 12 T.

Only the current densities of the coils in the central stack are limited by this equation. The current densities in the other PF coil groups are not constrained since the size constraints on these coils are not well defined. The above current limitation is applied at both the BOP and at the EOF. In calculating the field levels at the coils, the contributions from the other coils and the plasma are included. We use s_{alw} = 330 MPa, which results in good agreement with the allowable peak fields from more detailed design analysis. These values are used throughout this study.

The Harrison-Kukushkin analytic divertor and scrape-off layer model [17] is used to calculate the divertor heat loads and the plasma temperature at the divertor plates. This model uses an analytic treatment of the divertor plasma power balance, the pressure balance and the sheath and atomic conditions. The geometry is approximated by a three point slab model, for the divertor throat, divertor plate and the stagnation region adjacent to the main plasma. Correction factors are applied to adjust results to fit sophisticated 2-D calculations from the Braams B2 code. In TETRA we scale several input quantities to the divertor model with main plasma parameters. The field line connection length adjacent to the main plasma (from the "stagnation" point to the divertor entrance) L_t is scaled as:

$$L_t(m) = 11.0 \times B_t / B_p\ ,$$

which corresponds to a 45 m length for the baseline ITER physics phase case. The connection length in the divertor region is scaled as :

$$L_d(m) = 6.4 \times B_t / B_p\ ,$$

which corresponds to a 28 m length for the baseline ITER. Here B_p(T) is the average main plasma poloidal field and B_t is the toroidal field on axis. The ratio of the poloidal field to the toroidal field at the divertor plate (R_B) is scaled as:

$$R_B = 0.67 * B_p\ R_{stk}/B_t\ R,$$

where R_{stk} is the divertor strike point radius. These relationships are calibrated to

match MHD equilibria calculations for the nominal ITER physics phase plasma. Also we scale the parallel heat conductivity (Chi_{pl}) along the field line as:

$$Chi_{pl} = 2.1 \times 10^3 / [1 + 0.8 (Z_{eff} - 1)].$$

Two important calculated quantities from this model are the peak heat load on the divertor plate (H_{calc}) and the plasma temperature adjacent to the divertor plate (T_{calc}). These quantities are modified by:

$$H_{div} = H_{calc} \times (0.54 - 3.6\, T_{calc}\ (eV)), \text{ and}$$

$$T_{div} = T_{calc} \times (0.45 - 7.2/T_{calc}\ (eV))$$

to agree with earlier 2-D divertor modeling results -- the most recent ITER 2D runs have not been incoprporated. We use the scaled quantities H_{div}, and T_{div} as output quantities in TETRA.

REFERENCES

[1] J. R. GILLELAND, YU. A. SOKOLOV, K. TOMABECHI, R. TOSCHI, Nuc. Fusion, **29**, 1989, 1191.

[2] ITER Design Report, IAEA, Vienna, Oct. 1989.

[3] N. OHYABU, J. C. DEBOO, A. MAHDAVI, "Radiative Cooling in the Magnetically Expanded Boundary," Nuc. Fus. (1982 ?), or GA-A16434, 1982.

[4] International Tokamak Reactor Phase Two A Part III, Vol. 1., Report of the IAEA STI/PUB/795, Vienna (1988).

[5] J. CUMMINGS, S. COHEN, R. HULSE, M. REDI, "Power Radiated from ITER by Impurities," ITER-IL-PH-13-9-U-25, Sept. 1989.

[6] R. L. REID et al., "ETR/ITER Systems Code," ORNL/FEDC-87/7.

[7] N. A. UCKAN, ITER Physics Guidelines, Ver.1", ITER-TN-PII-8-7, 1989.

[8] R. L. CRANE, K. E. HILLSTROM, M. MINKOFF, "Solution of the general Nonlinear Programing Problem with Subroutine VMCON," ANL-80-64, 1980.

[9] J.GALAMBOS, "ITER Steady-State and Hybrid Operational Scenarios," ORNL/FEDC-90/1 , 1990.

[10] M. FENSTERMACHER, R. S. DEVOTO, R. H. BULMER, J.D. LEE, J. R. MILLER, J. H. SCHULTZ, "A Noninductively Driven Tokamak Reactor Based on ITER," Fus. Tech., **15**, 1989, 740.

[11] J. MILLER, LLNL, private communication, 1989.

[12] L.J. PERKINS, J. GALAMBOS, J. GILLELAND, D. BULMER, W. NEVINS, J.R. MILLER, "ITER at High Aspect Ratio :Is it time to Consider a Change for the Engineering Design Activityt?," UCRL-ID-104178, Lawrence Livermore National Laboratory, June 1990.

[13] E. STRAIT, "Avoidance of Disruptions in Low q, High Beta Discharges," D-III-D contribution to ITER R&D under ITER Task TH08-US, 190.

[14] R. H. BULMER, L.LODESTRO, W.M.NEVINS, L.D.PEARLSTEIN, "Bootstrap Current Improves Technology Phase Operating Scenarios",LLNL memo Feb., 1990.

[15] J.MANDREAKS, L.J.PERKINS, W.STACEY, *Proposed Work on ITER Impurity-Seedinging Operating Scenarios*, ITER memo ITER-IL-SA-1-0-20 (1990)

[16] M.F.A.HARRISON, *Analytical Modelling of Divertor and Scrapeoff -- The Harrison Kukushkin Model*, to be issued 1990

[17] N.FUJISAWA, *Bootstrap Current Assumptions*, ITER memo published during ITER joint-work session Feb-March 1989, Garching (1989)

[18] T.MIZOGUCHI et al, *Development of the Tokamak Reactor Conceptual Design Code TRESCODE*, JEARI-M 87-120 (1987)

VI. THE PROSPECTS FOR HIGHER ASPECT RATIOS: A PRELIMINARY ASSESSMENT

VI-1. INTRODUCTION

The present experimental confinement database is derived mainly from low aspect ratio machines in the vicinity of 3. In addition, as each of these aspect ratios remained either fixed or varied over only a narrow range, the aspect-ratio-dependence of all scalings for energy confinement derived from this database is clearly open to interpretation. As shown in Fig III-3, Chapter III, their predictions diverge at high aspect ratio. A recent analysis [1] has examined the implications of the aspect-ratio-dependence of confinement scaling on the ITER design point and has suggested that there may be benefits for high aspect ratio ITER designs, especially regarding technology phase performance. While this report is preliminary in nature, it is interesting to extract the salient features for discussion in this chapter. Validation, or otherwise, of its major conclusions deserves high priority in the early phase of the ITER Engineering Design Activity.

VI-2. ASPECT RATIO DEPENDENCE OF CONFINEMENT: IMPLICATIONS FOR ITER

VI-2.1 THE *ITER P*ower Scaling and the TFTR Results

At an international ITER Confinement Workshop in Garching in 1989, analysis of a larger L-mode database led to the definition of the *ITER Power* scaling [2] as:

$$\tau_E = 0.048\ I^{0.85}\ R^{1.2}\ a^{0.3}\ n_{20}^{0.1}\ B^{0.2}\ (A_i\kappa/P)^{0.5}$$

This has a statistical uncertainty of about 30%. According to Ref. 2, a comparison of this L-mode fit with H-mode data from ASDEX and JET indicated that an H-mode enhancement factor of H~2.2 might be expected.

Recent results by Grisham et al [3] provide interesting empirical support for the validity of the aspect-ratio-dependence of the *ITER Power* scaling as distinct from the other scaling expressions shown in Fig III-3 in Chapter 3 with their rather disparate predictions. By forming plasmas on both the inner and outer limiters of TFTR, they were able to obtain a wide range of aspects ratios from A=2.85 to 6.2 with plasma currents in the range I=0.5 to 1.52MA. Scans were performed in which I and A were varied simultaneously to keep the product of *I*A=constant*, with q_ψ fixed at slightly greater than 3 by adjustment of B. The results indicated that a constant value of the confinement parameter n-tau-T resulted over this wide range of aspect ratios with a scatter of only ~10-15%.

Returning to Fig. III-2(a)-(e), Chapter III, we note that curves of *I*A=constant* would be hyperbolae in I-A space and, very importantly, the form of the constraint boundary for the *ITER Power* scaling is very close to a hyperbola. This can be seen in Fig. III-3, where points are plotted of I*A=constant normalized to the ITER baseline

point (i.e. *I*A=22*2.79=61.4*). Note the excellent agreement with the *ITER Power* scaling as I and A are varied! The H=2 boundaries for *Goldston* and *T-10* scaling tend to overestimate the effect, i.e. they predict that contours of *I*A=constant* would improve n-tau-T at higher A and require only a small increase in aspect ratio to offset decreasing currents. By contrast, offset linear scalings such as *JAERI, Rebut-Lallia* and *ITER Offset*, underestimate the effect and would require large changes in aspect ratio to keep n-tau-T constant when plasma currents are decreased. The *ITER Power* scaling plots a middle path, with characteristics of the form *I*A=constant*, and requires modest changes in aspect ratio to offset decreasing currents.

Accordingly, if the *ITER Power* scaling correctly predicts the confinement at the ITER baseline design point, then these experimental results suggest that it may also be applicable for designs at higher aspect ratio and lower plasma currents. However, it is a larger extrapolation from the present database of the large machines.

VI-2.2 The *ITER H-Mode* Scaling

The latest support for this suggestion comes from the recent analysis of the new H-mode database by Cordey et al., resulting in a true *ITER H-mode* scaling [4]. Out of a total of 691 data points, 195 are from machines with moderate to high aspect ratios, i.e PDX (A~3.5), ASDEX (A~4) and PBX-M (A~5). Consequently, of all the presently favored scalings, this new formalism might be expected to provide the best prediction to date for the dependence of confinement on aspect ratio [5].

The application of this new scaling to our I-A-B_{tf} formalism is shown in Fig. III-3 in Chapter 3. Note, from that figure, that the aspect ratio dependence of this new H-mode scaling is even more favorable than the *ITER power* scaling in that it lies between that of the *ITER power* and *Goldston* scalings. If we were to follow the predictions of this scaling, even stronger trades of A for I could be made relative to *ITER Power* scaling.

VI-3 HIGHER ASPECT RATIO STUDY POINTS

As shown in Ref 1, according to the *ITER Power* scaling, a design point at, say, A=4, I=14.8MA in the B_{tf}=13T plane of Fig. III-2(d), Chapter III, has the same confinement capability as the ITER baseline at A=2.79, I=22MA (R=6m) in the Btf=11T plane of Fig. III-2(b). In other words, both require the same enhancement factor of $H_{ITER\text{-}power}$=2 to ignite under this scaling*. This led to the examination of a high aspect ratio study point with these characteristics, i.e A=4, I=14.8MA (R~6m) having the same confinement capability as the present low aspect ratio baseline under *ITER Power* scaling.

---

* Note that these two design points do not have the same energy confinement time. The former requires 3.09s, while ITER requires 3.82s. Rather, to ignite, both machines require the same enhancement factor of 2.0 over the energy confinement time predicted by *ITER Power* scaling. To the first order, this implies the same n-tau-T requirement. Actual requirements of $n_{DT}(0)*\tau_{Ei}*T_i(0)$ are 8.29×10^{21} m^{-3}.s.keV for the higher aspect ratio point and 8.46×10^{21} m^{-3}.s.keV for ITER.

In Table VI-1, we compare some of the major parameters of this study point with the present ITER baseline. Note that although the high aspect ratio point has a higher toroidal field at the coil relative to the present baseline, it operates under the same set of coil constraint limits (i.e, stress, protection and stability); field by itself is not a limiting parameter. Redesigning ITER at higher aspect ratios would, as shown in Chapter III, necessitate a higher field at the TF coil due to the nature of the constraint boundaries.

Note in Table VI-1 the superior technology phase performance of the high aspect ratio point under both steady state and hybrid operation, a consequence of, among other factors, significantly higher bootstrap current fractions. Note also the large inductive capability -- a direct consequence of the high aspect ratio -- which might permit the technology testing mission to be accomplished purely inductively. Attention would, however, have to be paid to current-profile stability. We caution that the parameters for this high aspect ratio machine in Table VI-1 are preliminary and have yet to be subjected to the scrutiny employed for the present baseline. They do, however suggest that further attention should be directed to the merits of such high aspect ratio designs, especially regarding the potential of improved steady state performance.

We might question how the high aspect ratio study point in Table VI-1 with a minor radius of only 1.5m could contain heat as well as ITER with its large minor radius of 2.15m? We could attempt a phenomenological reply that, although it has lower plasma current and minor radius, such a machine would have a significantly larger toroidal field on axis (7.0T relative to 4.85T) and, by virtue of its high aspect ratio (4.0 relative to 2.79), a lower toroidicity. However, because we do not yet understand energy confinement in tokamaks in terms of its formal dependence on design parameters, we cannot answer this question from a fundamental viewpoint.

While the predictions of both the *ITER Power* and *ITER H-mode* scalings, and the experimental results of Grisham et al., are certainly not the final word at this time, they do suggest that , as far as confinement is concerned, the trading of current for aspect ratio as demonstrated by the high aspect ratio study point in Table VI-1 may be about right. Additional evidence may be available soon from DIII-D which is planning aspect-ratio-dependent studies of confinement with A in the range ~3-5 in early 1991 [9]; this is relative to A=2.8 for the present DIII configuration. Unlike the aspect ratio studies on TFTR [3], DIII will be an elongated (κ~1.4-1.6), diverted plasma (double-null) operating in H-mode. JT60-upgrade may also commence operation next year and is, in principle, capable of forming plasmas up to A~4. On the other hand, it must also be noted that all large tokamak plasmas in present day experiments have low aspect ratios (A~3 or less).

VI-4 VERTICAL STABILITY AT HIGHER ASPECT RATIO

There has been concern that high aspect ratio plasmas would possess deleterious vertical stability properties at any reasonable elongation. The elongation of the high aspect ratio study point discussed above has been maintained at the same value as that of the ITER baseline, i.e ~2.0 at the 95% flux surface. Bulmer [6] has recently compared the vertical stability of this design with that of ITER using the new

TABLE VI-1. COMPARISON OF ITER AND A HIGH ASPECT RATIO STUDY POINT

	ITER BASELINE	*HIGH ASPECT RATIO STUDY POINT*
Characteristics		
Aspect ratio	2.79	4.0
Major/minor radius (m)	6.0/2.15	5.98/1.50
Plasma current (MA) / q_{ψ}(95%)	22.0 / 3.0	14.8 / 3.0
Toroidal field, axis/coil (T)	4.85/11.1	7.0/13.3[a]
Thermal/inductive stored energies (GJ)	0.580/2.24	0.346/1.35
Relative capital cost	1.00	~0.95[b]
Inductive, ignited performance		
Neutron wall loading (MW/m^2)	1.0	1.0
Fusion power (MW)	1080	784
Required Troyon beta coefficient (%)	1.99	1.73
Required H-mode enhancement for:		
ITER power confinement scaling	2.0	2.0[f]
ITER H-mode confinement scaling	0.66 - ~0.85[d]	0.62 - ~0.85[d]
Divertor peak heat load[c] (MW/m^2)	16.5	11.5
Volt-seconds: capability/burn (Vs)	326/46.1	417/179
Burn pulse length (s)	400	1660
No. of cycles for 1 - 3 MWy/m^2 fluence under purely inductive operation only	78,000 - 237,000	19,000 - 57,000
Technology phase performance[e]		
Steady-state operation under original beta and bootstrap models:		
Maximum attainable wall load[e] (MW/m^2)	0.42	1.10
Q	3.7	7.6
Bootstrap current fraction	0.33	0.46
Steady-state operation under improved beta and bootstrap models (Ref. 1):		
Maximum attainable wall load[e] (MW/m^2)	0.65	2.84[g]
Q	6.2	20
Bootstrap current fraction	0.54	0.82
Hybrid operation:		
Pulse length at $1MW/m^2$ wall load[e] (s)	~3,000	~9,000
No. of cycles for 1 - 3 MWy/m^2 fluence	11,000-32,000	4,000-11,000

a. At same coil design constraints as ITER (i.e same stress, protection and stability).
b. Would need validating under present ITER bottoms-up costing procedures
c. Includes safety factors of 2.75 (physics) and 1.5 (engineering)
d. Range reflects possible degradation due to ELMs; lowest values are for basic scaling.
e. Impurity-seeded operation with divertor, beta, and confinement constraints applied
f. Maintained constant relative to ITER baseline, i.e same confinement capability
g. Maximum wall load. Shielding and volumetric heat load constraints may preclude the realization of this high value in practice

formalism of Pearlstein et al. [7], a full MHD treatment with arbitrary passive structure and active components. Using the same distance from the plasma to the passive structure (note not same relative distance) in both cases, his preliminary studies indicate that the growth rates of the two cases are very similar, and of the order of ~45Hz.

Work has also also been performed on the vertical stability of CIT variants with aspect ratio varying in the range ~2.5-3.5 [8]. Any small effects seen at low aspect ratio appeared to saturate at A≥3 , leading to the conclusion of no dependence above this value.

Accordingly, the role of aspect ratio alone in vertical stability may be benign. While an ideal plasma with walls at infinity is certainly more vertically unstable at higher aspect ratio, there seems to be no dependence of vertical stability growth rates on aspect ratio when real passive and active structures are introduced, at least above aspect ratios of ~3. Rather, the design characteristics of these structures become the most important determining factor. Certainly, further work, experimental and thoeretical, is need on this topic (see below).

VI-5. BOOTSTRAP CURRENT AT HIGHER ASPECT RATIOS

Maximization of bootstrap current fraction is one of the most important factors in achieving attractive steady-state and hybrid scenarios for technology phase testing. Fig. VI-1 shows the I-A space at B_{tf}=12T similar to that of Fig. III-2(c) in Chapter III but under steady-state operation at a neutron wall loading of ~0.8MW/m^2. Contours of bootstrap current fraction are shown as determined by present ITER models; alternative models under consideration (see Chapter V) would tend to increase these bootstrap fractions by a factor of ≥1.5 [1].

Note that, unlike the ignition cases in Figs. III-2 and III-3 in Chapter III, all points in the I-A plot of Fig. VI-1 are at the beta limit of g_{Troyon}=3 (technology phase beta limit assuming a modicum of current profile control) in order to maximize the current-drive efficiency. The "neutron wall-load limit" boundary in the figure should be interpreted as the contour below which the neutron wall loading cannot be maintained at 0.8MW/m^2 and must be decreased continually for smaller machines at lower I-A coordinates. This then accounts for the drop in the bootstrap fractions shown below this limit.

From Fig. VI-1, we see that the bootstrap fraction I_{bs}/I increases strongly with increasing aspect ratio and the effect is even more marked had we also moved to a higher B_{tf} plane, i.e. B_{tf}=13 or 14T. The scaling trends of bootstrap current fraction vary as the square-root of the inverse aspect ratio multiplied by the poloidal beta and a simplified expression can be written (for illustrative purposes only --the results in Table VI-1 and Fig VI-1 were generated with the usual formalisms):

$$I_{bs}/I \sim \sqrt{(a/R)}\,\beta_p \sim \sqrt{(a/R)}*(B/B_p)^2\,\beta_t \sim g_{Troyon}\,\sqrt{(a/R)}*a*(B/I)$$

where, in the last term, we have made the substitution $B_p \sim I/a$ and $\beta_{t=g_{Troyon}}\, I/aB$. With reference to this last expansion in the equation, as we move to higher aspect ratio, lower currents, and higher field B on axis, the terms $\sqrt{(a/R)}$ and minor radius,

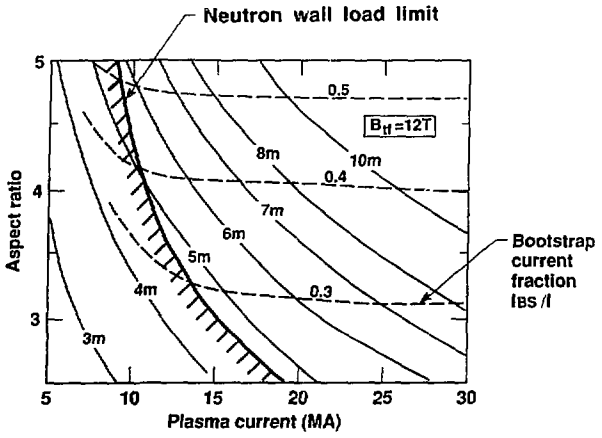

Fig. VI-1. I-A space for ITER-like machines at B_{tf}= 12T. Bootstrap current fractions (present ITER model) are shown for steady-state, current-driven operation at a neutron wall load of ~0.8 MW/m^2. Prospective new models would increase these bootstrap fractions by a factor of ≥1.5 [1]. The divertor heat loads are not constrained in this particular example; this does not affect the general trends of bootstrap scaling with aspect ratio, but rather would move the "neutron wall-load limit" (where 0.8MW/m^2 can no longer be maintained due to overlapping constraints) to larger machine sizes at higher {I,A} coordinates.

a, decrease while *B/I* increases. At the beta limit g_{Troyon}=constant, and the gain in B/I more than offsets the decrease in $\sqrt{(a/R)}$*a. In general, as we move to higher aspect ratio machines and require the same neutron wall loading, the beta poloidal increases faster than the square root of the inverse aspect ratio decreases. It is the dominance of the high beta poloidal which affords a strong apparent advantage to higher aspect ratio design points with regard to bootstrap current fraction.

VI.6 HIGHER ASPECT RATIOS -- INTERIM CONCLUSIONS AND CRITICAL ISSUES

In the present low aspect ratio ITER design, we have confidence that our baseline has a reasonable chance of achieving ignition under all of the presently favored energy-confinement scalings. However, as we noted in Chapter III above, the choice of this baseline design was dominated by considerations of prospective ignition performance under inductive operation. Formalisms for steady-state and divertor operation were only developed in the later stages of this project and must still be improved . With hindsight and the accumulated knowledge of three years of the ITER CDA, design selection based on simultaneous optimization of both modes of operation would have caused us to pay more attention to the potential advantages of high aspect ratio designs. This suggests a route for further optimization in the EDA .

TABLE VI-2. CRITICAL ISSUES FOR ITER HIGH ASPECT RATIO STUDIES

1. System and Operational Studies

- Optimum design point at high aspect ratio? What sets the upper limit on A?
- Technology phase operational characteristics at high aspect ratio?
- Characteristics of long pulse inductive mission at high A?
- Implications from the new *bi-modal* approach to design selection at high A [10]?

2. Confinement

- Confidence in the aspect ratio dependence of the new ITER H-mode scaling [3]? What are the expected extrapolation uncertainties at high A?
- Ability of near term experiments to support this issue?

3. Bootstrap and Beta Models

- Resolution of discrepancies (≥50%) in present bootstrap formalisms?
- Can we recommend an increase in ITER Troyon beta coefficient in terms of a parametric dependence on q_ψ and l_i?

4. Vertical Stability

- General trends in the variation of vertical stability with elongation and aspect ratio?
- Constraint for vertical stability? Is it, for example, a maximum growth rate or a power supply limit for the active circuits?

5. TF Magnets

- Higher aspect ratio ITER designs require higher fields at the TF coil under the same coil constraints (stress, protection, stability), a natural consequence of the form of the operational constraint boundaries for confinement, beta, volt-seconds, etc, -- see Chapter III. What problems ensue in the provision of ~ 13T fields for a high aspect ratio design at A=4?.
- Realization of very high aspect ratio designs with A~5-6 necessitates TF coil fields of ~14-15T. What is the ultimate limit on TF field given our present coil constraints?

6. PF Magnetics and Divertor Location

- Characteristics of the PF system for an A=4 study point?
- Are shaping requirements more stringent at high aspect ratio even though the vertical and radial builds are reduced?
- Divertor location, strike-point locations and exhaust duct geometries at high aspect ratio?

....table continued over

TABLE VI-2. CRITICAL ISSUES FOR ITER HIGH ASPECT RATIO STUDIES (Cont'd.)

7. Configuration, Access, Maintenance and Tritium Breeding

- Access problems at high aspect ratio?
- Can we use the same maintenance approach as in the present baseline?
- Implications for tritium breeding ratio in a high aspect ratio configuration?

8. Divertor Operation

- Divertor conditions are typically more favorable at high aspect ratio because of several factors including lower plasma currents, higher bootstrap fractions, longer connection lengths and higher densities (for the same beta limit); however, field line angles at the divertor plate may be problematic because of the low values of B_p/B_t. What limits should we place on incident angles at the divertor?
- Expected divertor conditions (2D simulations) under typical operating scenarios for the high aspect ratio design?
- Are any of the potential advanced divertor schemes more/less applicable at this design point (i.e higher A, B_t, n_e, and lower I)?.

9. Transient Implications

- Implications for thermal and electromagnetic disruption loads relative to the present baseline (e.g. effect of lower lower plasma current, lower thermal and inductive stored energies, runaway electrons, etc)?

10. Safety

- Safety implications for a high aspect ratio machine relative to the ITER baseline (e.g: lower fusion power, lower tritium inventory, lower plasma stored energy - thermal and inductive, but higher TF stored energy, etc)?

11. Miscellaneous Issues

- ***Alpha Loss via TAE Modes***: Does this problem get better at high A and high B_t? Can we optimize the design to minimize its effect?
- ***Tritium Supply***: Given that high aspect ratio designs have lower fusion power for the same neutron wall loading, are there favorable implications for tritium processing and supply?
- ***Costing***: Cost difference relative to the present baseline?

Studies now underway, indicate that higher aspect ratio, lower current design points may lead to more attractive machines, especially in terms of technology phase performance [1]. This suggests that further attention should be directed to the merits of such designs for ITER in the form of a "critical issues" study in 1991. A list of such issues is provided in Table VI-2. An expanded list can be found in Ref. 10.

Finally, we note that an aspect ratio of 4 is not necessarily a limit for candidate designs and that machines up to A~5 may be viable depending on constraints and performance requirements [1]. Nevertheless, the high aspect ratio study point at A=4 in Table VI-1 should provide a suitable study point for benchmark and critical issues studies in 1991.

REFERENCES

[1] L.J.PERKINS, J.D.GALAMBOS, J.R.GILLELAND, et al., *The International Thermonuclear Reactor at High Aspect Ratio*, Lawrence Livermore National Laboratory, UCRL-ID-104178, (1990)

[2] P.YUSHMANOV, T.TAKIZUKA, K.RIEDEL, et al., "Tokamak Energy Scaling Expressions and Their Uncertainty", to be published in *Nuclear Fusion* 1990[2]

[3] L.GRISHAM, S.SCOTT, R.GOLDSTON, et al., *Scaling of Confinement with Major Radius in TFTR"*, Proc. European Phys. Soc, Amsterdam, Netherlands, June 1990.

[4] J.G.CORDEY et al., *A Preliminary Analysis of the ITER Energy Confinement H-Mode Database*, 13th Internat. IAEA Conf. on Plasma Physics and Controlled Nuclear Fusion Research, Washington, DC, 1-8 October 1990, paper IAEA-CN-53/F-3-19, IAEA, Vienna (to be published 1991)

[5] J.G.CORDEY, JET Joint Undertaking, Abingdon,UK, private communication, (1990).

[6] R.H.BULMER, Lawrence Livermore National Laboratory, Livermore, CA, private communication (1990)

[7] D.PEARLSTEIN, S.HANEY and J.FREIDBERG, *A Variational Procedure for Vertical Stability*, 32nd Annual Meeting of the Division of Plasma Physics of the APS, Cincinnati, OH , (Nov. 1990)

[8] R.STAMBAUGH, General Atomics, San Diego, CA, private communication (1990)

[9] T.TAYLOR, General Atomics, San Diego, CA, private communication (1990)

[10] L.J.PERKINS, *ITER Systems and Operational Studies: Proposed Workplan for First Year of the EDA*, ITER memo, ITER-IL-SA-1-0-29

VII. ADVANCED OPERATING MODELS

VII.1 INTRODUCTION

We briefly examine two operating modes for the machine which lie somewhat beyond the normal operational scenarios, namely: (1) "advanced" operation at higher power levels more akin to those expected in a commercial power reactor together with an assessment of the possibility of net electric power generation, and (2) the investigation of D-^{3}He operation in order to determine if the present understanding of tokamak physics might extrapolate to interesting conditions. These studies are preliminary in nature and, appropriate to the "conceptual" nature of the present activity, should be treated as scoping studies to demonstrate potential flexibility.

VII.2 FEASIBILITY OF ADVANCED OPERATION

VII.2.1 Scope

Advanced operation of ITER, which has been studied previously[1-3] might include: achievement of reactor-typical power densities, high temperature/high efficiency blanket operation, net electric power generation, high end-of-life fluences, steady state or very long pulse operation, and self-sufficient tritium breeding. This study focused mainly on the first three. A summary of the work is presented here, and a more detailed account can be found in Reference 4. The study was organized into two assessment categories: performance/sensitivity and impact on systems.

VII.2.2 Performance Sensitivities

Performance was assessed under two sets of operating constraints: a nominal set, which incorporated the base set of ITER physics and technology constraints and an optimistic set where the ITER "rules" were extended to higher performance values [4] that might be realized in the future. Three operating modes were examined: purely inductive, conventional current drive, and advanced current drive. "Advanced" current drive refers to those speculative schemes, such as helicity injection through divertor biasing, which push on the bulk electron population and have the potential for high inherent efficiencies. These are distinct from "conventional" schemes, such as neutral beams, lower hybrid, electron cyclotron, etc., which drive only tail electrons. The results are summarized in Figures VII-1 and VII-2.

The figures show that net electric power may be possible, depending on operating constraints, operating mode, and wall loading. Figure VII-1 shows net electric power as a function of wall loading for all operating modes under nominal operating constraints. Advanced current drive shows considerable benefit over the inductive mode even though they have similar physics (i.e high Q operation). This is largely due to cycle averaging of the net electric power over the inductive burn pulse. The performance with conventional current drive is severely degraded as the wall loading is increased. This is because as the wall loading increases at fixed beta limit,

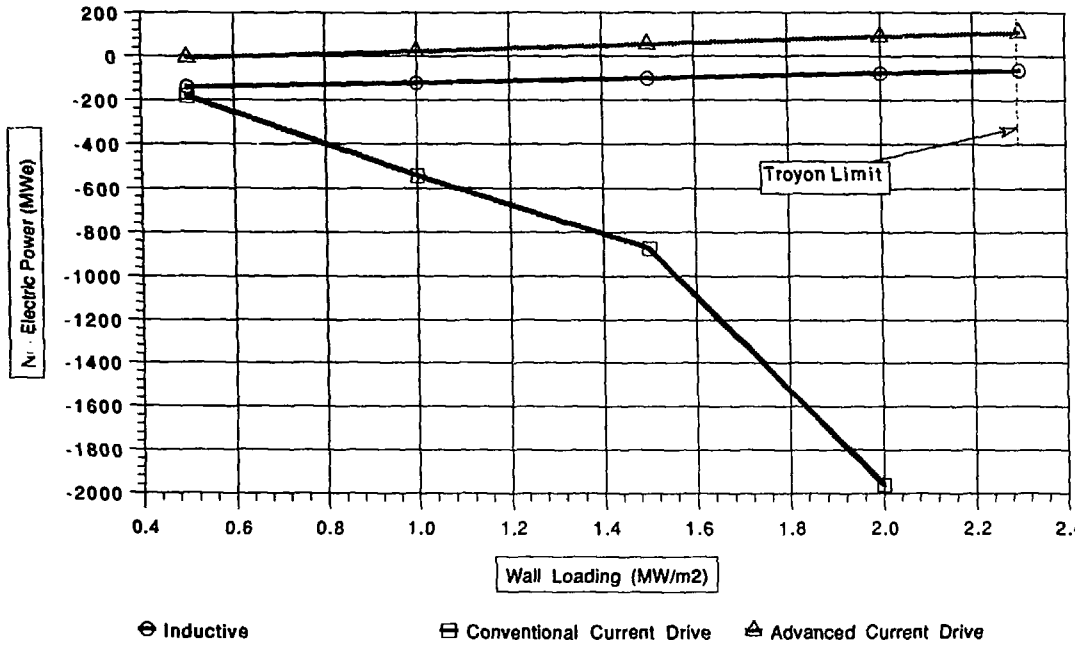

Fig. VII-1. Net Electric Power versus Wall Loading for Nominal Constraint Values.

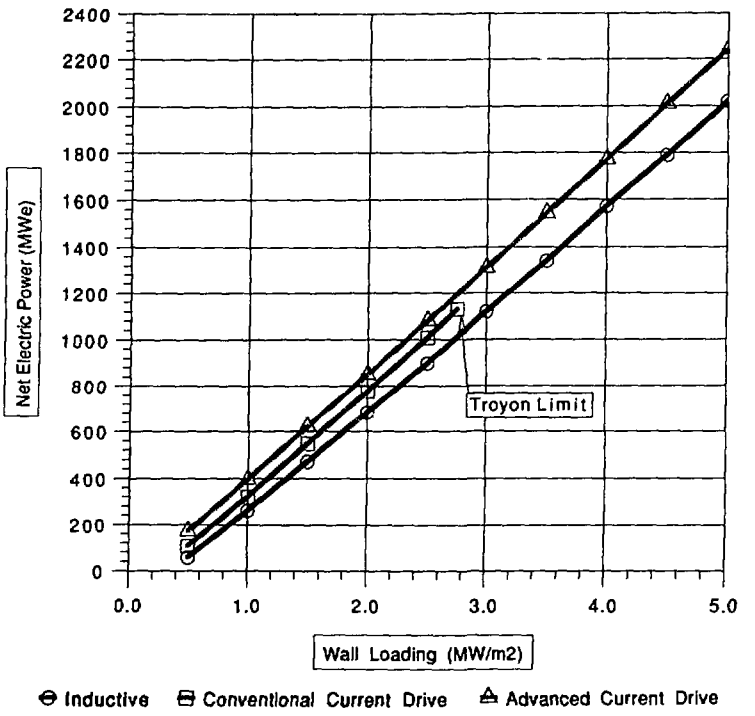

Fig. VII-2. Net Electric Power versus Wall Loading for Optimistic Constraint Values.

the density must increase while the temperature decreases. These both act to reduce the efficiency at which the neutral beam can drive current. The required neutral beam power therefore increases; because it does so at a rate faster than the fusion power is increasing with wall loading, the result is a steep decline in net electric power.

In Figure VII-2, the performance of the operating modes is compared using more optimistic constraints [4] and performance is improved relative to the nominal constraint case, particularly for conventional current drive. In such a case, net electric power would, in principle, be available in ITER.

Sensitivity of performance to some of the major constraints was also investigated. The most critical constraint was found to be the thermal conversion efficiency. If the goal of net electric power is pursued for ITER, considerable attention should be given to assuring that acceptable conversion efficiency can be obtained in the high temperature blanket modules.

VII.2.3 Implications of an Advanced Operation on ITER Systems.

Divertor: The ability of the divertor to remove heat may limit the wall loading to below the value necessary to achieve net power. This appears to be the case for purely inductive operation under nominal constraints. However, as seen from Fig. VII-1, the

advanced current drive mode can produce net electricity under nominal constraints at a wall loading less than that where divertor heat removal capabilities become a limitation. However, although advanced current drive schemes are expected to deposit only modest power levels in the torus, our speculative scheme of helicity injection by divertor biasing dissipates this power mainly in the scrapeoff layer. This aspect requires further attention; note however, that such advanced schemes work at high density similar to that of ignited operation.When considering divertor temperature and the potential for erosion, the wall loading under optimistic constraints may be even further reduced [3]. Depending on the divertor material, the wall loading required for net power under optimistic constraints may not be achievable because of excessive erosion. Under nominal constraints, divertor temperature and erosion concerns are not as limiting as the divertor heat load concern.

Shielding: If a higher fusion power is required to achieve net electric power (this depends on operating mode and operating constraints -- Fig. VII-1 or 2), or if the machine mission is extended, materials will be exposed to higher fluxes and/or fluences. If the current shielding configuration of the ITER baseline is retained, the nuclear heating limit in the magnets, the radiation damage limit in the magnet insulation, and the biological dose limit outside the cryostat will be exceeded. To avoid exceeding these limits, additional shielding would be required. Depending on actual flux and fluence values, the additional shielding requirement would be on the order of 10 cm [4].

Heat Transport/Thermal-hydraulics: To obtain net electric power from ITER, it will be necessary to alter the conditions and configuration of the blanket cooling system, and make appropriate additions/modifications to the balance of plant. A substantial hot blanket would be necessary. Thermal conversion efficiency was identified as the most critical constraint affecting the net electric power produced. Thus, considerable attention should be given to design of the energy conversion system to maximize thermal conversion efficiency. A steam rankine cycle would likely be adopted for energy conversion, requiring a steam generator and turbine system to be added to the balance of plant. A thermal storage system to maintain the blanket at elevated temperatures during downtime would be an additional requirement.

Blanket/Tritium Systems: If higher fusion power is required to generate net electricity, the tritium needs of the machine would increase. Thus, it would be necessary to breed more tritium or find external sources of supply. Increasing breeding requirements would increase demands on the breeder processing system, and may also affect availability, as blanket changeouts to specifically replace the consumed breeder may become necessary. The breeder blanket itself must be compatible with the high temperature blanket required for efficient energy conversion. At higher fusion powers, more tritium must be burned in the torus. This implies a greater fueling rate to the torus, and if fractional burn-up remains constant, this means greater exhaust flows. The increased throughput will place greater demands on the vacuum pumping systems and will required increased processing capability in the tritium systems.

Safety: Safety may be adversely affected if fusion power or machine duration increases. Onsite inventories of tritium and activation products would increase. Radioactive effluents and wastes from the site would likely increase. A high temperature blanket presents overpressure concerns and may provide a means for mobilizing radioactivity. It would be more difficult to demonstrate safe operation with higher inventories and more severe conditions.The frequency and severity of accidents may also increase. There will also be safety related siting and cost implications.

Configuration: Configurational changes will be necessary to accommodate the goal of net electric power production. A steam generator, turbine, and thermal storage system will be required. The in-blanket piping arrangement may have to be modified. Additional shielding may be necessary. The capacity of the tritium systems might have to increase. Additional safety features would be needed. A larger, more pressure tolerant building may also be required to house the additional equipment, and to withstand the higher potential overpressure from the high temperature coolant.

Cost: Extending the ITER mission would add to the cost of the program due to: additions to the heat transport system to allow for energy conversion, a thermal storage system, increased capacity of tritium systems, tritium purchases (if needed), additional shielding, additional safety systems, and a larger more pressure tolerant building.

VII.2.4 Electricity Generation Demonstration in a Single Sector

The challenge of extracting net electric power from ITER may be more easily met if only a single sector (say 1/16) is considered. Net electric power could be demonstrated if the gross electric power from the sector was greater than roughly one-sixteenth of the recirculating power for the full blanket. Concerns associated with the divertor and shielding, which are only related to the plasma power level would be unchanged. The heat transport/energy conversion system, however, could be considerably scaled down. A thermal shield between the energy producing sector and the remainder of the blanket would be needed to isolate the relevant sector and eliminate losses to the colder portions of the blanket. Safety concerns associated with the high temperature coolant would be reduced as the volume of hot coolant would be much less. It may not be necessary to provide a larger more pressure tolerant building to accommodate additional equipment and a higher overpressure source term. Costs associated with single sector energy extraction would not be as great. The cost of the building and of the heat transport/energy conversion equipment would not be as high as that associated with energy conversion from the full blanket. In summary, obtaining net electric power from a single sector of the ITER blanket might be a more manageable objective.

VII.3 PLASMA OPERATION IN D-^{3}He

VII.1. Introduction

The question considered here is whether approximate breakeven conditions (D-^{3}He fusion power equal to the injection power sustaining the plasma) can be achieved in ITER using the same physics scaling laws used in determining the performance with D-T fuel. Only a summary of the work is presented here. Further details are available in Ref. 5.

VII.3.2 D-^{3}He Performance

Plasma operation would require high temperature (Te~30keV, Ti~40keV), to study transport, power balance, fueling mechanisms, impurity control, etc. The assessment of D-^{3}He operation in ITER has been done using a power balance code (DHE3TOK) similar to the physics portion of the US ITER systems codes, but specialized for the peculiarities of D-^{3}He fuel, including relativistic corrections to bremsstrahlung and synchrotron radiation. The figure of merit used to evaluate the performance of ITER with D-^{3}He fuel is the energy multiplication, Q, which is the ratio of the fusion power produced in the plasma to the injected power required to sustain the plasma.

Shown in Fig. VII-3 is Q versus ion temperature (all temperatures quoted in this chapter are density weighted and volume averaged). We see that Q improves with ion temperature and reaches a maximum at about 35 to 50 keV. The Q-values for the 28 MA case are considerably better than those for the nominal 22 MA reference case because confinement improves with plasma current.

Representative parameters are shown for the optimum ion temperature for these 4 cases in Table VII-1. Transport losses dominate the total energy loss, with both synchrotron and bremsstrahlung considerably smaller.

Fig. VII-4 shows the sensitivity in the H-mode multiplier (*ITER Power* scaling) used in calculating energy confinement. As expected, Q improves with the H-mode multiplier. Above H~2.5 it saturates, however, due to the ohmic confinement limit.

VII.5. Tentative Conclusions on D-^{3}He Operation

Under the nominal constraints assumed for conventional ITER operation, a D-^{3}He plasma might be expected to achieve Q values of ~0.3 but would require appreciable injection powers approaching 200MW. Confinement enhancement of up to H=2.5 and higher plasma currents up to 28MA would increase this value to Q~0.6. with injection power requirements of ~125MW. Note, however, that a given Q in D-^{3}He is equivalent to a Q five times larger in D-T from the point of view of the impact of fusion reactions on the plasma power balance. This is because essentially 100 % of the fusion energy is in the form of charged particles for the D-^{3}He reaction, whereas it is only 20 % for the D-T reaction Note, however, that the low density plasma and the high fraction of the fusion power output in charged particles may considerably worsen the divertor conditions relative to DT. One possibility is the potential for a large fraction of the output power to be in directed radiation, leading to the concept of

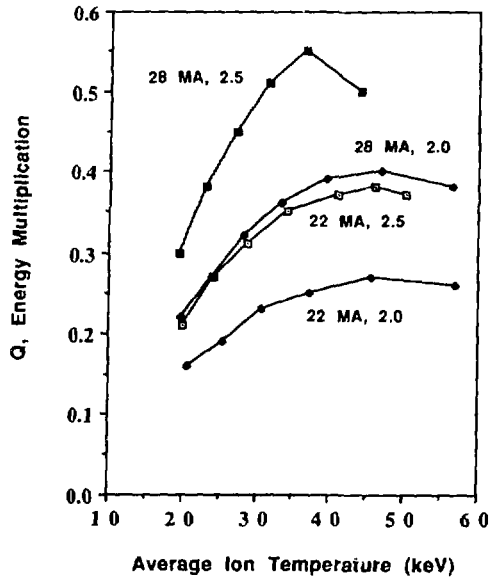

Fig. VII-3. D-^{3}He operation in ITER: Variation of Q with average ion temperature. The four curves are parameterized by the plasma current and H-mode multiplier (ITER Power scaling).

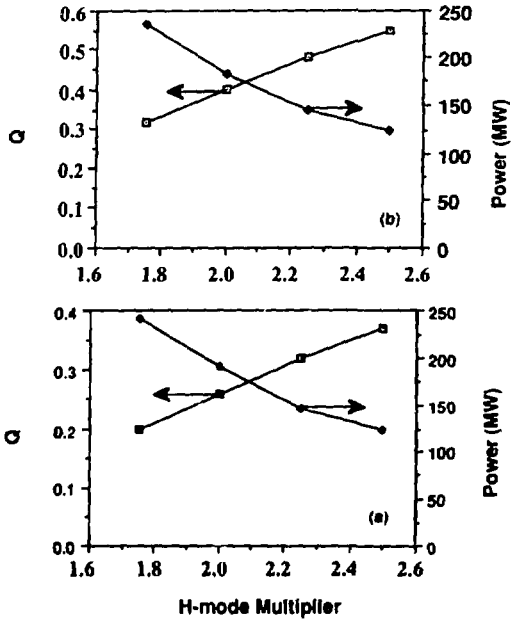

Fig. VII-4. Effect of the H-mode multiplier (ITER Power scaling) on Q and auxiliary power requirements, for plasma currents of (a) 22MA and (b) 28 MA.

synchroton power conversion via waveguide-loaded rectennas. In such a case, conduction flow to the divertor would be less.

Questions requiring further analysis for D-^{3}He operation in ITER include the effect of low density operation on the divertor, and ripple loss of fast ions. Attention must also be addressed to the accuracy of modelling radiation power especially synchrotron losses which can be appreciable at these temperatures under certain

TABLE VII-1. REPRESENTATIVE PARAMETERS FOR D-^{3}He OPERATION IN ITER

Plasma current (MA)	**22**	**22**	**28**	**28**
H-mode multiplier for *ITER-Power* scaling	**2.0**	**2.5**	**2.0**	**2.5**
Q	.27	.38	.40	.55
Injection power (MW)	186	122	183	124
Fusion power (MW)	49	46	72	68
Ion density (10^{13}/cm^3)	3.1	3.0	3.7	4.5
Ion temperature (keV)	46	46	47	37
Electron temperature (keV)	30	32	33	30
τ_E (s)	3.4	5.4	4.3	6.7
Slowing down time (s)	5.8	6.5	5.6	6.5
Particle conf. time (s)	10	16	13	20
Troyon coefficient	2.5	2.5	2.5	2.5
Transport power (MW)	195	124	198	131
Synchrotron power (MW)	28	32	39	33
Bremsstrahlung (MW)	13	12	19	27

circumstances. In summary, operating ITER with D-^{3}He would provide useful data on confinement and transport of burning plasmas under D-^{3}He-relevant conditions and would contribute to the database for possible next step D-^{3}He experiments.

REFERENCES

[1] L.J. PERKINS AND D.T. BLACKFIELD, "High Power Operation of ITER", LLNL-ITER-89-002, January 1989.

[2] W.R. SPEARS, "ITER As A Demonstration Power Reactor", ITER memo ITER-IL-SA-1-9-8, May 1989.

[3] J. SHEFFIELD AND R.L. REID, "A Slightly Different Logic for the ITER Design and Program", submitted for publication in Fusion Technology, May 1990.

[4] S.J. BRERETON AND L.J. PERKINS, "Potential for, and Implications of, Advanced Technology Phase Operation in the International Thermonuclear Experimental Reactor, Lawrence Livermore National Laboratory, UCRL-ID-105292, November 1990.

[5] G.A EMMERT, Potential for D-^{3}He Operation in ITER, Rep. UWFDM-842, Fusion Technology Institute, University of Wisconsin, Madison, WI (1990).

VIII. IMPLICATIONS FOR COMMERCIAL FUSION REACTORS

During the ITER Conceptual Design Activity a number of parametric surveys and design studies of commercial tokamak power reactors have been made. These studies have been based to varying extents on ITER physics assumptions. Therefore, to varying extents, they represent extrapolations of where ITER might lead, technology permitting, if that physics performance were realised. Only those studies that most closely fit to the assumptions of ITER, and therefore indicate most closely to where the ITER device is leading, are considered [1,2,3]

All these studies consider slightly different options for the input reactor parameter assumptions. Consequently they would have somewhat different output parameters, e.g net power, neutron fluence, etc. in a machine of given size. However, this aspect is of secondary importance. A general assumption of these studies has been to consider higher peak field values in the range 14-15 T, compared to the 11 T values in ITER, assuming that the (about 25%) higher resulting stresses can be accommodated in the more optimised coil designs which will then be likely to be available.

Sometimes a beta scaling coefficient higher than, or plasma safety factor lower than, the ITER baseline constraint is also assumed, again on the assumption that they will not need to be worse than that required for the ITER technology phase. Higher bootstrap current contributions and current drive system efficiencies are also assumed, on the basis that the knowledge and ability to tailor the plasma behaviour will have advanced sufficiently to allow these improvements. The resulting main cases from these steady-state driven studies are shown in Table VIII-1 in comparison with ITER and the potential operation of a machine of ITER size (see section VI).

As was shown in Chapter VII, even a machine the size of ITER equipped with the improved current drive and particle exhaust systems expected to be developed during the life of ITER, and with shielding thicknesses adjusted to keep the same TF coil dose and neutron fluence as in the present ITER design, would be able to produce about 2 GW of fusion power. If this could be converted to electricity with only an overall 25% thermal conversion efficiency, a few hundred MW of electricity could be generated in such a machine. For devices from the above studies, which have been optimised to produce a net electrical power of about 1200 MW, assuming a thermal conversion efficiency of 40%, the increase in size over that of ITER is rather modest, and the results show that the range covered by plasma parameter options to be studied in the ITER experimental programme may even allow some overall size reduction in devices after ITER.

To attain this reactor performance, without significant machine size increase over that of ITER, a number of plasma physics and technological objectives will need to be achieved relative to those expected in basic ITER operation:

- magnet stress levels about 25% higher;
- thermal conversion efficiencies of about 40%;
- slightly increased plasma elongation and/or beta scaling coefficient and/or slightly reduced plasma safety factor;

TABLE VIII-1. ITER-EXTRAPOLATED REACTOR STUDIES

	ITER	ITER SIZE	POWER REACTORS [1]	[1]	[1]	[2]	[3]	[3]
Peak tor. field (T)	10.7	←	14.0	←	←	←	13.5	14.9
Plasma elongation (95%)	2.0	←	2.0	←	2.5	2.0	←	2.25
Beta scaling coefficient	3.0	3.5	3.0	3.3	3.5	3.0	←	4.0
Plasma Safety factor q-psi	3.4	3.0	4.1	3.1	3.1	3.0	2.9	←
Alpha particle fraction	0.10	←	0.05	←	←	0.05	←	←
Z_{eff}	3.81	1.65	1.5	←	←	1.83	1.54	←
Bootstrap fraction	0.28	0.32	0.30	←	←	←	0.30	0.50
CD efficiency (nIR/P)	0.42	0.75	0.74	0.76	0.77	0.99	0.54	0.70
Major radius (m)	6.0	←	7.0	6.4	6.0	6.0	7.1	5.3
Minor radius (m)	2.15	2.03	2.4	1.8	1.4	1.6	2.0	1.4
Plasma current (MA)	19.8	19.3	25.0	21.6	20.6	17.0	22.4	16.6
On-axis tor. field (T)	4.85	←	7.4	7.0	7.5	7.1	6.4	6.2
Electron temperature (keV)	19.0	15.0	28.0	28.0	32.0	20.0	←	←
Electron density ($10^{20}m^{-3}$)	0.74	1.24	0.65	0.87	0.99	1.27	1.05	1.45
Neutron wall load (MW/m^2)	0.8	2.1	2.3	3.0	3.6	3.3	3.1	4.2
Lifetime fluence (MWy/m^2)	3	18	43	56	68	55	58	78
Goldston scaling HG	2.0	1.6	1.5	1.3	1.2	1.6	1.1	1.4
Fusion power (MW)	830	2040	3120	2905	3107	2630	3900	3050
Thermal efficiency	-	0.25	0.4	←	←	←	0.35	←
Current Drive power (MW)	150	130	107	111	←	92	217	91
Thermal power (MW)	-	2580	3420	3430	3430	3850	4920	3780
Circulating power (MW)	-	430	167	171	171	340	524	310
Net electrical power (MW)	-	215	1200	←	←	←	←	←

- about a factor 2 higher current drive efficiency, or an enhanced bootstrap effect;
- an adequately high temperature energy efficient blanket of similar attenuation in the space presently allowed for the water-cooled driver blanket;
- tolerance of heat and particle loadings on the first wall about 3 times that typical in ITER;
- reduction of the heat and particle loads on the divertor, by control of the scrape-off layer physics, so that these are not 3 times higher than in ITER;
- material damage levels 3-10 times that attainable in ITER;

The ability to overcome these challenges in subsequent machines will to a large extent be demonstrated by the studies to be carried out on the ITER device during its testing programme. Clearly, however, additional facilities, e.g. in materials testing, will also be needed to give confidence in the commercial viability of the reactor.

REFERENCES

[1] R.S.DEVOTO, et al., "Projections for a Steady-State Tokamak Reactor Based on ITER", Lawrence Livermore National Laboratory, UCID-21519 Rev.1 (1989)

[2] A.I.MELDIANOV et al., "Calculations of Power Tokamak Reactor Characteristics on ITER Plasma Physics Database", Kurchatov Institute of Atomic Energy Report, 1989

[3] P.I.H.COOKE, R.HANCOX, W.R.SPEARS, "A Reference Tokamak Reactor", Culham Laboratory Report CLM-R298, 1989

INTERNATIONAL
ATOMIC ENERGY AGENCY
VIENNA, 1991